

**A Theoretical Investigation of Inversion Layer Transducers  
(ILT) for Ultrasonic Skin Thickness Measurement**

**Yasser Estantouli**

Submitted in July 2004

For the degree of

**Doctor of Philosophy**

The Bioengineering Unit &  
The Centre for Ultrasonic Engineering  
University of Strathclyde

## **Copyright Notice:**

The copyright of this thesis belongs to the author under the terms of the United Kingdom Copyright Acts as qualified by the University of Strathclyde Regulation 3.49. Due acknowledgment must always be made of the use of any material contained in, or derived from this thesis.

## Acknowledgements

I would like to thank my supervisors Prof. Gordon Hayward and Prof. Joseph Barbenel for their help and support throughout the progress of this work.

I would also like to thank all the CUE staff for the nice time that I spent in this big family, which I considered as my second home. Thanks also go to the Bioengineering staff.

Thanks to all the football team members whom enabled me to have a very nice games.

My appreciation also goes to Dr. Paul Reynolds and Dr. Richard O'Leary for their help in PZFlex.

I would also like to thank Nishal Ramadas for his help in programming the mathematical model using MATLAB.

Great thanks to my family back home, mother, father, brothers and my sister for their patience and support.

I would like to thank deeply from my heart, my Wife, Rima for her patience and support during my work and the long time that I left her alone with the two angels, latterly, my sons Mekdad and Moaaz.

# Table of Contents

<b>Acknowledgments</b>	<b>ii</b>
<b>Abstract</b>	<b>vii</b>
<b>List of Symbols</b>	<b>viii</b>
Chapter 1- Introduction	1
1.1 Background	2
1.2 Aims	4
1.3 Contributions of the Thesis	5
1.3.1 A New Model of the Inversion Layer Transducers	5
1.3.2 The Use of FE Modelling to Simulate Ultrasonic Wave Propagation through Skin	6
1.3.3 An Evaluation of Ultrasonic Transducer Technology	7
1.3.4 Publications Arising from the Work of this Thesis	7
1.4 Overview of the Thesis	9
Chapter 2- The Human Skin	13
2.1 The Human Skin	14
2.2 Function	14
2.3 Structure of the Skin	14
2.3.1 Epidermis	15
2.3.2 Dermis	18
2.3.3 The Appendages of the Skin	19
2.3.4 The Dermis-Epidermis Interface	20
2.3.5 Subcutaneous Tissue	21
2.3.6 The Surface Pattern of the Skin	21
2.4 The Inhomogeneous Structure of the Skin	24
2.5 The Mechanical Properties of the Skin	24
2.6 Water Effect on the Skin	26

2.7 Skin Thickness Measurement	27
Chapter 3- Skin Imaging & Thickness Measurement	28
3. Introduction	29
3.1 Skin Imaging and Measurement	29
3.1.1 Thickness Measurement	29
3.1.2 2-D and 3-D Skin Imaging	30
3.1.3 Comparison of Methods	31
3.1.4 Validation of Ultrasound Thickness Measurement	32
3.2 Clinical Use of Thickness Measurements	32
3.2.1 Skin Thickness	33
3.2.2 Skin Diseases	33
3.3 Principles and Physics of Ultrasound	35
3.3.1 Source and Detection of Signal	36
3.3.2 Coupling	39
3.3.3 Focusing	39
3.3.4 Improving the Acoustic Mismatch	42
3.3.5 Ultrasound Modes of Operation	43
3.4 Ultrasonic Properties of the Skin	46
3.5 Pulse Width and Skin Measurement	48
3.6 Review of the Ultrasonography of the Skin	49
Chapter 4- PZFlex, FEM Technique Non Planar and Dry Coupling Low Frequency Models	60
4.1 Principles of the FE modelling	61
4.2 Materials Definition in PZFlex	63
4.3 Modelling Accuracy	66
4.4 The Effect of the Skin-Fat Interface on the Backscattered Signal	73
4.4.1 The Planar Boundary	73

4.4.2 The Effect of a Non-Planar Interface	74
4.4.3 The Effect of a Planar Diffusive Boundary	78
4.5 Front Face Configuration	79
4.6 Conclusion	85
 Chapter 5- High Frequency Modelling	 87
5.1 Modelling of the Real Interfaces of the Human Skin	88
5.2 Comparison of Planar and Realistic Interfaces	90
5.3 Diffuse Interfaces	92
5.4 Results and Discussion	93
5.5 Future Work	101
 Chapter 6- Heat Treated LiNbO <sub>3</sub> Transducer Design	 103
6.1 Original LiNbO <sub>3</sub>	104
6.2 Heat Treated LiNbO <sub>3</sub>	105
6.3 PZFlex Modelling	107
6.3.1 Thickness	107
6.3.2 Imperfect Interface	108
6.4 Impedance Profile	110
6.5 The Effect of Backing	114
6.6 The Influence of a Front Face Matching Layer	119
6.6.1 The Fractional Bandwidth (FBW)	120
6.7 Experimental Result	123
6.8 Concluding Remarks and Discussion	125
 Chapter 7- Mathematical Model	 127
7.1 Introduction	128
7.2 The Thickness Mode Receiver	128
7.2.1 Basic Equations for Piezoelectric Resonator	129
7.2.2 Boundary Conditions and Equation Development	136

7.2.3 Some Specific Conditions of Electrical and Mechanical Loading	146
7.2.4 The Pulse Width in Reception Mode	152
7.3 The Device as a Transmitter	159
7.3.1 Relationship Between Force and Charge for Transmitter	161
7.3.2 Relationship Between Voltage and Charge for Transmitter	164
7.3.3 Developing the Transfer Function of the Transmitter	166
7.3.4 The Pulse Echo Mode	181
7.4 Electrical Impedance Analysis	183
7.5 The Feedback System Block Diagrams and Physical Insight	191
7.5.1 The Receiver Transfer Function Feedback System	191
7.5.2 The Transmitter Transfer Function Feedback System	196
7.5.3 The Transducer Admittance Transfer Function Feedback System	204
7.6 Concluding Remarks	206
 Chapter 8- Concluding Remarks & Future Work	 207
8.1 Concluding Summary	208
8.2 Future Work	211
8.2.1 FEM Analysis	211
8.2.2 Manufacturing	211
8.2.3 Skin Measurement System	212
 <b>References</b>	 213

## **Appendixes**

Appendix A: The mechanical properties for the materials used in PZFlex

Appendix B: MATLAB program to build table from an image.

## **Abstract**

The human skin is the outermost organ of the body. The thickness of the skin can give useful clinical information on its condition. In this thesis the complicated structure of the skin was described and methods of skin thickness measurement critically reviewed. Ultrasound was identified as a non-invasive method having several advantages over the other methods, such as safety, ease of use and low cost.

The existing ultrasonic systems have not been successful to quantify the skin structure properly, due to lack of high resolution transducers and the biology of the skin structure.

The PZFlex Finite Element Method (FEM) package was used to model the skin, an ultrasonic thickness measurement system, and their interaction, in order to define the system structure and parameters. Initially, the skin was modelled as one planar layer of a linear isotropic material and 5MHz transducer was used to minimize computational effort. A non-planar structure was then modelled and compared to the planar interface to see the effect of the additional complexity on the backscattered signal and to clarify the axial and lateral resolution requirements for skin thickness measurement. Different front face configurations of the transducer were also modelled to investigate the effect of the geometry on the backscattered signal as a starting point to introduce practical coupling. A more realistic skin structure was then modelled at 80 MHz, by super-imposing a FEM mesh on a micrograph of the skin and the backscattered ultrasound signal from the real skin interfaces compared to a signal from planar interfaces. An appraisal of the existing technology was concluded and the requirements for an ideal skin thickness measurement system were then addressed.

A monolithic  $\text{LiNbO}_3$  transducer incorporating inversion layers (IL) was modelled using PZFlex to investigate the usefulness of these transducers for skin measurement. A novel mathematical 1-D linear systems model was developed for a transducer incorporating one front face inversion layer. This model gave a physical insight into, and more understanding of, the transducer behaviour. It was found that, although ILT's offer improved sensitivity and bandwidth for skin thickness measurement, they suffer from similar problems to conventional devices and a new transducer technology is needed for ultra high resolution applications on real skin surfaces.

The new theory offers substantial base for the design of ILT's, which will have significant applications in other areas, such as harmonic imaging and multi-frequency sonar.

## LIST OF SYMBOLES

Symbol	Description	Units
Z	Specific Acoustic impedance	kg /m <sup>2</sup> .s, MRayls
c, V <sub>c</sub>	Longitudinal Acoustic velocity	m/s
ρ	The density of the medium	kg/m <sup>3</sup>
f	The frequency	Hz
λ	The wavelength	m
T	Transmission Coefficient	
R	Reflection Coefficient	
Z <sub>nf</sub>	The length of the near field of the non-focused transducer	m
r = D / 2	The radius of the transducer	m
D	The transducer diameter	m
δ <sub>lat</sub>	The lateral resolution	m
AR, δ <sub>ax</sub>	The axial resolution	m
F = Fl / D	F number,	
Fl	The focal length	m
T = $\frac{2d}{V_c}$	Transit time	s
d	The thickness of the transducer	m
$\hat{Y}_x^D$	The elastic constant measured under constant electrical displacement	newtons/m <sup>2</sup>
ε <sub>x</sub> <sup>s</sup>	The absolute permittivity of the transducer material measured under constant strain	farad/m
D <sub>x</sub>	The electrical displacement	coulombs/m <sup>2</sup>
E <sub>x</sub>	The electrical field strength	volts/m
Γ <sub>x</sub>	The tensile or compressive stress	newtons/m <sup>2</sup>
S <sub>x</sub>	The strain, or fractional change in length	
h <sub>33</sub>	The piezoelectric constant relating the stress and charge or the electrical field and mechanical strain, measured under constant electrical displacement.	v/m

$\xi_x$	The mechanical displacement	
The suffix $_{33}$	indicates that it is applicable to the thickness direction.	
The suffix $_x$	indicates the x-direction	
$A' = \pi r^2$	The area of the transducer surface	$m^2$
$Q$	The net charge on the transducer surface	coulombs
$F_x$	The force in the x direction.	newton
$C_0$	The bulk capacitance of the transducer	farad

# **CHAPTER 1**

## **Introduction**

## **1.1 Background:**

This project is an evaluation of ultrasonic skin measurement, with the ultimate objective of quantifying accurately skin structure. To this end, a Finite Element Modelling package, PZFlex, has been used to simulate different ultrasonic transducer configurations and to understand ultrasonic wave propagation through various interfaces of the skin organ.

Human skin thickness measurement and imaging is a helpful tool for diagnosing the condition of the skin. Some diseases or malfunctions of the skin will influence its thickness. Hence, the measurement of the skin can help the physician to assess any change produced by disease, such as skin tumours, monitor the progress of disease or treatment and assess the efficiency of cosmetic factors.

The skin is a thin tissue compared to the other human tissues, and thus it requires high frequency transducers to resolve this low thickness. A very high frequency is required (> 100MHz) to resolve the different layers of the skin such as the stratum corneum, the outer layer of the skin, which may have a thickness of only 7 $\mu$ m.

In the last few decades, work by different researchers has contributed to the development of high frequency transducers of 100 MHz and above, which was helpful for measuring low thickness objects in many fields. In this context, lithium niobate (LiNbO<sub>3</sub>), was preferable to other piezoelectric materials because of its reasonable sensitivity and higher speed of sound which allows for the development of the very low thickness transducers at high frequencies.

Snook et al [1] performed a series of studies of the fabrication of high frequency transducers using a variety of single –element piezoelectric materials, i.e. PVDF, LiNbO<sub>3</sub>, PbTiO<sub>3</sub> and PZT ceramics. Their results showed that the transducers incorporating LiNbO<sub>3</sub> and PbTiO<sub>3</sub> have excellent sensitivity with a good bandwidth.

Kerr [2] investigated skin thickness measurement using the PiezoCAD modelling package. Several piezoelectric materials were compared for transducer performance and the results showed that the LiNbO<sub>3</sub> was a good compromise for the different requirements of high frequency transducers.

Though, ultrasound offers a relatively inexpensive and good means of obtaining the data required for thickness measurement and imaging, the characteristics needed for high frequency transducers suitable for skin thickness measurement are difficult to achieve, specifically the requirements for a short pulse width at 100 MHz and such a device is not yet available. The complex properties of the skin, incorporating an inhomogeneous structure, non planar and diffuse boundaries, also inhibit the use of inversion methods to obtain clear data to be used for skin structural measurement.

Wojcik et al [3] used the PZFlex package with another, more specific package, for tissue modelling (PSFlex), to simulate the ultrasonic wave propagation in a non-linear tissue structure, and obtained good results. As always, the properties of the materials used in the model, especially the tissues, must be accurately known to obtain reliable results.

In this thesis, PZFlex was adopted to simulate the ultrasonic signal propagation in a real skin structure to investigate the effect of planar, diffusive and real boundaries on the backscattered signal.

A new inversion layer transducer (ILT) was investigated to evaluate the efficiency of such transducers in fulfilling the requirements needed for skin thickness measurement. A novel mathematical model was developed to provide a better understanding and physical insight of the ILT devices.

## **1.2 Aims:**

The main aim of this study is to perform a detailed appraisal of the current transducer technology and clarify ultrasonic wave propagation through a realistic skin structure, in order to design a system that will yield improved data and better understanding of the interpretation of the reflected signals from a real skin structure. This incorporates the following objectives:

### **Resolving the thinnest layer of the skin:**

To design a high frequency transducer with sufficient temporal resolution to delineate the thinnest layer in the skin which is of the order of few micrometers. This should take account of suitable backing or matching layer(s) and the need for a focused transducer. The transducer used in the system is required to have a wide frequency response which corresponds to a short time response and this is desirable for the low transit time of the thin skin layers. This will increase the resolution of the system thus improving the system ability to resolve the low thickness.

### **Quantify the difficulties with practical ultrasonic measurement of the skin:**

The geometrical structure is an important issue in affecting the backscattered signal from the object under study. The structure of the skin is inhomogeneous and complex and the

effect of this structure, including the surface geometry, the layer non-uniformity and the different mechanical properties of the skin layers, on the identification of the reflections from these layers is important. This information can be used to improve the transducer design and behaviour to extract information about the skin. Also, the possibility of having a 'diffuse' boundary between the layers of the skin will reduce the amplitude of the reflected signal and increase the demand for a highly sensitive transducer. In this context, a diffuse boundary is defined as one possessing a graded transition in acoustic impedance between two adjacent layers. In other words, the mechanical boundary transition between two adjacent layers is relatively smooth, resulting in a reduction of the effective reflection coefficient. This is considered a more realistic scenario for practical skin structures.

#### **Transducer Mechanical Interfacing:**

Dry coupling is an important issue and required to be explored, since the use of water as a coupling agent might hydrate the stratum corneum causing artefact in the output result. As an initial stage of the design of dry coupling the shape of the front face of the transducer incorporating rubber cover was investigated.

### **1.3 Contributions of the Thesis:**

#### **1.3.1 A new Model of the Inversion Layer Transducers (ILT):**

In an attempt to overcome the deficiencies with current ultrasonic transducer technology, a new type of device, the ILT, was investigated. To understand such

devices, a new mathematical model has been developed and verified using finite element analysis.

### **1.3.2 The use of FE Modelling to Simulate Ultrasonic Wave Propagation Through Skin:**

The real structure of the skin is inhomogeneous, anisotropic, visco-elastic and non-linear, with an irregular pattern of interfaces separating the different layers of the skin, which makes it difficult to identify and recognize the reflected signals from these layers. For the purpose of simplifying the models, the skin was modelled as a linear elastic material throughout the stages of this project.

As part of the ultrasonic system evaluation process, a range of FE models were established. The most important comprised:

- The effect of custom modelled non planar interfaces between skin and fat on the backscattered signal was studied.
- The effect of having a diffuse boundary between two different tissues on the output backscattered signal was modelled. The results showed that this will reduce the amplitude of the backscattered signal.
- The effect of the real interfaces of the different layers of the human skin structure on the high frequencies ultrasonic backscattered signal was modelled. A micrograph of the cross section of the skin was superimposed on the FEM mesh of the model to mimic the real structure of the skin. The effect of such real skin interface on the backscattered signal and the propagation of ultrasonic wave were

reported and some critical recommendations made for high frequency transducer design.

- The use of rubber interface between the transducer and the skin and the effect of the shape of the rubber material was modelled and reported, and some recommendations given for further investigation of dry coupling medium for skin thickness measurement at high frequencies.

### **1.3.3 An Evaluation of Ultrasonic Transducer Technology:**

The finding of this thesis and those of other works, were used to evaluate the practical potential for using ultrasound in accurate characterisation of skin structure. Unfortunately, these are negative, due to inadequacies inherent in known transducer technology. However, this analysis is considered to provide a proper basis for future device, processing and system development.

### **1.3.4 Publications Arising from the Work of this Thesis:**

1. Y. Estanbouli, G. Hayward and J. C. Barbenel, "A Theoretical Investigation of Ultrasonic Transducer Design for Measurement of Skin", Proceedings of the IEEE Ultrasonics Symposium, October 2002, Munich-Germany, pp 1245-1248.

2. Y. Estanbouli, G. Hayward and J. C. Barbenel, "A Study of Inversion Layer Transducers", Presented at US Office of Naval Research Transducers Materials and Transducers Workshop, May 2003, The Penn Stater Conference Centre, State College, Pennsylvania, USA.
3. Y. Estanbouli, G. Hayward and J. C. Barbenel, "A Theoretical Investigation for Ultrasonic Measurement of Skin Thickness", Presented at the Ultrasonics International Conference, June 2003, Granada-Spain.
4. Y. Estanbouli, G. Hayward and J. C. Barbenel, "A Study of Inversion Layer Transducers", Proceedings of the IEEE Ultrasonics Symposium, October 2003 Hawaii-USA, pp 1322-1325.
5. Y. Estanbouli, G. Hayward and J. C. Barbenel, "A Study of Ultrasonic Skin Thickness Measurement Using Finite Element Modelling", Presented at British Medical Ultrasound Society (BMUS) 35th Annual Scientific Meeting, December 2003, Harrogate, UK.
6. K. Mackenzie, D. Kelly, G. Hayward, G. Abel, Y. Estanbouli and W. Galbraith, "Experimental Measurement of Ultrasonic Backscatter from Gas Filled Microspheres Using Pseudo Random Code Sequences and Ultra-Wideband Transducer Technology", Presented at British Medical Ultrasound Society (BMUS) 35th Annual Scientific Meeting, December 2003, Harrogate, UK.

## **Papers in Press:**

Y. Estanbouli, G. Hayward, S. N. Ramadas and J. C. Barbenel, “A Linear Systems Model of the Thickness Mode Piezoelectric Transducer Containing Dual Piezoelectric Zones”, to be published in the Proceedings of the IEEE Ultrasonics Symposium, August 2004, Montreal, Canada.

## **Papers in Preparation:**

IEEE Journal Paper “A Linear Systems Model of the Thickness Mode Piezoelectric Transducer Containing Dual Piezoelectric Zones” , IEEE Transaction on Ultrasonics, Ferroelectrics and Frequency Control.

## **1.4 Overview of the Thesis:**

### **Chapter (1):**

This Chapter gives an introduction to the thesis, outlining the background of the project, the aims and the contributions made by the work, a thesis overview and a list of publications presented during the progress of the work.

## **Chapter (2):**

In this chapter the structure and the functions of the human skin are described. The overall structure of the skin containing the different layers forming the human skin and the anatomy of each layer is described in some detail because of its relevance to skin thickness measurement. The requirements of skin thickness measurement from a medical perspective are discussed at the end of this Chapter.

## **Chapter (3):**

The diseases of the skin and their effect on thickness measurements are discussed. Brief comparisons are made of the different techniques used for skin thickness measurement, together with the underlying physics of each method. A brief but comprehensive overview of ultrasonic techniques used for skin thickness measurement is given. A critical review of the up-to-date ultrasonic skin thickness measurement is included in this Chapter. The requirements for an ideal skin thickness measurement system for the FE modelling are outlined.

## **Chapter (4):**

This Chapter explains the FE modelling technique and gives some examples at low frequency (5 MHz). A brief study describes the effect of the shape of a silicone rubber front face between the transducer and skin surface on the low frequency backscattered signal.

The effect of specific irregular skin-fat interface geometries on the low frequency backscattered signal were modelled and described. The requirements of sufficient axial and lateral resolution were demonstrated. The effect of having diffuse boundary was also investigated.

### **Chapter (5):**

A model incorporating a real skin structure was developed by the superimposition of the FEM mesh on a skin micrograph and the effect of the realistic skin interfaces on the backscattered signal modelled at high frequency, i.e. 80 MHz, which is theoretically sufficient to resolve the thickness of the modelled skin layers. The propagation of the ultrasonic pressure wave in this real structure was modelled in this Chapter and compared with planar skin layers interfaces.

A diffuse epidermal-dermal interface and its effect on the backscattered signal was modelled.

At the end of the Chapter an appraisal of current transducer technology along with the requirements for ideal ultrasonic skin thickness measurement system were addressed.

### **Chapter (6):**

The performance of heat treated  $\text{LiNbO}_3$  transducers incorporating a number of inversion layers, i.e. opposite polarity piezoelectric layers in the thickness direction was explored using FE models. The advantages of such transducers for skin thickness measurements were outlined.

## **Chapter (7):**

A mathematical model was developed in this Chapter for an inversion layer transducer incorporating one front face inversion layer to provide physical insight and better understanding of the behaviour of such transducers. The ability of using ILT's for skin characterisation was addressed at the end of the Chapter.

## **Chapter (8):**

This is a concluding Chapter, which summarises the thesis results and achievements and gives recommendations for further work.

An analysis of the real potential of using ultrasound in skin thickness measurement and characterisation was discussed.

## **CHAPTER 2**

### **The Human Skin**

## **2.1 The Human Skin:**

The skin is the largest organ of the body with an average area of more than  $1.7\text{m}^2$  and weighs about 4.5 kg. In just  $6.45\text{ cm}^2$  of skin there are approximately 30 million cells, 100 fat glands, 600 sweat glands, 65 hairs, numerous muscles, and thousands of nerve endings [4, 5]. The human skin ranges in thickness from 0.5mm in the eyelid to more than 2mm in the palms of the hands and soles of the feet [4].

## **2.2 Function:**

The skin is multi-function organ and performs complex roles in human physiology, e.g.:

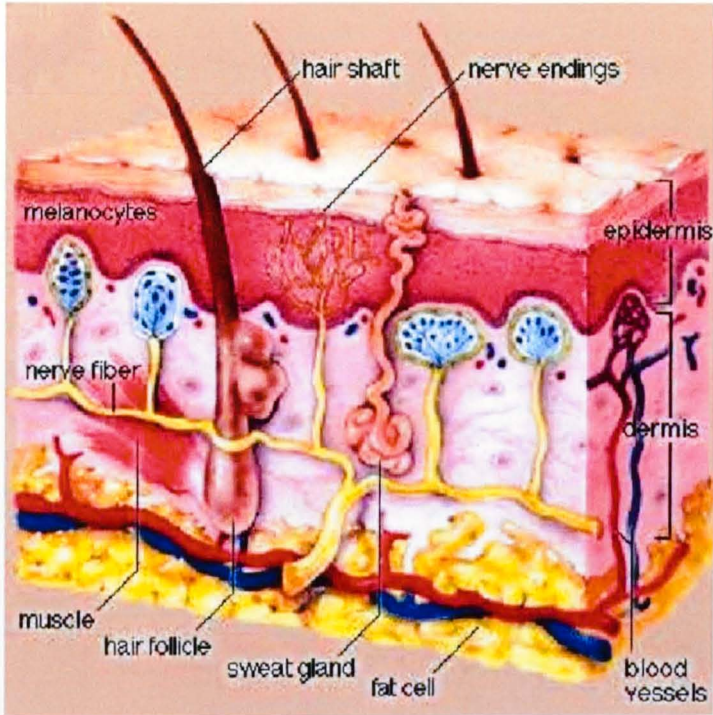
- Protects the rest of the body from toxins, injuries, the sun, and temperature extremes in the external environment
- Preserves the stability of the body's inner environment and keeps it in place
- Plays a role in the regulation of body temperature
- Communicates information about physical and emotional states

These, and some other, functions of the skin are mentioned later and related to the skin structure.

## **2.3 Structure of the Skin:**

The skin [Fig (2.1)] is made up of a thin cellular but avascular outer layer (called the epidermis) and a thicker inner layer (called the dermis). Below the dermis is the

subcutaneous tissue, which contains fat. Buried in the skin are nerves that sense cold, heat, pain, pressure, and touch. Sebaceous glands secrete a lubricating substance called sebum. Deep within the skin, but communicating with the surface, are the sweat glands, which produce perspiration when the body is too hot.



[www.kyaz.com/English/AboutHumanBody.html](http://www.kyaz.com/English/AboutHumanBody.html)

Fig (2.1): The 3-D structure of the skin.

### 2.3.1 Epidermis

The epidermis varies in thickness (50-100  $\mu\text{m}$ ) depending on the body site, sex and age of the individual. It is particularly thick (about 1 mm) in the palms and the soles, where friction is greater. Mechanical simulation of the skin accelerates the production of epidermal cells and causes thickening of the epidermis.

Although it is very thin, the epidermis is composed of many layers of cells. In the lowest layer of the epidermis, the basal layer (the living epidermis), new cells are constantly being reproduced, pushing older cells to the surface. These cells get their nourishment and oxygen from capillaries in the dermis. As skin cells move farther away from their source of nourishment and move out of the basal layer towards the horny, most superficial, layer they flatten and shrink, lose their nuclei, and become filled with a protein called keratin, becoming keratinocytes that make up a layer of dead cells (the dead epidermis or the so called stratum corneum). After serving a brief protective function, the keratinocytes are gradually sloughed off. This process of converting a living cell to a dead keratinocyte, called keratinization, takes about 4 weeks. This transformation process of the cells as they migrate from the basal layer to the horny layer produces changes in cell shape, size and structure, producing 5 characteristic layers in the epidermis namely: stratum germinativum (the basal layer), stratum spinosum, stratum granulosum, stratum lucidum, and stratum corneum.

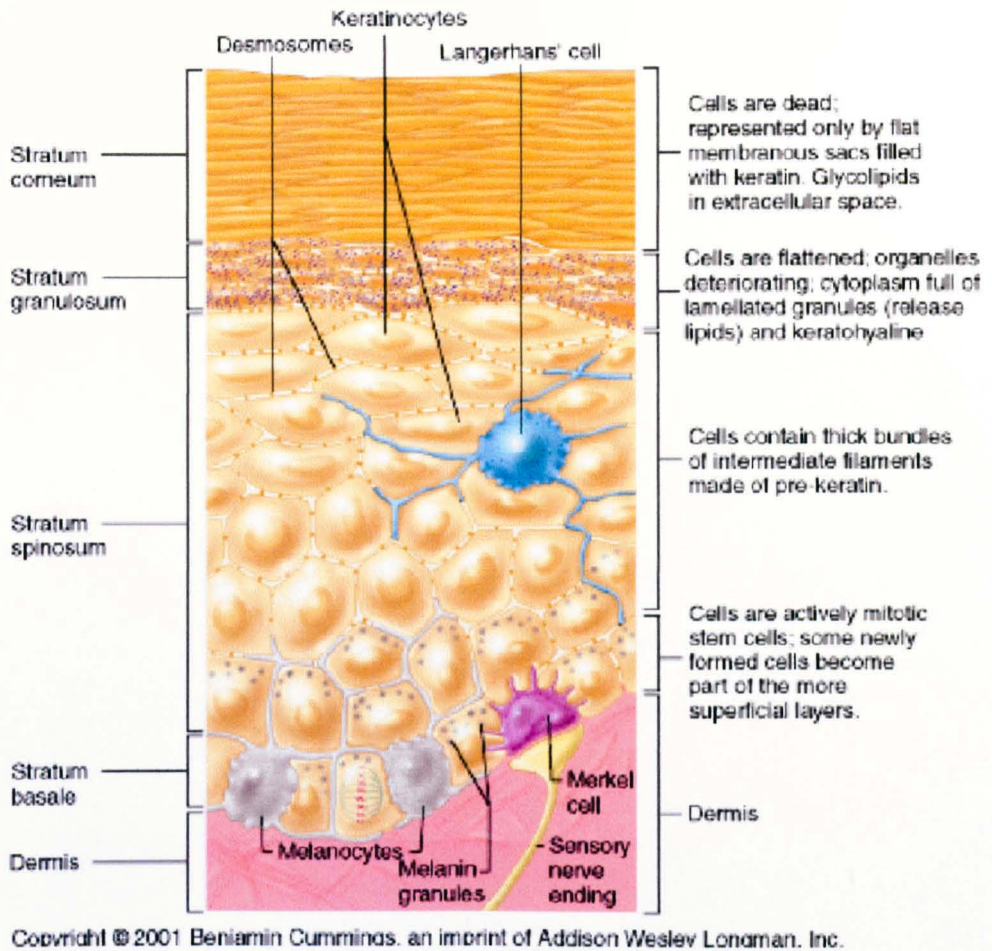


Fig (2.2): The structure of the epidermis.

Other epidermal cells, called melanocytes, manufacture and distribute melanin, the protein that adds pigment to skin and protects the body from ultraviolet rays. Skin colour is determined by the amount of protein produced by these cells, not by the number of melanocytes, which is fairly constant in all races.

Hair and nails are specialized keratin structures and are considered part of the epidermis. While animals have fur and claws for protection and defence, these corresponding structures

are largely cosmetic in humans.

### **2.3.2 Dermis:**

The dermis, or the "true skin," is a connective tissue composed of networks of the fibrous proteins collagen, elastin and reticulin permeated by a semi-gel matrix of ground substance made of a carbohydrate material known as glycosaminoglycan. The collagen provide the skin with its tensile strength and toughness while the elastin contributes the elastic properties of the skin. Within this layer are systems and structures common to other organs such as lymph channels, blood vessels, nerve fibres, and muscle cells, but unique to the dermis are hair follicles, sebaceous glands, and sweat glands, that are derived from the epidermis and open onto the skin surface.

The dermis can be subdivided into two main layers. The main part, the reticular dermis, is formed of an irregular arrangement of coarse fibres, but the upper layer, the papillary dermis, contains more delicate fibres of collagen, reticulin, and elastin separating the epidermis from the coarse fibres.

The dermis also regulates body temperature through a network of capillaries. In hot weather these vessels dilate to give off heat, causing the skin to flush. In cold weather, they constrict, conserving heat, causing pallor. The blood in these vessels nourishes the skin and provides protection for the cellular and fluid systems. Blood vessels in the dermis are responsive to emotional stress, causing the colour changes mentioned previously. The skin, unlike animals, is uniquely human, since it can betray emotion by blushing (embarrassment),

turning red (anger), blanching (fear), sweating (tension), and forming goosebumps (cold or terror).

Nerve endings in the dermis are the source of the body's sense of touch. They sense heat, cold, and pressure, providing both pain and pleasure.

### **2.3.3 The Appendages of the Skin:**

The appendages are derived from the epidermis, but located in the dermis and are continuous with the extended surface of the skin, passing through the epidermis. The hair follicle manufactures a keratin structure, hair. These follicles are found everywhere on the body except for the palms and soles, though most of the hairs produced are fine, light hairs that, unlike the hair of the scalp, are scarcely visible to the naked eye. The sebaceous glands are attached to the hair follicles and through the follicles excrete an oily substance called sebum, which both lubricates and protects the skin.

There are two distinctive sweat-producing glands, the apocrine and the eccrine. The apocrine gland is best known for producing body odour but otherwise has no known physiological function and is apparently a vestige from times past. In the ear it forms a portion of what we see as earwax. It is also present under the arms, around the nipples and navel, and in the anal-genital area.

The eccrine glands are an advanced and extensive system of temperature control. Several million of these glands are distributed over the entire body, with the highest concentration in

the palms, soles, forehead, and underarms.

Sweat, a dilute salt solution, evaporates from the skin's surface to cool the body. Excessive sweating without replacement of lost water can cause heat stroke. Eccrine glands sweat in response to physical activity and hot environments, but emotional stress and eating spicy foods can also cause perspiration.

Table (2.1): Typical dimensions of the skin structure [6].

	Depth $\mu\text{m}$	Width $\mu\text{m}$
Stratum Corneum (SC)	10-20*	
Epidermis	50-100	
Dermis (corium)	1200-1800	
Terminal Hair follicle	1500-4000	50-100
Vellus Hair follicle	800-100	30-60
Sebaceous gland	150-2500	150-500

\* The thickness of the SC may be much more than this in some anatomical sites such as soles [4].

### 2.3.4 The Dermis-Epidermis Interface:

The interfaces of the diverse layers of the skin have an effect on the ultrasonic backscattered signal and hence in ultrasonic skin measurements. The epidermal-dermal junction forms such an interface. It is uneven and wavy showing a complex topology composed of pegs and sockets with finger like contour of dermal protrusions called dermal papillae projecting

towards the skin surface and downward projections from the epidermis called rete ridges. This complex form of interface enhances the stability of the epidermal-dermal junction.

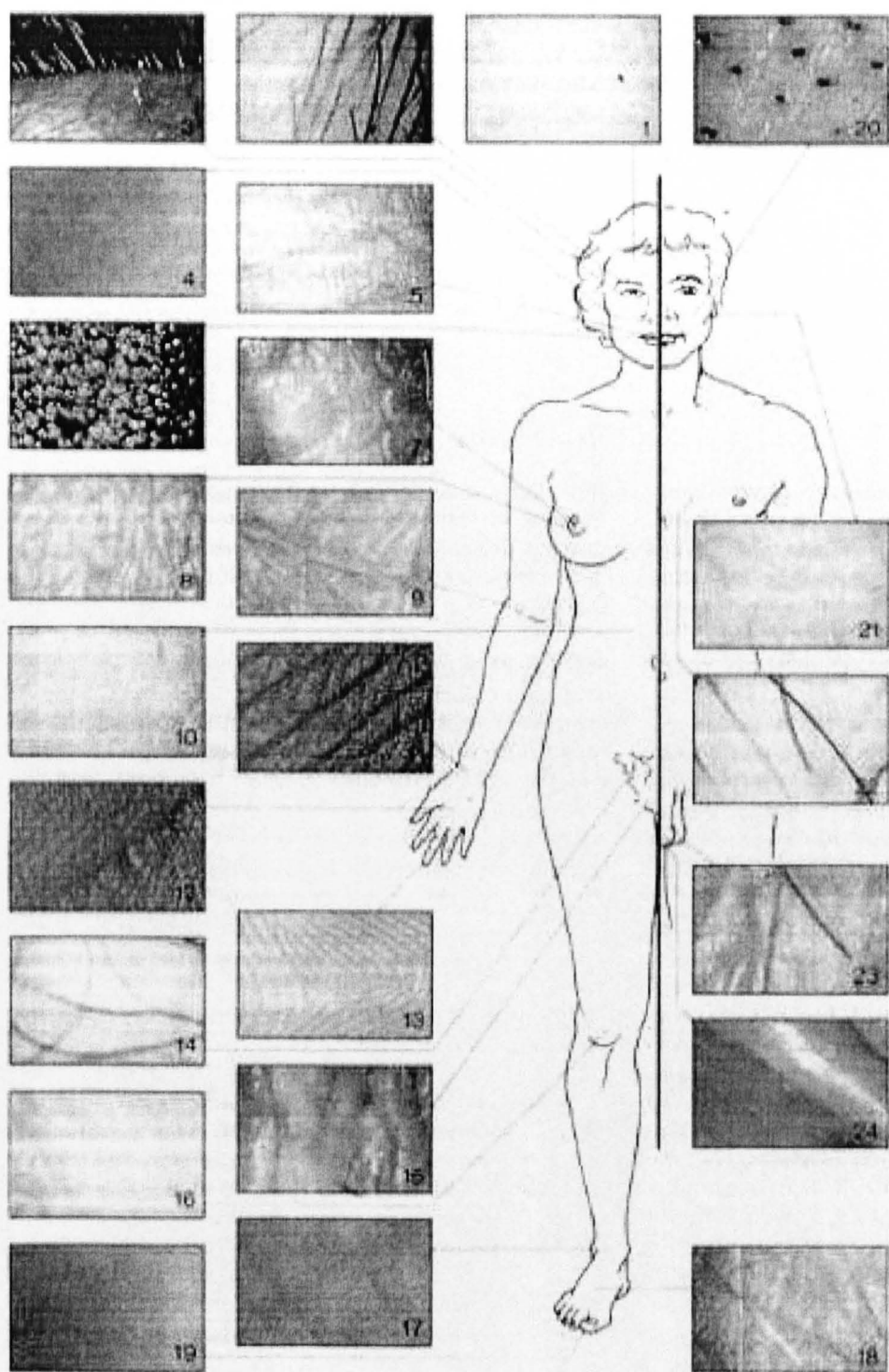
### **2.3.5 Subcutaneous Tissue:**

The subcutaneous tissue is another layer of connective tissue below the dermis that may contain fat. It is unevenly distributed over the body, and there are wide individual differences in distribution. In addition to providing protection and insulation, the subcutaneous tissue serves as a depository for reserve fuel to be drawn upon whenever the amount of calories taken in is less than the amount burned up through activity. It is also instrumental in manufacturing vitamin D.

### **2.3.6 The Surface Pattern of the Skin:**

The arrangement and interlocking of adjacent keratinocytes, the epidermal rete ridges, the dermal papillary structure, and the cutaneous appendages all contribute to the surface form. Both external and internal processes, e.g., ageing, dehydration, hydration continuously remodel the cutaneous landscape.

The real skin surface pattern is not uniform, but can be described as a flat plateau, divided into neat geometric patterns by intersecting furrows, ridges and other irregularities. The direction of the furrows and their depth is site dependent (Figure 2.3). This pattern allows the epidermis to stretch during the normal body movement. The surface form is site dependent and related to skin extensibility.



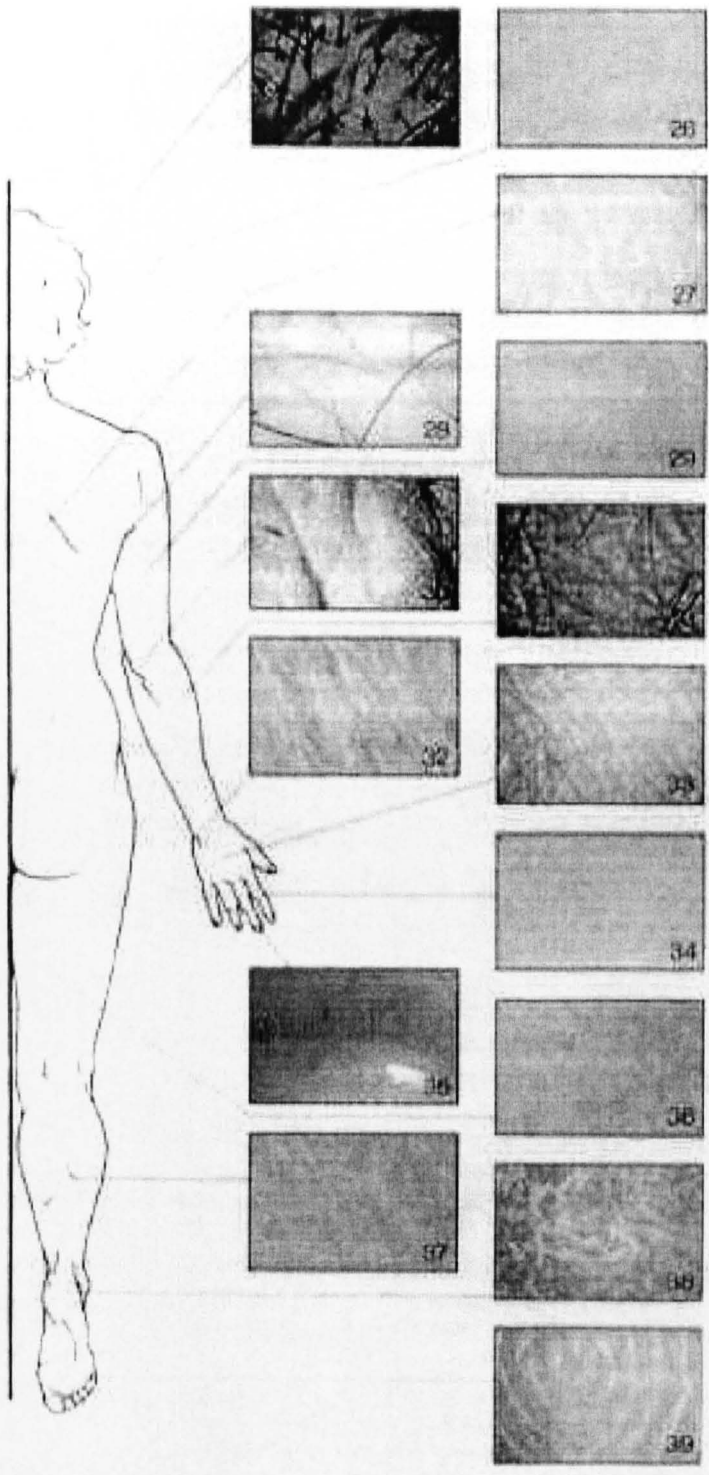


Figure (2.3): Surface pattern of the human skin and its site dependency [7].

## **2.4 The Inhomogeneous Structure of the Skin:**

The inhomogeneity of the skin structure leads to inhomogeneous mechanical properties, because the physical properties vary within the skin layers and each layer has different properties.

The interfaces between the different layers of the skin have irregular surfaces. These interfaces may also be diffuse rather than abrupt, e.g. there is a basement membrane between the cells of the epidermis and the dermis.

The combination of the different layers of the skin contributes to its complex mechanical properties and helps the skin to perform its multiple functions.

## **2.5 The Mechanical Properties of the Skin:**

The complex structure of the skin containing different materials, such as, collagen and elastin, each with different mechanical properties and the interaction between these materials will lead to the complex mechanical behaviour of the skin [7, 8].

Brown et al, 1973 reviewed the function, structure and mechanical properties of the skin [8]. In their review they explained the relationship between the structure and the properties of the skin and that the stress-strain relationship is not linear. In most regions of the body, the skin is in a state of resting tension and its behaviour varies in different parts of the body and in different directions at a single site. There may also be slight differences between in vivo and in vitro results [8].

Wan Abas and Barbenel [9] explained the stress-strain relationship and gave a range for the Poisson ratio for small tensile loads for human skin in vitro. The study showed that

the stress-strain relationship of the skin behaves nonlinearly and that the skin is an anisotropic tissue.

In the handbook of non-invasive methods and the skin [7], several researchers have discussed skin imaging techniques and the mechanical properties of the skin.

Farinelli and Berardescaa described many factors, which affect the skin properties such as sex, age and body site. Goh mentioned the influence of the environmental and seasonal variations like solar radiation, temperature and humidity on the skin, specially the stratum corneum. The stress-strain relationship as demonstrated by Agache is not linear, and that the stratum corneum is the stiffest layer in the skin, so its role in the whole skin mechanical behaviour is overlooked [7].

Different measurement systems of the mechanical properties of the skin showed that the value of elasticity depends on the applied stress and the mechanical system used for the study.

The whole skin properties have been investigated by simple tension in the plane of the skin both in vitro [9] and in vivo [7, 8]. The results all confirm that the skin has complicated mechanical properties. It is:

- non-linear, having a characteristic non-linear stress-strain relationship.
- Anisotropic.
- Visco-elastic

The SC is potentially important for ultrasonic imaging because it is the surface of contact with the coupling medium. Water or gel used widely as coupling medium may cause artifact to the skin measurement because it affects the properties of the SC.

The properties of the SC have been investigated, mainly in excised specimen [7]. Its property is related to the water content; this is explained in more details in the next section. The main skin properties required to undergo the ultrasonic skin measurement are the velocity, the density, the acoustic impedance which is the multiplication of the velocity and the density, and the ultrasonic attenuation.

The skin properties used in this thesis are given in the next chapter. For more accurate modelling of the skin much more accurate and detailed properties of each of the diverse layers of the skin are required, such as attenuation values and the non linearity parameter.

## **2.6 Water Effect on the Skin:**

The main effect of water on the skin will be on the outer layer, i.e. the stratum corneum (SC). The SC is one of the human body tissues with the lowest water content. The range of water content is approximately 10-30% [10]. The water content depends on the ambient relative humidity.

The SC water contents either directly or indirectly influences the barrier repair processes of the skin epithelium. It is possible that a change in water content of only a few percent may significantly affect the physical properties of the SC, and such small changes in water content may be very difficult to detect. As an example, there is a ratio of about

100 between the elasticity moduli measured in dry and humid conditions. In moist conditions the SC shows rubber like behaviour [8].

There is a hydration gradient between the external and the internal layers in the skin, which is responsible for the continuous flow of water vapour across the SC.

Hydration of the SC has two main effects in addition to changing the modulus; it increases the SC thickness and the diffusion constant. The thickness may increase up to four times the original thickness after hydration [7]. The surface topography of the skin is also affected by moisture, but both dry and moist skin have a rough surface.

For the purpose of this thesis it is important to take in account the effect of water on the skin, which has been used as a coupling medium for ultrasonic scanning, to promote the use of dry coupling or rubber delay line.

## **2.7 Skin Thickness Measurement:**

Measurement of skin thickness gives a good indication of the condition of the skin and can be used for clinical diagnosis and the monitoring of the progress of disease and therapy. It provides a method of localising and locating the site of abnormality within the skin structure.

More details about skin diseases and thickness measurement are given in the next chapter.

## **CHAPTER 3**

### **Skin Imaging & Thickness Measurement**

### **3. Introduction:**

There are different methods for skin imaging and thickness measurement. One main classification of these methods is according to their invasiveness of the skin, which can be classified into three categories; non-invasive, semi-invasive and invasive. For many reasons the non-invasive methods are preferable. There are many different principles for the non-invasive methods as mentioned before, e.g., NMR (MRI), X-ray, and Ultrasonic imaging. The ultrasonic technique is preferable for many reasons, including safety and cost [11, 12].

### **3.1 Skin Imaging and Measurement:**

Ultrasonic skin imaging is a non-invasive tool to obtain information about skin structures and dimensions which can be used clinically to assess the conditions of the skin and to detect the existents of any skin abnormalities. Ultrasound can be used to produce 1-D (thickness measurement), 2-D or 3-D images of the skin structure.

#### **3.1.1 Thickness Measurement:**

Ultrasound provides a simple method of directly obtaining measurements of the thickness of the skin and the position of structures providing echoes. A beam of ultrasound is directed into the skin and the received echoes produced by discontinuities of structure seen as A or B scan (Fig 3.1).

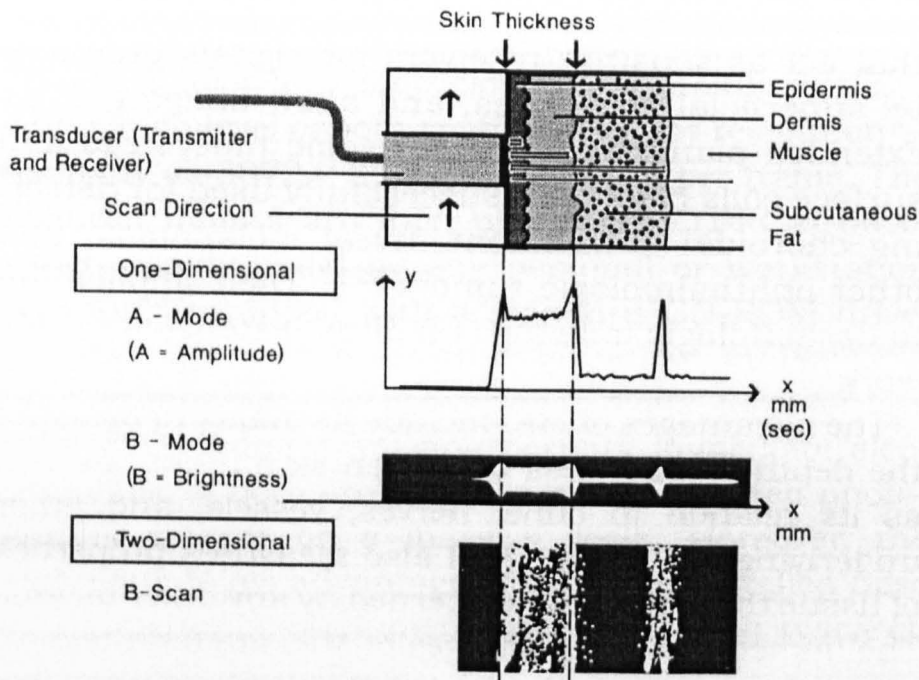


Fig (3.1): 1-D and 2-D ultrasonic skin imaging [7].

The most echogenic structure is the dermal fat junction giving measurements of the full thickness of the skin. Other echoes arise from other junctions, e.g. entry echo and epidermal dermal junction, and discontinuities in the tissue layers, either normal or due to the presence of abnormal structures.

### 3.1.2 2-D and 3-D Skin Imaging:

Imaging of the skin structure to obtain 2-D images can be performed using different techniques such as ultrasound, X-Ray and MRI.

X-ray images represent broadly the electron density in the tissue [13]. Xerography has been successfully adapted for determining skin thickness.

MRI maps the density and behaviour of tissue protons that have been stimulated by radio waves in the presence of a strong magnetic field. The protons seen are typically those of hydrogen atoms within water or other tissue molecules. The application of MRI to dermatology has become practical with the advent of specialised surface coils that acts as sensitive receivers for signals produced by superficial structures. It can be used for skin thickness measurement of a given lesion and its relation to bone, nerves, vessels and the underlying tissues.

3-D images of the skin structure can be build up of 2-D images. In ultrasonic imaging 3-D images have been obtainable and this is a recent field of study in the last few decades. In this case 2-D slices, together with the information about their positions and orientations, constitute 3D dataset describing the scanned volume. Recently 3D images in real time showing movement have also become possible.

### **3.1.3 Comparison of Methods:**

Imaging techniques for clinical purposes are based on many factors such as resolution, contrast mechanism, speed, convenience, acceptability by the patient and safety. For tissues, ultrasonography scores highly for all these factors [14].

The resolution of MRI for dermatological application is in the order of 35 to 70  $\mu\text{m}$  in the depth direction, which is enough to delineate the epidermis [7]. The main disadvantages of this method are the high cost and complex nature of the equipment.

Even though Xerography has been adapted for determining skin thickness it is seldom used in practice because of expenses, site limitation (generally only the extremities can be imaged), and potentially harmful effects of x ray.

### **3.1.4 Validation of Ultrasound Thickness Measurement:**

Skin thickness measurement can be performed in vivo or in vitro, but in vitro measurements required surgical biopsy. General studies of ultrasound measurements produced lower thickness compared to radiology, and both methods have good correlation as was demonstrated by Tan et al [15]. Serup et al [7] showed that it is difficult to delineate the dermis-fat interface using radiology. In general ultrasound is preferable to radiology for many reasons as mentioned before.

### **3.2 Clinical Use of Thickness Measurements:**

Skin imaging is useful tool for assessment of skin structure and dimensions in both diseased and healthy skin. Imaging can give clinical evaluation and assessment of a new therapeutic agent, provide a method for assessing tissue edema and wound healing as well as measuring thickness to evaluate disease and the monitoring of treatment. Skin cancer can also be evaluated and studied using the different imaging techniques to measure the thickness and volume. In diseased skin, thickness in specific lesion of the different layers of the skin, or in more than one layer, may be affected depending on the disease and its particular effect.

### **3.2.1 Skin Thickness:**

Ultrasonic skin imaging has been widely used in the last few years at frequencies of 15 MHz and above. The overall thickness of the skin can be detected by frequencies of about 10-15 MHz. However, higher frequencies are required to produce enough resolution to detect information about more specific structures of the different layers of the skin.

The dermis can be detected with ultrasonic frequency of about 20 MHz, but to delineate the epidermis a resolution of about 50  $\mu\text{m}$  and hence a frequency of about 50 MHz is required. To detect more details of the layers of the epidermis, such as SC, a higher frequency (>100 MHz) is required.

### **3.2.2 Skin Diseases:**

In at least 10 percent of all patients, seen by primary-care physicians, complain of skin problems [4].

Skin diseases, regarding ultrasonography, will have two main effects that can be detected; i.e. changes in the dimensions and echogenicity of the characterised tissue.

The diseases of the epidermis, for example, may induce scaling, crusting or oozing. The epidermis may become thicker or thinner.

The following are some examples of the diseases that can affect the skin and be monitored using ultrasound.

**Psoriasis:** A skin disease marked by red, itchy, scaly patches. Thickening of the epidermis, make it possible to visualise the epidermal structure at low frequencies (20MHz) , here the hyperkeratosis is prominent and the epidermal echo is enhanced.

**Inflammation:** inflammatory skin diseases will mainly cause thickening of the skin.

**Scleroderma and morphea (fibrosis of the skin):** Scleroderma is a chronic hardening and contraction of the skin and connective tissue, either locally or throughout the body. There is an accumulation of collagen fibres in the skin and the echogenicity of the dermis increases.

**Wound healing after carcinoma:** carcinoma is a cancer arising in the epithelial tissue of the skin or of the lining of the internal organs. Data obtained from ultrasonography can be used to monitor treatment and healing as a function of wound size and location.

**Burn depth measurements:** Burn depth measurements can be used to assess the extent and severity of burn injury and hence the treatment regimen.

**Skin ageing:** skin ageing will affect the properties of the skin mainly causing atrophy and irreversible structural change and a redistribution of the fluid in the aged dermis. This effect is shown as a reduction in thickness with age.

**Skin tumours:** it can be detected by two or three dimensional imaging, and is characterised by low echogenic areas

**Carcinoma:** good correlation was obtained with histology in determining the tumour depth.

**Melanoma:** a tumour of melanin-forming cells, especially a malignant tumour associated with skin cancer. Ultrasound can provide information about the depth and location of the tumour.

**Other diseases:** Many other different diseases can be studied and monitored using ultrasound, e.g. diseases of skin appendages and subcutaneous inflammation.

It is worth mentioning here that the thickness of the healthy skin is affected by many factors, such as, age, sex, and body site. It is also dependent on the individuals [7, 8]. Males, for example, have a greater skin thickness than females; extremities skin is thinner than truncal skin.

### **3.3 Principles and Physics of Ultrasound:**

Since this work is concerned with ultrasound this technique is explained in more detail here. The ultrasound beam consists of mechanical vibration that travels through the medium under test. When the ultrasonic beam encounters a boundary between two media of different acoustic impedances, some part will be reflected and the rest will be transmitted. The reflected backscattered signal can be used to obtain information about the subject.

#### **Attenuation:**

The ultrasonic signal, when travelling in any medium, will attenuate.

The attenuation is a result of two main factors, scattering and absorption. Scattering takes place if the boundary between two media has surface irregularities of the order of magnitude of the wavelength or less. The reflected wave is then fragmented into random directions relative to the boundary and the intensity of the wave is reduced. Absorption occurs when the mechanical energy is converted into heat in the medium.

### **3.3.1 Source and Detection of Signal:**

This ultrasonic vibration may be obtained when an electrical field is applied to specific materials, called piezoelectric materials, through a phenomenon called the inverse piezoelectric effect. These materials also are found to create electric charges on their surface under compression or extensional forces, a phenomenon defined as the direct piezoelectric effect. The levels of energy involved for medical applications are similar in magnitude to the energy levels in the sound of normal conversation, and this is unlikely to produce a damaging effect [13].

The general ultrasonic transducer consists of a piezoelectric material placed between two media, an absorbing backing material adhered to the rear face of the transducer with a bonding line and matching layer(s) to optimise the energy coupling into the load media. The transducer is then connected to the electrical drive/receive system. A schematic diagram of this structure is shown in Fig 3.1a.

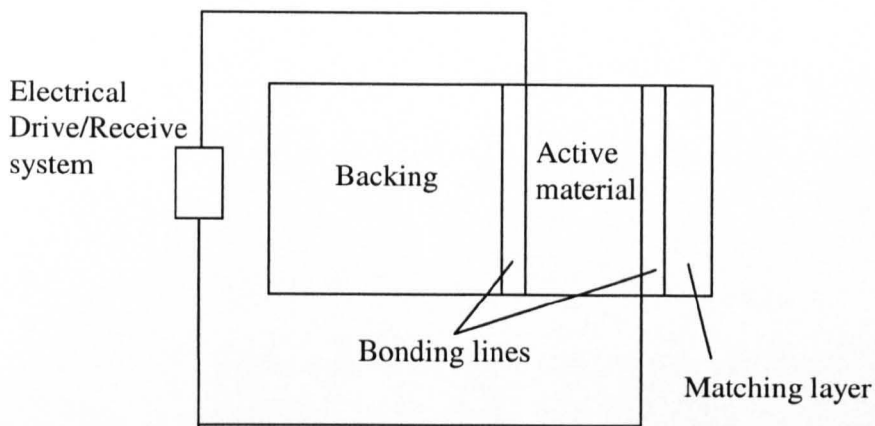


Fig (3.1a): The structure of a general piezoelectric transducer.

The specific acoustic impedance for any medium is defined by:

$$Z = \rho c \text{ kg /m}^2\cdot\text{s} \quad \text{—————} \quad 3.1$$

Where:  $\rho$  is the density of the medium [ $\text{kg/m}^3$ ]

$c$  is the sound velocity in the medium [ $\text{m/s}$ ]

The relation between the wavelength and the velocity is given by the formula:

$$\lambda = c / f \quad \text{—————} \quad 3.2$$

Where:  $c$  is the velocity [ $\text{m/s}$ ]

$f$  is the frequency [ $\text{Hz}$ ]

$\lambda$  is the wavelength [ $\text{m}$ ]

The length of the received echo pulse determines the axial resolution, and is governed by the transducer construction and position of the field point within the beam [16]. The mechanical and electrical loading of the transducer influence the bandwidth of the resonant system and thus the length or duration of the generated stress pulse.

Using a backing material with an impedance near to that of the transducer will reduce the multiple reflections within the transducer, thus reducing the pulse width and increasing the axial resolution, but this will cause a large loss in the sensitivity due to the loss of energy into the backing.

When an acoustic wave is travelling in a media of different materials, the amount of force transmitted or reflected at the boundary between two media of different acoustic impedances is determined by the transmission and reflection coefficient as follows:

$$T = \frac{2Z_2}{Z_2 + Z_1} \quad \text{Transmission Coefficient} \quad \text{—————} \quad 3.3$$

$$R = \frac{Z_2 - Z_1}{Z_2 + Z_1} \quad \text{Reflection Coefficient} \quad \text{—————} \quad 3.4$$

Where  $Z_1$  and  $Z_2$  are the acoustic impedances of medium 1 and 2. If the mismatch of the acoustic impedance between these two media is high then less energy will be transmitted and more will be reflected.

Using a quarter wavelength-matching layer(s) in front of the transducer can reduce reflections from the front face of the transducer and this will increase the sensitivity.

The axial resolution (AR) can be defined simply by the following formula [17]:

$$AR = c \cdot t / 2 \quad \text{—————} \quad 3.5$$

Where:  $c$  is the sound velocity in the medium

$t$  is the time duration of the pulse (the pulse width)

The pulse width time duration is defined as the time taken for the wave amplitude to fall to 10% of its peak value. Since the peak value may occur during the negative cycle of the wave, the rectified pulse must be taken in account.

The velocities in the different human tissues do not differ very much, hence the pulse width is the main factor to improve the resolution, the lower, the better the resolution.

Figure (3.3) illustrates the effect of pulse width on resolution in more detail.

### **3.3.2 Coupling:**

Using a coupling medium, like water or gel, provides many advantages, e.g., the axial multiple reflection artifact in superficial layers of tissue is reduced due to the improvement of matching between the transducer and the skin and a continuous path for the wave is provided, which allows more energy to propagate into the tissue.

### **3.3.3 Focusing:**

In the non-focused transducer there are two main fields of the ultrasonic beam, the near field and the far field as illustrated in Fig (3.1b). In medical diagnosis, it is desirable to operate as close to the near field as possible. A high frequency transducer with small radius can give a near field long enough to extend to tissue depth of interest. Table 3.1

shows some values for a number of ultrasonic frequencies with the disc radii for ultrasound propagation in water.

The axial resolution is some 5 times or more, better than the lateral resolution at the same frequency. The lateral resolution in the near field can be improved if the beam is focused. The lateral resolution depends on the width of the ultrasonic beam. Focusing narrows the beam and has the dual effect of improving the resolution and producing a more accurate image of any small reflectors as well.

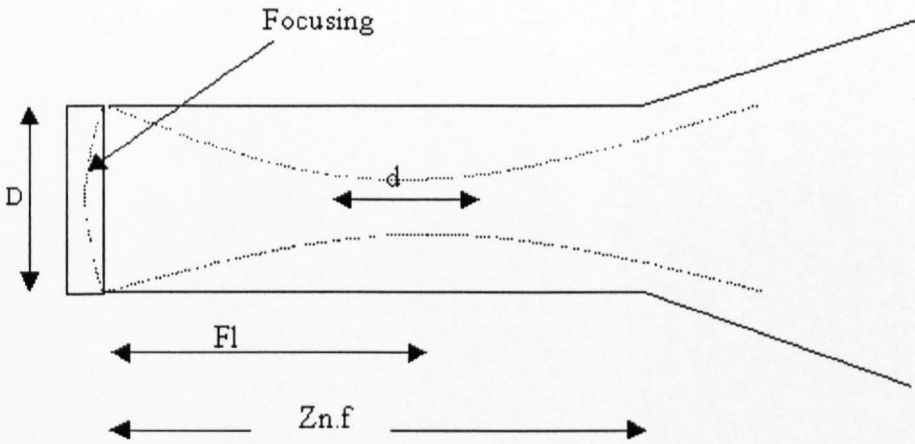


Fig (3.1b): Illustrating the focused and non-focused transducer ultrasonic beam field.

Focusing can be achieved either by curving the front face of the transducer as illustrated in Figure 3.1b, or by using a focusing lens in front of the transducer.  $Z_{n.f}$  is the length of the near field in the non-focused transducer.  $D$  is the transducer aperture. The length of the focal area is defined by  $d$ . For the non-focused transducer, in the far field, the beam is divergent and the energy is dispersed.

The length of the near field of the non-focused transducer is given by the formula [13, 16]:

$$Z_{nf} = r^2 / \lambda - \lambda / 4 \cong r^2 / \lambda \quad \text{—————} \quad 3.6$$

Where:  $r = D / 2$  (The radius of the transducer)

For a focused transducer the resolution is given by the following formula [18]:

$$\delta_{lat} = 1.02c / Ff \quad \text{,the lateral resolution} \quad \text{—————} \quad 3.7$$

$$\delta_{ax} = 2c \ln 2 / \pi \Delta f \quad \text{,the axial resolution}$$

Where:  $c$  speed of sound

$f$  centre frequency

$\Delta f$  Band width

$F = Fl / D$ , F number, Fl is the focal length and D is the transducer aperture (the diameter in the case of a circular device) as in Fig 3.1b.

Table (3.1): Near field length at some frequencies for propagation in water [13].

Disc Radius [m]	Frequency [MHz]	Znf. (Near field length) [m]
0.005	1.0	0.016
	10.	0.167
0.010	1.0	0.065
	10.0	0.667
0.020	1.0	0.263
	10.0	2.667

### 3.3.4 Improving the Acoustic Mismatch:

As mentioned before, using a matching layer of a quarter wavelength at a specific frequency will improve the sensitivity of the transducer. The impedance of this layer is given in the following equation:

$$Z_{ml} = \sqrt{Z_t Z_l} \quad \text{—————} \quad 3.7a$$

where:

$Z_{ml}$  is the acoustic impedance of the matching layer between the two media  $Z_t$ , the transducer and  $Z_l$ , the load medium.

A number of multiple matching layers can be used to further improve matching. In this case each layer will have the optimum impedance value with respect to the adjacent layers.

Mast [19] published a paper reporting a study performed on several human soft tissues, including skin, to predict the relationship between different acoustic parameters. Four main parameters were studied namely sound speed, density, and absorption and non-linearity parameter  $B/A$ , (which characterise the non-linearity of the medium). The study used linear regression analysis and the values used obtained from different sources. This study showed that the non-linear parameter is correlated with speed and density, and confirmed that tissues rich with collagen (proteins) have a relatively higher sound speed and density, while tissues rich with lipids have lower sound speed and density.

### **3.3.5 Ultrasound Modes of Operation:**

There are two main modes of transmitting and receiving ultrasound:

**Pitch-catch mode:** two transducers are used, one for transmitting and the other for receiving.

**Pulse-echo mode:** the same transducer is used for transmitting and receiving. The sound emission is not continuous but pulsed. The equipment automatically and rapidly switches between emission of sound and registration of the echo coming back to the same transducer from the objects being studied. The pulse is fired to the transducer at regular intervals at a frequency called pulse-repetition frequency. The ratio of the pulse duration to the pulse interval is called the Duty Cycle.

There are different types of scanning in ultrasound which will lead to different imaging modes.

In A-scan, i.e. Amplitude versus time, a line of peaks representing echoes from different layers. These echoes are plotted on screen as a function of depth and used to measure distances.

In B-scan, a number of A-scans are depicted and processed electronically to produce a cross sectional image of the object in 2-D.

C-Scan: Scanning a horizontal picture is depicted. The transducer is moved horizontally over an area along x and y-axis.

3D images by ultrasound are also possible and this is a relatively recent field of study in the last few years. In this case 2D slices, together with the information about their positions and orientations, constitute 3D dataset describing the scanned volume. Recently 3D images in real time with movement are also possible.

In M-mode, the motility may be characterised using special procedures. In this case a rapid sequence of B-mode scans whose images follow each other in sequence on screen enables the operator to see and measure ranges of motion, as the organ boundaries that produce reflections move relative to the probe. M-mode ultrasound has been put to particular use in studying the motion of the heart or of arterial walls.

In Doppler ultrasound the velocity of moving objects can be measured, where the movement will produce a change in frequency for the signal emitted from the moving reflector, and the Doppler frequency is proportional to the velocity.

Ultrasonic thickness measurement, using A-scan and pulse-echo mode, involves detection of the time taken for a signal to reflect from layer boundaries; the thickness between these two layers can be obtained when the ultrasonic velocity is known. Fig (3.2) illustrates this in more detail.

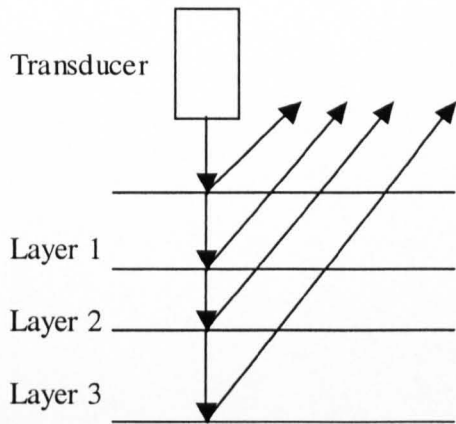


Fig (3.2): The ultrasound principle in determining the thickness.

The principle of the use of ultrasound to measure the thickness of any material is very simple. When an ultrasonic signal propagates through a material of thickness  $d$  it will take a time  $T$  to cross that thickness. If the ultrasonic velocity  $c$  in that material is known then the thickness can be calculated from the formula:  $d = c T$  [m].

Fig (3.2) demonstrates a multi-layer structure (similar to that of the skin). The thickness for the three different layers is  $d_1 = c_1 T_1$ ,  $d_2 = c_2 T_2$ ,  $d_3 = c_3 T_3$  respectively. Where  $c_1$ ,  $c_2$ ,  $c_3$  are the ultrasonic velocities for the layers and  $T_1$ ,  $T_2$ ,  $T_3$  are the times taken for the signal to cross each layer respectively.

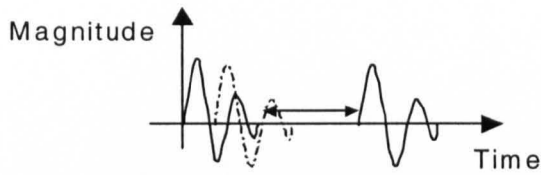


Fig (3.3): Impulse response distortion.

Fig (3.3) illustrates the importance of the pulse width in determining the resolution.

When the two reflected pulses of the front and back face of the same layer are too close they will overlap and look like one pulse and the thickness will not be resolved. The pulse width, as mentioned before, is calculated from the rectified pulse as the minimum time for the signal amplitude to fall to 10% of its peak amplitude.

### 3.4 Ultrasonic Properties of the Skin:

The values of the acoustic velocity, impedance, density and attenuation for each tissue layer are required for the measurements and calculations of skin thickness. Many researchers have performed studies to determine the values of these parameters of the skin; however, the values obtained vary. The acoustic velocity of the skin is the most commonly documented parameter, and this, in turn, will give the acoustic impedance as in equation 3.1.

In Chapter (4) of this thesis skin and fat were modelled to study the effect of non-planar interfaces on the back scattered signal. The properties of these two materials are shown in table (3.2) [7].

The tissues were modelled as acoustic fluids and the shear velocity for both skin and fat was assumed to be zero. The attenuation for both tissues was taken as water (0.002 dB/cm).

Table (3.2): The acoustic properties of skin and fat.

	Density kg/m <sup>3</sup>	Velocity m/s
Skin	1100	1480
Fat	925	1427

Later on, in Chapter (5) the skin was differentiated into more specific layers with different properties of each in order to model the effect of the real skin structure on the backscattered signal. The properties of these layers are given in table (3.3).

Table (3.3): The acoustic properties of the different layers of the skin.

The skin layer	Density kg/m <sup>3</sup>	Longitudinal Velocity m/s
stratum corneum	1500	1550
Epidermis	1150 (1100-1190)	1540
Dermis	1116	1580

All the skin layers were modelled as an acoustic fluid, as stated previously. The attenuation was assumed to be the same as that of the water.

### 3.5 Pulse Width and Skin Measurement:

The transit time for the ultrasonic wave to cross each layer can be obtained from the thickness of each layer and the ultrasonic velocity in that layer. When the transducer system is in the pulse echo mode the wave will cross each layer twice giving a transit time as follows:

$$\text{Transit time} = \frac{2d}{vc} \quad \text{—————} \quad 3.8$$

Where:  $d$  is the thickness of the layer  
 $vc$  the acoustic velocity in that layer.

The stratum corneum is the thinnest layer of the skin and has a minimum thickness of about  $7\mu\text{m}$ . Equation 3.8 and the values of the parameters in table 3.3 predict the transit time will be about  $9.03\text{ns}$ . To resolve this thickness the transducer must have sufficient axial resolution and hence a time duration pulse width of less than this time. Therefore the frequency required to resolve the thinnest layer of the skin can be calculated from the following equation:

$$f = \frac{1}{T} \quad \text{—————} \quad 3.9$$

Where:  $T$  is the pulse time duration.

Substituting  $T = 9.03 \text{ ns}$  in equation 3.9 yields:

$$f = 110.74 \text{ MHz}$$

Therefore an ultrasonic transducer with a minimum operating frequency of about 110.74 MHz is required to resolve the thinnest layer of the skin. The frequency of an ultrasonic transducer operating in the thickness mode is related to its thickness and this will be discussed in more detail in following chapters.

### **3.6 Review of the Ultrasonography of the Skin:**

Skin thickness measurement using ultrasound has some practical difficulties because of the complex structure and the inhomogeneity of the skin and the irregularity of the interfaces between the different layers of the skin.

For example, high resolution in both the axial and lateral dimensions is required. In A-mode imaging the resolution is related to the centre frequency of the transducer. The higher the frequency the better the resolution, but at the same time the penetration ability will decrease [7]. The frequency used for skin imaging purposes should be  $> 20 \text{ MHz}$ , 50 MHz or higher may be needed for scanning of the epidermis [11, 12]. To visualise the stratum corneum, which is very thin, the frequency should be  $>100\text{MHz}$  [7, 11, 12]. The centre frequency is not the only factor that affects the resolution of the signal, but the bandwidth is also a very important issue. A Fractional Bandwidth (FBW) of about 100% is required for an acceptable ultrasonic signal from the skin [7]. The FBW is given by the formula  $\frac{BW}{f_c} \cdot 100\%$ , where: BW is the bandwidth and  $f_c$  is the center frequency.

The axial resolution is mainly determined by the bandwidth. The lateral resolution is proportional to the centre frequency.

Serup et al [7]; used a 20 MHz transducer with 0.05 mm axial resolution and 0.15-0.35 mm lateral resolution (Dermascan C, Cortex Technology, Hadsund, Denmark) and indicated that ultrasonography had a good correlation with histology in determining the thickness. Although histology has a higher resolution, ultrasonography is non-invasive and gives immediate results [7]. They also found that the echogenicity of the skin increased during the daytime and is affected, as mentioned previously, by many biological variables. All these factors should be taken in account when any study including ultrasonic examination is performed.

Many trials have been carried out to construct an effective ultrasonic system for skin thickness measurement.

In 1978 Cantrell et al, published a paper describing acoustic impedance variations at burn-nonburn interfaces in porcine skin [20]. They used two methods for skin thickness measurements, a 15MHz ultrasonic transducer, with a resolution of approximately 0.2mm and a micrometer. The micrometer was used to measure the thickness in vitro, and then by using the pulse-echo ultrasound the time between the reflections was measured. The in vitro measured thickness and the reflection time were then used to measure the ultrasonic velocity in the skin. This was repeated for many samples and the average velocity was calculated ( $1.72 \times 10^5$  cm/s). This velocity was approximately constant in all skin tissues- necrotic, viable and normal. Using this velocity and the

ultrasound, the thickness was measured in vivo. In this study they indicated that the knowledge of the thickness of necrotic tissue to within 15% is adequate, and this system can give values to within this limit.

A year later, Alexander and Miller performed some experiments to determine the thickness of the human skin in vivo with a 15 MHz A-scan pulsed ultrasound, using the system Model 300 Biometric Ruler from the Sonometrics systems, Inc. [21]. They compared the ultrasonic result with radiological method of proven accuracy. The correlation of these two methods was about 0.99 ( $P < 0.05$ ). But the dermis/subcutaneous fat reflection was not always distinguished. The resolution of this system was not enough to visualise the stratum corneum/epidermis interface or the epidermis/dermis interface.

In 1981, Chin Y. Tan et al, using a similar A-scan system to Alexander and Miller, performed a study similar to that of Alexander and Miller to measure the thickness of the skin in corticosteroid induced dermal thinning. Here the result was also compared with the xeroradiographic method [22]. The study was performed on 48 healthy adults. The correlation was 0.89 ( $P < 0.001$ ) in the pre-treatment normal skin and 0.96 ( $P < 0.001$ ) in the post-treatment thinned skin.

One year later Tan et al, using similar system to Alexander and Miller and two independent observers, published a paper describing a study to assess the reproducibility and validity of the skin thickness measurement using ultrasound. They also investigated the variation of skin thickness with age, sex, and body site [15]. They used both in vivo and in vitro measurements, and they noticed that the in vitro measurement gave greater thickness. The reproducibility was good (correlation = 0.88 for two observers). The

dermis-subcutaneous fat junction is not uniformly straight, and in this study ultrasound tended to measure the thinnest part of the skin. It was suggested making several measurements to take in account the least and greatest thickness and then take the average.

In 1989, Rigal et al studied the ageing of the human skin by ultrasound imaging, using B-mode cross sectional images of the skin [23]. The frequency was 25 MHz, reaching a depth of 4mm with a lateral resolution of about 250 $\mu$ m and axial resolution of 80 $\mu$ m. The transducer was housed in a Perspex tip filled with an aqueous coupling gel. It was found that the dorsal skin was 17% thicker than the ventral one, but neither are different beyond 70 years old. The limit of the dermis in A-scan was difficult to be delineated; therefore it was difficult to determine which echo corresponds to the dermis-hypodermis interface. In this study the thickness was 15% greater than that found by Tan et al.

In 1996, Passmann & Ermert, used a PZT strongly focused 100MHz transducer. They claimed that the system would have an axial resolution of 8.5 $\mu$ m and lateral resolution of about 27 $\mu$ m. "The axial resolution was measured as the -6dB width of the envelope of an echo signal of a polished glass-plate". The system was accompanied by advanced imaging and signal processing techniques to enable sufficient penetration depth to obtain a good visualisation of the skin [18]. The signal processing technique adopted here called pulse compression technique in combination with depth dependent pre-filtered non-linear frequency modulated chirp signal, of which the mathematical description can be found in [24]. Strengthening focus will shorten the focal length; therefore a B-scan

system was not enough to get sufficient depth, which led them to use the B/D (Brightness/Depth) scanning technique. In this technique different A-scans were taken for the same skin section at different depths and then processed together to get axial 2-D skin images reaching a depth of about 3mm. They achieved a compromise between a good lateral resolution and high axial resolution and the required penetration depth. The system had a complex software and hardware, and the effect of using water or gel on the skin and on their measurement was ignored in this study. The constructed image does not show or clearly resolve the structure of the skin. This might be due to the PZT transducer used here and this material has low efficiency and sensitivity at 100MHz as was demonstrated by Kerr [2] and also, the way the axial resolution was calculated is not very accurate.

In 1999, El Gammal et al; used a 100 MHz transducer similar to that of Passmann & Ermert with a mechanical focusing procedure (three dimensional x/y/z motor units were used to keep a constant distance between the transducer and the skin). The B/D scanning technique was used also. Using the same method of Passmann & Ermert they also claimed to obtain an axial resolution of 8.5 $\mu$ m and 27 $\mu$ m laterally with a depth of 3.2mm [25]. This high resolution allowed far more details of the upper skin layers as compared with 20-40 MHz sonography. The SC, however, was not detected. Again the effect of water was neglected.

In 1999, Thiboutot reviewed many studies of the application of ultrasound technology to the skin for a range of frequencies [6]. The usefulness of ultrasound as a non-invasive

method for the assessment of many skin diseases and the measurement of skin thickness was explained, e.g., he mentioned that the surface features and the thickness of the epidermis change in skin disease. He concluded that ultrasound *may* become a valuable tool in the objective assessment of safety and efficiency of dermatological therapies for a variety of conditions [6].

High frequency ultrasound transducers have major difficulties. Lopath et al reviewed some of these difficulties, such as active material selection, passive components, acoustic and electrical matching [26]. They tested two different types of active materials for high frequency performance, the lead titanate (PT) and the PZT fibre composites, and tried to examine some of the issues facing high frequency ultrasound. For the first type they examined the use of a transmission line transformer to improve the electrical match at two frequencies 25 and 40 MHz. At 40 MHz the transformer was shown to improve the response only modestly and increased the bandwidth a few percent. At 25 MHz the bandwidth improved almost 60%, however the sensitivity increased only 1dB. For the second type, they investigated the effect of various volume fractions and passive backings. Parylene C was shown to be an effective matching layer for these composites, improving bandwidth of the 30% volume fraction transducers by 20% and sensitivity by 5 dB.

Lebertre et al studied the effect of the epidermis on the dermis backscatter [27]. Using a 35 MHz focused transducer on a fresh abdominal human skin in vitro, they conclude that

the epidermis absorbs and reflects more than 50% of the incident and backscattered energy.

Iraniha et al used a 5 MHz non-contact transducer (1 inch from the burn surface, acoustically matched to air) with a low power level to determine the burn depth [28]. This method allowed a good judgement of wound healing from the B-mode image without causing pain or discomfort to the patient. This study was not used for the measurement of the exact depth of burn but used for the identification of the integrity of the deep capillary plexus for the categorisation of wounds into a healing group or non healing group.

Ritter et al developed a new composite linear array transducer of 48 elements with a 30 MHz centre frequency [29]. They tested the transducer on a phantom and images of ex-vivo human eye were also obtained. The resolution was about 100 $\mu$ m.

Agner reported a review study of different papers in which A-mode ultrasound scanning was used for skin thickness measurement [7]. It was explained that the velocity of ultrasound in any medium depended on the density as well as the elasticity of the medium. He demonstrated that the sound velocity in the subcutaneous fat was considerably lower than the epidermis and dermis, which means that the interface between the dermis and fat was sharply outlined and clearly demarcated. He reported that B or C scanning was more helpful than A-scanning in tumour measurement.

Seidenari, using a Dermascan C (Cortex technology, Hadsund, Denmark) system, mentioned several aspects that should be considered when imaging the skin [7]. For example, the distance between the probe and the skin is very important and should be constant; and the quantity of gel between the probe and the skin should be standardised, because this will affect the signal by affecting the attenuation. She mentioned, also, that the orientation of the collagen fibres, which strongly influences the acoustic properties of the dermis changes under different tension forces, e.g., increasing the pressure of the probe onto the skin.

Hoffmann et al, using two commercially available systems (Dermascan C, Cortex, Denmark and DUB 20 S, Taberna Pro medium, Germany), performed a study of B-scanning of diseased skin for some diseases. They explained that A-scan skin thickness measurement has some problems, because as far as differentiation of histological structure is concerned, it is very difficult to determine where the individual reflections have arisen [7]. Nearly all tumors appeared echopoor. Hair follicles and/or glands lying next to tumor may lead a considerable exaggeration of the tumor thickness. They conclude that differential diagnosis of various inflammatory skin disease based on 20 MHz sonography was not possible. However, high frequency sonography was useful for the measurement of tumor thickness and for monitoring the progress of treatment, and this was also true for evaluation of progression and regression of scleroderma.

Kerr explained some of the issues related to the measurement of skin thickness using ultrasound [2]. It was shown that even the thickness of the bonding line used to connect the backing layer to the transducer would affect the transducer performance and a

bonding line having a thickness of  $0.1\mu\text{m}$  would produce more reverberation in the pulse echo impulse response. Modelling a thickness of  $1\mu\text{m}$  (arguably the minimum achievable in practice) produced a long pulse width reducing the axial resolution significantly and it was concluded that “ the final transducer design must have no bond line and therefore the chosen backing material must be adhesive and prepared *in situ*”. It was also shown that the backing material would affect the bandwidth and hence the pulse width and an optimum backing was required which was difficult to achieve in practice because of the high acoustic impedance of the backing material. Adding the matching layer(s) improve the efficiency but at the same time reduce the bandwidth and hence the axial resolution and a compromise was required.

This review shows the different difficulties accompanied with skin thickness measurement mainly outlined as follows:

- The data obtained from the skin structure are difficult to interpret due to the complex structure of the skin. So, a clear understanding of the ultrasonic wave propagation in the skin structure is required to help interpreting the data.
- The existing transducers do not have the required resolution to resolve the thin layers of the skin specifically the SC, which has a thickness of approximately  $7\mu\text{m}$  at some body sites. Also the transducer is required to have a wide bandwidth and high sensitivity.
- The parameters required for the measurements are difficult to obtain.

- The bandwidth needs to be considered carefully taking in account the effect of backing and matching. For a 100MHz transducer a bandwidth of approximately 100MHz is required to obtain sufficient axial resolution. The backing has to be attached to the transducer via a bond line, but the later in turn will increase the pulse width and hence reduce the axial resolution. To avoid this the backing block needs to be prepared in situ, but backing blocks of sufficient acoustic impedance cannot be 'poured' onto the transducer during manufacturing and is difficult to achieve in practice due to the high acoustic impedance of the backing material.
- Using water or gel as coupling medium is required to create a continuous path for the acoustic waves into the skin and eliminate the effect of air. Doing this might affect the SC causing hydration and changing the SC properties producing artefact in the results.

In all of this work, two issues are of paramount importance. Firstly, no suitable transducers have been devised to meet the axial resolution requirements with adequate sensitivity. Indeed, there is an excellent case to support the hypothesis that current piezoelectric transducers technology will never fill this gap. Secondly, a more complete understanding of the issues relating to ultrasound wave propagation through skin is required. This is also necessary to create the specifications for the required transducer characteristics.

In order to have more understanding of the effect of the skin structure on the ultrasonic wave propagation, and the effect of non-planar layer interfaces a FEM

package was adopted in this thesis, i.e. PZFlex, explained in more details in Chapter (4). The transducer and the skin were modelled to provide an insight into the interaction of the transducer and the skin-structure in order to clarify the design requirements of a high frequency transducer suitable for skin measurement.

## **CHAPTER 4**

### **PZFlex, FEM Technique**

### **Non Planar and Dry Coupling Low Frequency Models**

## **4.1 Principles of the FE Modelling:**

The Finite Element Method (FEM) or Finite Element Analysis (FEA) is an approximate mathematical method for analysing the behaviour of structures subjected to a variety of loads. The body is divided into a structure consisting of a mesh of small elements that are joined at nodes. The sub-element shape is simple, generally a triangle or rectangle for a 2-D structure as illustrated in Fig 4.1, and the global problem can be transformed to a matrix of simple element equations which are connected by the condition that common nodes undergo the same change of global state. This behaviour is described by mathematical equations as a combination of the behaviour of all the elements in the mesh. The solution is formed from the summation of the interaction between elements in the structure, where each set of elements is considered small enough to enable their behaviour, e.g. the stress-applied forces relationship, the strain-displacement relationship, and the stress-strain law, to be assumed linear [30]. The overall behaviour of the structure is determined from the collective contribution of each set of elements.

FEM is an effective way of analysing complicated structures such as skin, which contains multiple non-uniform layers. The FEA was carried out to study the interaction of the skin and ultrasonic signals as a guide to transducer selection and manufacture. In this thesis the PZFlex FE modelling package was used.

Wojcik et al [3], as mentioned before, used the PZFlex package with another, more specific package, for tissue modelling (PSFlex), to demonstrate ultrasonic wave propagation in the abdominal wall.

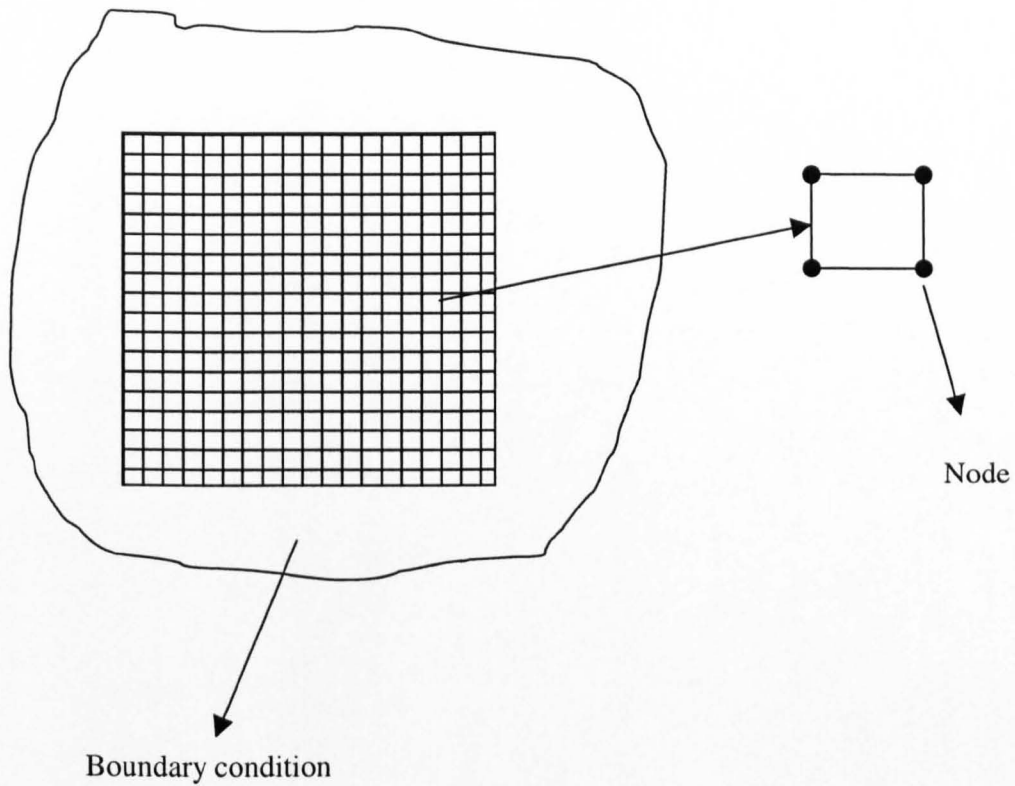


Fig (4.1): The principle of FE modelling. Any structure such as the large rectangle shown above can be divided into a finite number of sub-elements (small rectangles). Four nodes (illustrated to the right of the figure) define each element. The process of dividing the structure into elements is called the meshing of the structure. The conditions surrounding the mesh, the boundary conditions, are also defined in the model for each side of the model. The number of elements or nodes is defined in the model. The larger the number of elements the better the modelling result but that will be at the expense of the memory size and the processing time of the computer.

## **4.2 Materials Definition in PZFlex:**

There are several types of material behaviour that can be defined in the PZFlex environment. The main one that is used to define the piezoelectric materials is LEAN (Linear Elastic Anisotropic). There are other types that can be used to define materials such as ELAS (Linear Elastic Material), TISU (non-linear Tissue material). Other non-mechanical parameters may be used, such as thermal and electrical properties.

In FE modelling it is important to use correct material properties in order to get an accurate result. The main problem with the mechanical properties of the skin is that the mechanical parameters are not fixed but may change according to variables, such as age, sex, outer environment and body site. It also differs between individuals.

Both the skin and fat can be modelled as ELAS or TISU type.

Modelling biological tissues as linear elastic and isotropic is easier but less accurate than TISU, and in this case we need just three parameters to define the skin or fat, these are density, longitudinal and shear velocity. For the TISU type more parameters are needed, such as the non-linearity parameter, which characterise the non-linearity of the medium, and some pressure parameters, such as the estimate of maximum pressure and the pressure cut-off.

The material damping is another important issue in FEM because the higher the damping, the lower the received signal amplitude. For skin and fat, water damping was used as a starting point, but in reality the damping in both tissues is higher than water. The damping will affect the signal amplitude when it is propagating through the material.

The next stage will be to define the lithium niobate as a piezoelectric material to be used for the single layer transducer in the frequency range 100-200 MHz. The reasons for using this material are the reasonable electromechanical coupling, the robust single crystal structure, and the higher speed of sound that allows the fabrication of sensitive thickness mode resonator in the desired frequency range [31].

The mechanical and physical properties of the skin used for low frequency modelling in this chapter were taken from [32] by Duck and [7] by Serup et al. The main properties used were:

The density of the skin = 1100 kg/m<sup>3</sup>

The density of the fat = 925 kg/m<sup>3</sup>

The longitudinal acoustic velocity in the skin = 1480 m/s [7]

The longitudinal acoustic velocity in the fat = 1427 m/s

The shear acoustic velocity for both the skin and the fat were set to zero, the tissue being modelled as an acoustic fluid [3, 33].

In any piezoelectric transducer, different physical phenomena are interacting, i.e. the electrical and mechanical domains. The system of equations must be solved simultaneously to describe and analyse the behaviour of the transducer. The electrical and the mechanical domains are interrelated by the piezoelectric matrix, as explained by Bennett [34], through the following two equations:

$$T = [c^E] S - [e] E \quad \text{—————} \quad 4.1$$

$$D = [e]^t S + [\epsilon^S] E$$

Where: T is the 3D stress tensor

[c] is the stiffness tensor given in the material properties

S is the 3D strain tensor

D is the electrical charge density tensor

[ε] denotes the dielectric tensor defined by the material properties

E is the electrical field tensor

[e] the piezoelectric stress tensor defined in the material properties

The superscript <sup>E</sup> means under conditions of constant electric field

The superscript <sup>S</sup> means under conditions of constant strain;

The superscript <sup>t</sup> indicates the transpose of the matrix.

In PZFlex, three main 3D matrixes of parameter values are used for piezoelectric materials. These are: the stiffness constants (6\*6 matrix); the piezoelectric constants (3\*6 matrix); and the dielectric constants (3\*3 matrix).

The dielectric matrix defines the electrical permittivity in typical units of farad/meter and it is a 3x3 diagonal matrix for 3D models.

The piezoelectric matrix relates the electrical field to stress or voltage to displacement behaviour of the piezoelectric material and has the units of coulombs/meter<sup>2</sup> and this is a 3x6 matrix in 3D model.

The stiffness matrix is symmetric and has the unit of newtons/meter<sup>2</sup>, it is a 6x6 matrix in 3D.

### 4.3 Modelling Accuracy:

A piece of Lead zirconate titanate ceramic PZT-5H (30\*30\*5 mm–PZ29), was modelled and the impedance output was compared to the experimental impedance analyser output for the same piece to check the model accuracy. The matching was good as shown in Fig (4.2).

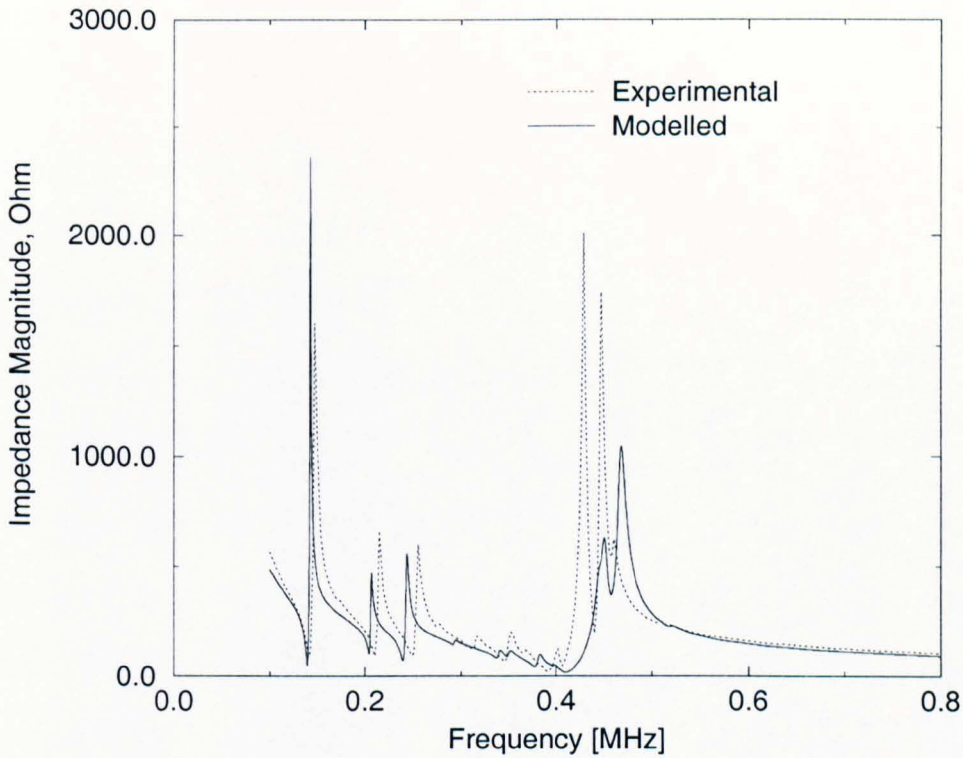


Fig (4.2): Comparing the impedance analyser output with the impedance predicted by the FEA using the PZFlex Package, for a piece of PZT5H material with the dimensions (30\*30\*5mm).

From the graph in Fig 4.2 it can be seen that the electrical resonance frequency for the main thickness resonance (at the lowest impedance) is about 411 kHz. The mechanical

resonance frequency when calculated for this specimen was 435 kHz. The slight difference in the graph shape between the modelled and the experimental data might be due the effect of the radial modes which interfere with the thickness mode. The radial modes exist because the thickness of the specimen (5mm) is not  $< 20$  times the lateral dimensions (30mm) [35], and the model is exaggerating these modes. Also the parameters defining the PZT5H material are not perfect, because standard values were used and these can vary by about 10%.

The same thing was done with a piece of lithium niobate (10\*10\*0.266 mm). The result was acceptable Fig (4.3), but not as good as with PZT-5H. The lithium niobate has directionally dependent properties according to the cut direction of the material. For high frequencies (low thickness) the 36° Y-cut lithium niobate is used. The mechanical properties of lithium niobate given by the company from which the material was bought (Boston- Optics) [36] were not accurate for that orientation cut. A better output was obtained, Fig (4.3), when three parameters, the  $C_{33}$  stiffness constant, the  $e_{33}$  piezoelectric constant and the  $E_{zz}$  dielectric constant were changed. These parameters were chosen because different orientation or cut of the material will affect them, and they are related to the thickness mode resonator, denoted by the subscript  $_{33}$  or  $_{zz}$  that is used here. Changing the orientation of the cut will affect both the velocity and the electromechanical coupling factor of the material and these in turn will affect  $C_{33}$ ,  $E_{zz}$  and  $E_{33}$ . These parameters were changed as follows:

$C_{33}$  The stiffness constant changed from  $2.424 * 10^{11}$  to  $1.85 * 10^{11}$  [N/m<sup>2</sup>]

$E_{zz}$  The dielectric constant changed from 28.7 to 64

$E_{33}$  The piezoelectric constant from 1.8 to 6.2 [C/m<sup>2</sup>]

Later a new code, Piezoelectric Resonance Analysis Program, PRAP CODE [37], became available and was used to measure these parameters more accurately. “This software package allows the determination of complex elastic, piezoelectric, and dielectric properties of piezoelectric resonators” [37]. The result is shown in Fig (4.4). The measured parameters are given in Appendix A. The measurements justify the changes given above for these parameters.

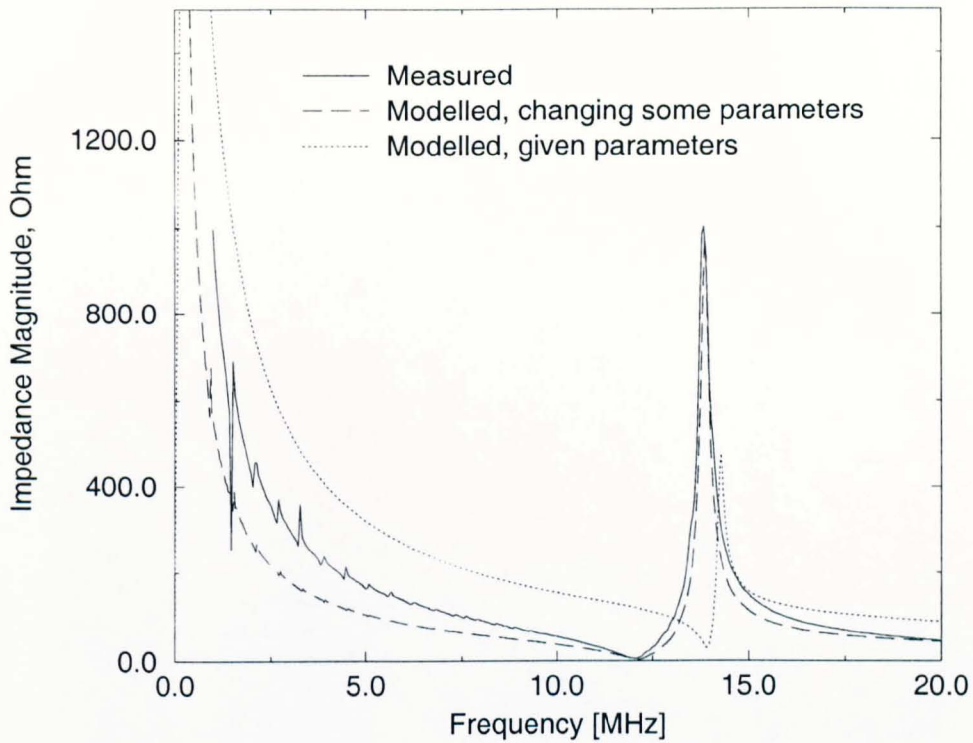


Fig (4.3): Comparing the impedance analyser output with the impedance predicted by FEA using the PZFlex Package, for a piece of lithium niobate material with the dimensions (10\*10\*0.266) mm. The mechanical and the electrical resonance occur at about 13.8 and 12.4 MHz respectively.

The dotted line is the modelled impedance using the data given by the company.

The continuous curve is the measured impedance with the impedance analyser.

The dashed curve is after changing the three parameters.

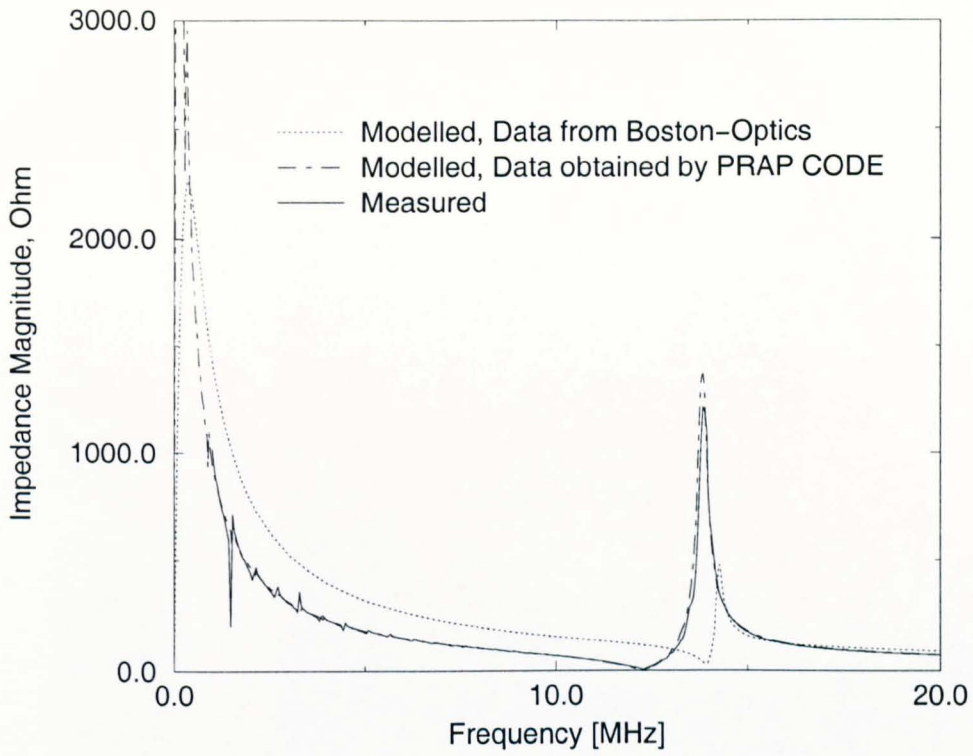


Fig (4.4): Comparing the modelled electrical impedance for the Lithium Niobate using two sets of data for the mechanical properties, the properties from Boston-Optics and the properties measured using the PRAP CODE.

The continuous line is the experimental impedance measured by the impedance analyser.

As a starting point, the effect of adding a matched backing to a PZT-5H transducer, Fig (4.5), was modelled using PZFlex .

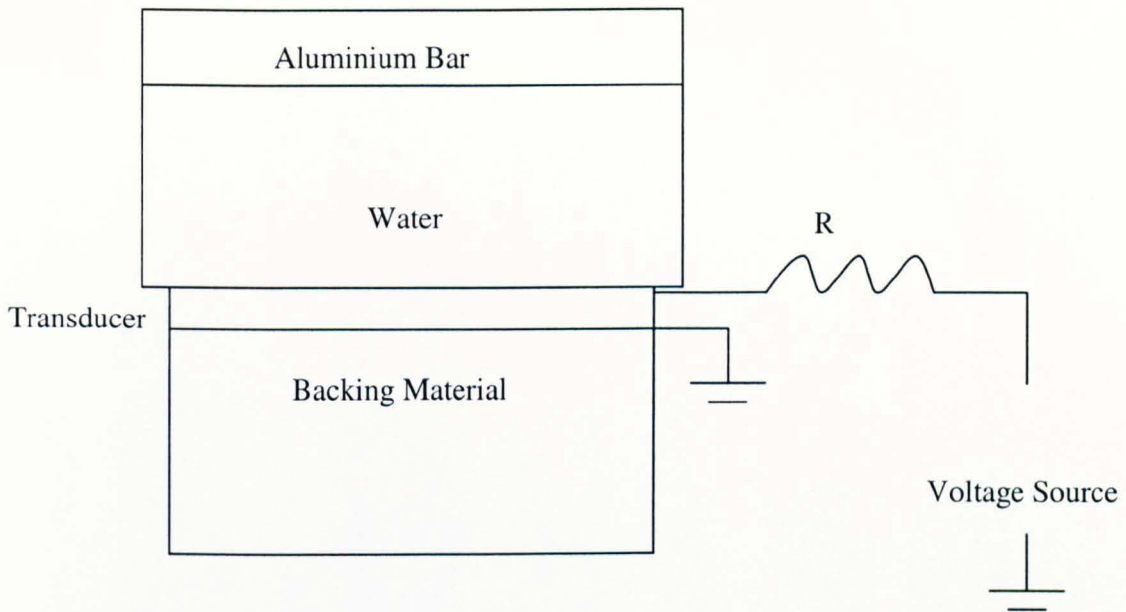


Fig (4.5): The initial model. A transducer of 5 MHz -PZT5H material with a backing material (tungsten epoxy) was modelled in water. The reflected signal from an aluminium bar located at 3mm from the transducer was detected. A resistor R was used to connect the transducer to the voltage source (A single cycle sine wave of 1 V amplitude and 5MHz frequency). The bond line which bonds the backing material to the transducer was assumed ideal, i.e. zero thickness.

In the FEM mesh, for the different materials (water, tungsten, PZT5H, and aluminium) the number of elements was determined from the smallest wavelength in the different materials. The wavelength is given by the formula:  $\lambda = c / f$ .

Where:  $c$  is the ultrasonic wave-velocity in the material and  $f$  is the frequency

The smallest wavelength occurs for the lowest velocity material; for this configuration the lowest velocity is in water ( $c = 1480$  m/s). The number of elements in the mesh was taken to be 15 elements per wavelength. So for 5 MHz,  $\lambda$  for water will be  $296 \mu\text{m}$  and the number of elements will be 15 per  $296 \mu\text{m}$  or about 51 elements per mm.

The transducer here is about 0.45 mm thick and 5mm wide.

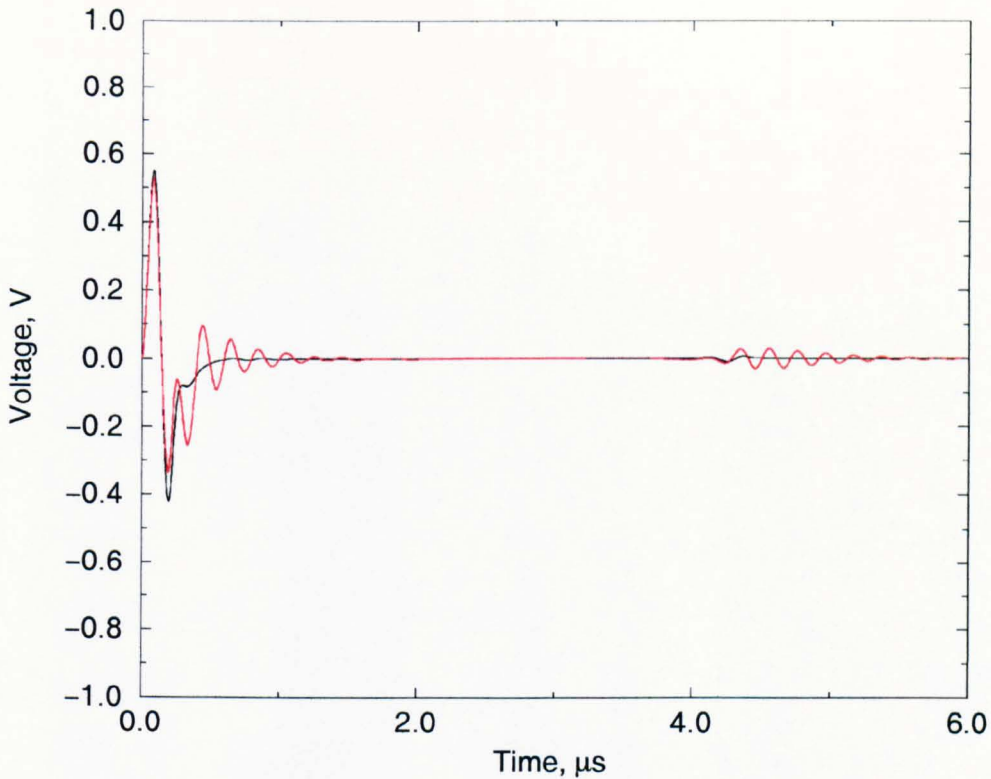


Fig (4.6): The effect, on the output signal, of adding the backing layer to the piezoelectric material. With the backing layer, the black graph, the output from the transducer showed less ringing effect and a shorter pulse width is achieved. At the same time the efficiency, related to the voltage peak to peak amplitude, is less in this case.

Fig 4.6 shows clearly that adding the backing will improve the pulse width and hence the axial resolution, but at the same time the efficiency will be reduced and a compromise is required.

## **4.4 The Effect of the Skin-Fat Interface on the Backscattered Signal:**

### **4.4.1 The Planar Boundary:**

A planar skin-fat boundary was modelled to be compared with the non-planar custom modelled interfaces given in subsequent sections. The back scattered ultrasonic signal from a planar interface between two materials with different acoustic impedance depends on the difference between the two impedances. The greater the difference the larger the reflected signal. When the two acoustic impedances are matched, no reflection will occur and the entire signal will be transmitted.

All dimensions were scaled to a transducer centre frequency of 5 MHz in order to minimise simulation run time. For simplicity, a thickness mode disc of piezoelectric ceramic material (PZT-5H), with a mechanical backing of identical acoustic impedance, was used as the active element. Electrically, the device was resistively loaded with 50 ohms during both transmission and reception. Skin and fat were modelled as homogeneous isotropic linear elastic materials. The average skin thickness was 1mm and fat thickness 4mm, with corresponding densities of  $1100 \text{ kg/m}^3$  and  $925 \text{ kg/m}^3$  respectively [32]. Longitudinal sound velocity in skin was 1480 m/s [7] and 1427 m/s for fat [32]. As a starting point for the study, the attenuation for both skin and fat were

assumed to be 0.002 dB/cm at 1 MHz increasing in proportion to the square of frequency.

A frequency of 5 MHz produces a time pulse duration of 0.2  $\mu$ s for a single pulse. The ultrasonic velocity was 1480 m/s, hence the minimum thickness of skin, that can be detected for this transit time as given in equation 3.8 is 148 $\mu$ m.

#### 4.4.2 The Effect of a Non-Planar Interface:

The back-scattered signal will be modified if the skin-fat interface is not planar. For the purpose of demonstration, two simplified boundaries between the skin and fat are presented: random-rectangular, with skin thickness ranging between 0.6-0.85mm and semi-elliptical, with a minimum skin depth of 0.56mm.

The effect of these two models of a non-planar interface were investigated and compared to a planar boundary.

The two idealised and rather extreme non-planar interfaces are shown in Figs 4.7a and 4.8a. The back-scattered signal from these interfaces is shown in Figs 4.7b and 4.8b.

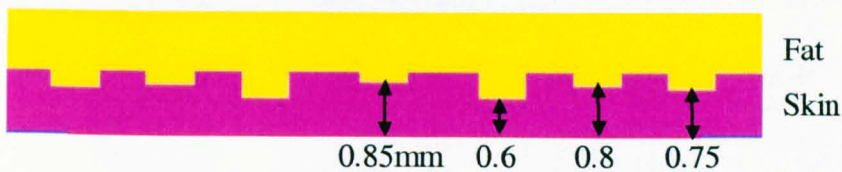


Fig (4.7a): Random rectangular skin-fat interface.

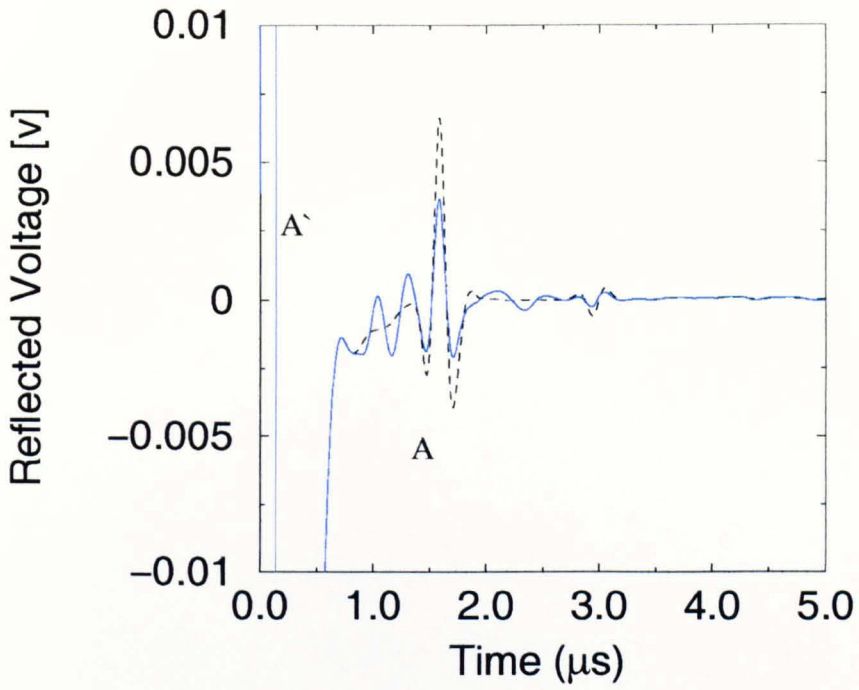


Fig (4.7b): The backscattered signal produced by the random rectangular interface between the skin and fat compared to the planar skin-fat interface (dashed line). A` is the initial wave generated by the transducer. A are the reflections from the skin-fat structure.



Fig (4.8a): Semi-elliptical skin-fat interface.

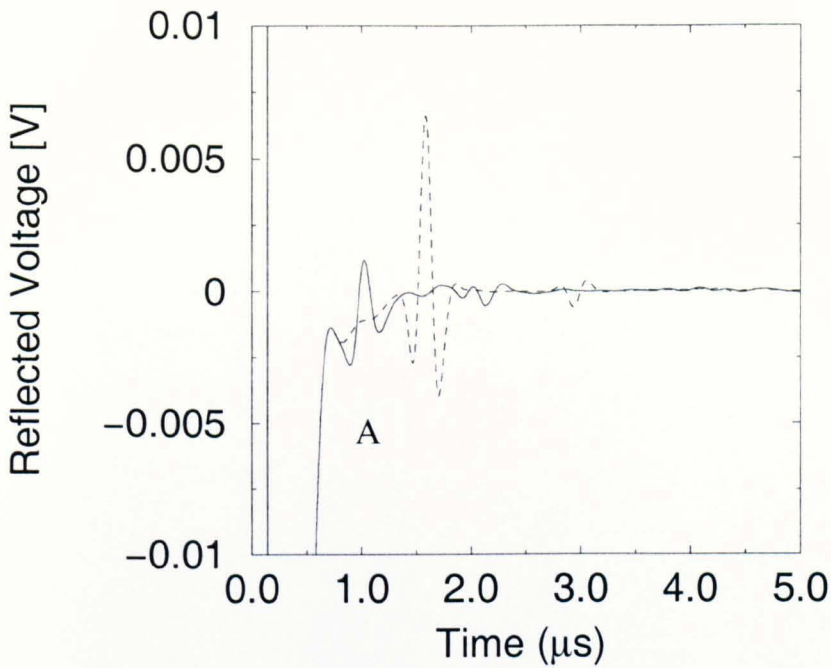


Fig (4.8b): The backscattered signal produced by the semi-elliptical interface between skin and fat compared to the planar skin-fat interface (dashed line).

As expected, the different skin-fat interfaces influence both the amplitude and phase of the reflected signals. In the case of the random-rectangular model, shown in Figs 4.7a and b, there is a reflection at the 1mm skin thickness (A), with earlier reflections produced by the layer indentations. These earlier reflections correspond to skin thickness of 0.6 and 0.75 mm, while the reflections from 0.8 and 0.85 mm thickness overlapped with the 0.75mm thickness reflection. This is because, as mentioned before, the minimum thickness in the axial direction that can be detected by the 5 MHz transducer is  $148\mu\text{m}$ . The  $50\mu\text{m}$  difference that exists between the 0.75, 0.8 and 0.85mm thickness was not detected. The lateral resolution required to detect such random structure will be

of the order of the smallest width of these indentations in the lateral direction. For the random structure considered this will be of the order of about 0.87mm.

For the elliptical skin-fat interface shown in Figs 4.8a and b, relatively little of the reflecting surface is at 1mm depth and the predominant reflection is produced by the part of the ellipse defining the minimum skin thickness. In both cases, the ultrasonic beam profile was designed to encompass most of the reflecting surface and these results serve to illustrate the requirement for strong axial focusing of the ultrasonic field.

The non planar structure causes changes to the backscattered signal creating scattering of energy and the resulted amplitude of the reflected signal reduced and more reverberations appeared. The wave when hitting the non planar interface was scattered unevenly in different directions and only a small part propagated back to the transducer. These structures need careful consideration to be resolved properly, such as performing spatial averaging with a highly focused transducer. The interpretation of the backscattered signal and to relate it to the interface structure becomes more difficult and highly focused transducer is required.

The material properties used in the calculations and measurement are of great importance. If the velocity of the material, for example, is not accurate it will produce a different value from the real thickness of the structure. For the skin, as mentioned before, the properties of the different layers are not available in accurate and repeatable measurements and this requires an extended research and standardised methods.

### 4.4.3 The Effect of a Planar Diffusive Boundary:

The effect of diffusive or graded boundary between skin and fat as an example was also modelled and compared to a planar abrupt boundary. To model a diffusive boundary, up to 14 intermediate layers, with a total thickness of 0.7 mm were interposed between the skin and fat. The acoustic impedance for these layers increased gradually from that of the fat to that of the skin, using a Gaussian profile. The velocity of these layers was constant (1450 m/s), but the density increased from  $925 \text{ kg/m}^3$  (fat) to  $1100 \text{ kg/m}^3$  (skin). The number of these layers was increased gradually until no reflection was detected from these layers.

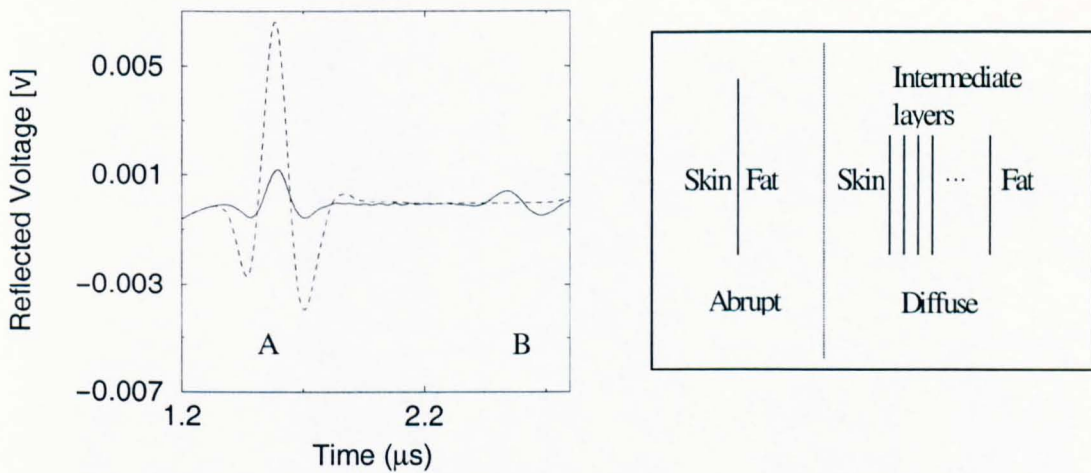


Fig (4.9): The signal reflected from the diffusive boundary between skin and fat for 14 layers (solid line), compared to the reflection from abrupt boundary (dashed line). A is the reflection from the skin-first intermediate layer and B is the reflection from the last intermediate layer-fat. The structure of the abrupt and diffuse boundary is shown to the right.

As expected, a diffusive boundary reduced the amplitudes of the reflected signals. In Fig 4.9, which corresponds to a 14 layer planar interface, the skin - fat interface is just detectable. The relative amplitudes of the 2 reflections in Figure (4.9) depend on the properties of the intermediate layers; increasing their sound velocity to a value nearer that of skin reduces the amplitude of A and increases that of B. Reducing the sound velocity has the opposite effect.

The amplitude of A reduced with the presence of the diffuse boundary because the acoustic impedance of the skin is more matched to the first intermediate layer than to the fat. The reflections from the intermediate layers were not detected because the acoustic impedances of these layers are very closely matched.

Although the modelling and analysis relate to the interface between the dermis and fat, similar effects will occur at the junction between the epidermis and dermis. The interface has a complicated geometry and both tissues show a gradation of structure, and hence mechanical properties, adjacent to their junction. This type of structure makes it very difficult for the ultrasonic system to detect such interfaces because of the closely matched acoustic impedance of these interfaces. The transducer is required to have high efficiency and sensitivity with high axial resolution and the processing of data is very important to decide which reflection comes from which layer.

#### **4.5 Front Face Configuration:**

The use of soft rubber delay line at the front face of the transducer will serve many purposes. It will provide an alternative coupling medium to the skin surface rather than

water, provide protection to the transducer front face and separate the main reverberations of the transducer and the return echoes from the skin. The shape and the properties of the rubber material are very important. Using water as a coupling medium with the SC may cause hydration and an artifact in the output backscattered signal as was discussed in Chapter 2. The use of silicone rubber of different shapes at the front face of the transducer, shown in Figs 4.10a-12a was modelled. The effect of these shapes of a rubber shoe mounted at the top of the transducer on the output backscattered signal was studied.

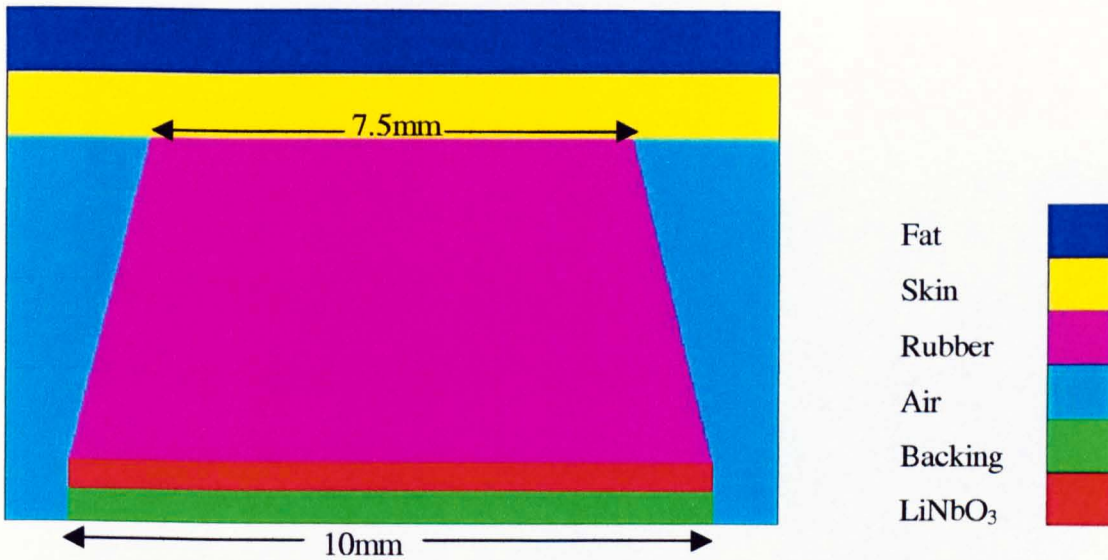


Fig (4.10a): Frustum dry coupling rubber. The graph shows, from the bottom to the top, the backing, the transducer, the front face rubber in direct contact with the skin surface and the skin-fat structure.

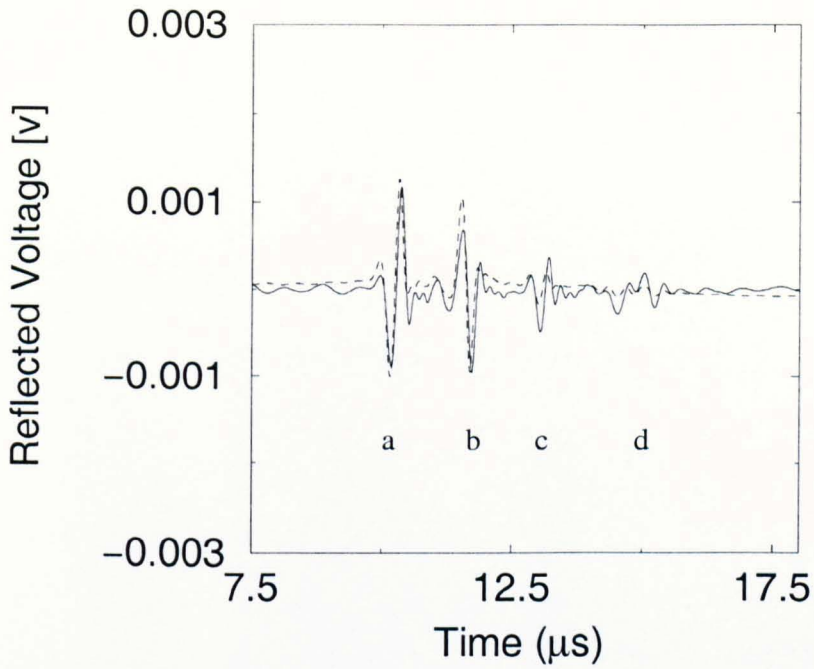


Fig (4.10b): The reflected signal for a frustum (solid line), compared to the signal using cylindrical rubber contact (dashed line). a is the reflection from the rubber skin interface; b is the reflection from the skin-fat interface; c is the signal introduced by diffracted waves from the transducer boundary; (d) is a reflection from rubber-air boundary. All the boundaries are modeled as planar interfaces.



Fig (4.11a): Complete hemisphere dry coupling rubber.

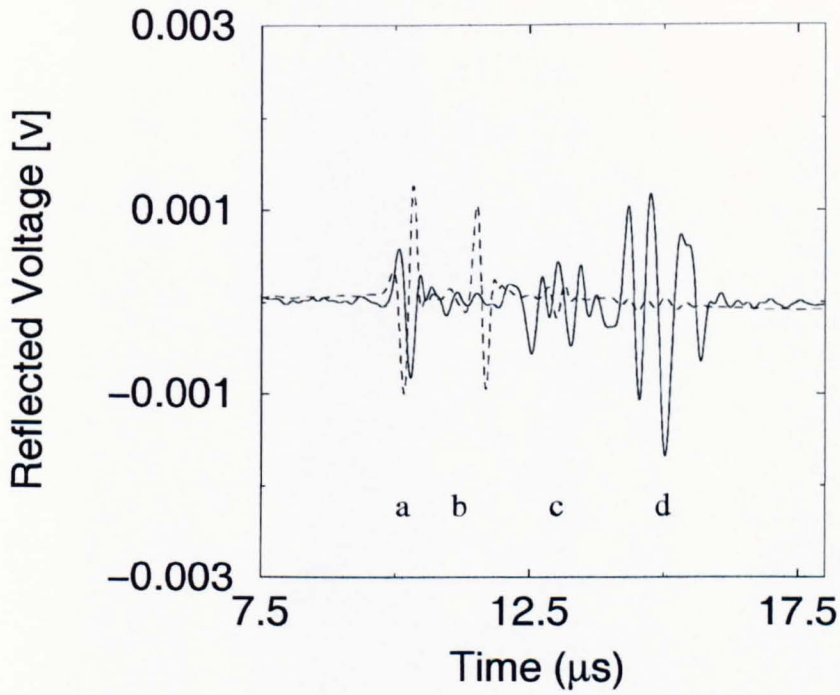


Fig (4.11b): The reflected signal for a complete hemisphere (solid line). Key as in Fig 4.10b.

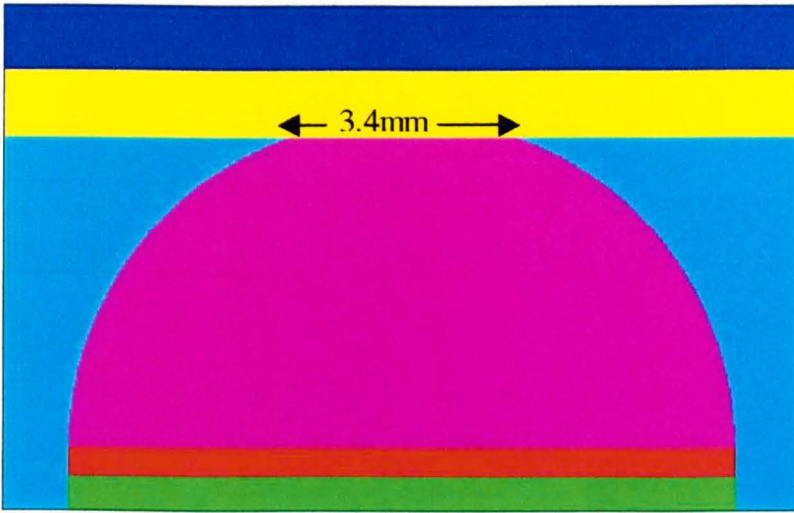


Fig (4.12a): Flattened hemisphere dry coupling rubber.

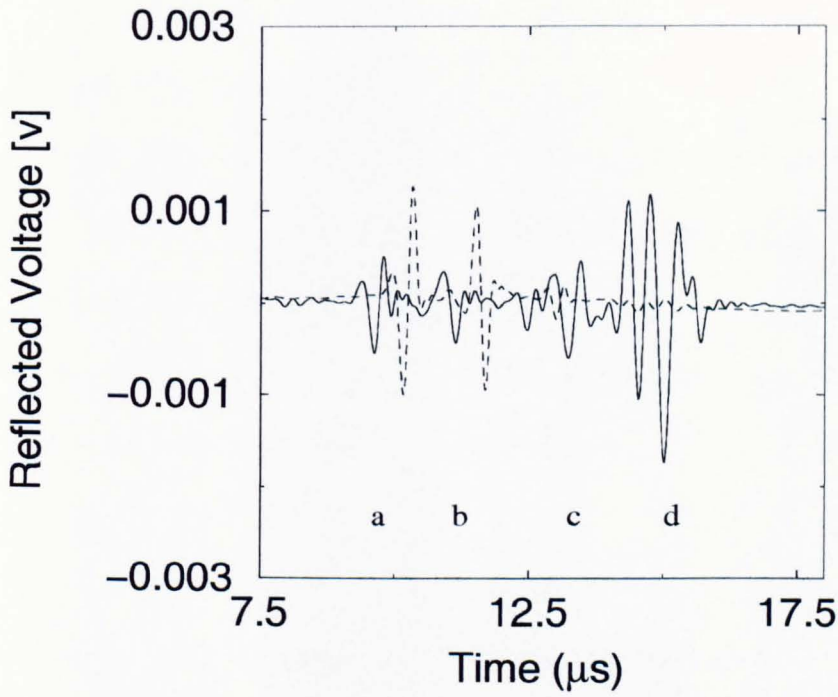


Fig (4.12b): The reflected signal for a flattened hemisphere (solid line). Key as in Fig 4.10b.

A low loss rubber with an acoustic impedance closely matched to that of the skin surface was positioned on the transducer front face. Three different geometries of silicone rubber, approximately 5mm in thickness, were considered. A frustum of a right circular cone (in 2-D, a trapezium with a maximum width of 10 mm and SC contact width of 7.5 mm) shown in Fig 4.10a, a hemisphere (a semi-circle in 2-D); Fig 4.11a and a hemisphere with its apex removed to produce a larger contact area with the SC (a 3.4 mm contact width in 2-D); Fig 4.12a. The backscattered signal from these interfaces were compared to that for ideal coupling via a cylindrical rubber layer, with a contact area equivalent to that of the transducer.

The material properties of RTV 664 rubber (GE Silicones, UK Ltd.) were measured [38], and are provided in Appendix A.

The shape of the rubber dry contact will influence the signal reflected from the skin in 2 ways. The surface of the skin is not planar and it has been suggested that a small area of surface of contact with the skin is needed to eliminate the effect of air between the rubber and the skin, which will reduce the acoustic energy coupling with the skin [39]. Reflections from the internal surface of the rubber will also reduce the return energy from the skin structure.

Figs 4.10b-12b show the output signals for 3 geometries. As expected, the reflected signal using the frustum (Fig 4.10b) is very similar to that obtained using a cylinder, which suggests that this could be an effective geometry, although further modelling is needed to incorporate a non-planar skin surface and to determine the optimal cone angle. The hemisphere geometries are much less satisfactory, producing reflected signals in

which it is difficult to identify either the skin surface or the skin-fat interface. There are also large additional reflections from the rubber-skin interface.

The interface geometry is critical for dry coupling. The smallest possible contact area is desirable because it will reduce the effect of air gaps between the transducer and the skin which in turn reduces the signal transmitted into the skin, but this in turn can degrade lateral resolution and also introduces problems with signal to noise ratio. A compromise is required, as is the case with operating frequency. To resolve all of the skin structure, a highly damped transducer, with a centre frequency around 100 MHz is required. The use of such a frequency is problematic for the dry contact mode of operation described in this chapter.

#### **4.6 Conclusion:**

The simplified configurations of the non-planar interface between skin and fat simulated in this chapter showed an effect on the output backscattered signal reducing the amplitude and increasing the reverberations. Such structures require a focused transducer to resolve the geometry. The diffuse boundary, as shown, will even for planar interfaces, have a significant impact on the backscattered signal reducing the amplitude because of the close matching of the acoustic impedance of the adjacent layers. A transducer with good sensitivity is required to resolve the diffuse boundary.

Therefore, to resolve such a multi-layer structure with non-planar and diffuse interfaces, a highly sensitive, strongly focused transducer with spatial averaging of the data and possibly the application of signal inversion methods such as impedeography is required.

The front face design also must be considered carefully. In the situation under consideration the cylindrical or trapezoidal design gives the best result. The material used for the front face must have a very low loss with an acoustic impedance close to water.

In the light of the cases considered and before a proper specifications for the transducer can be listed, a more realistic simulation of skin structure is required. This was performed in the next Chapter.

## **CHAPTER 5**

### **High Frequency Modeling**

## **5.1 Modeling of the Real Interfaces of the Human Skin:**

The real human skin interfaces separating the different layers, as explained before, are not planar but rather irregular, particularly the epidermal-dermal interface that shows a complex topology marked by peg and socket or ridge/groove interdigitations. This is expected to affect the ultrasonic backscattered wave.

In this study a skin micrograph was used to produce an FE model to investigate the effects of these interfaces. The micrograph was pre-processed before the FEM analysis in order to remove the inhomogeneities of the skin structure. The skin micrograph used here is for ischial skin and was taken from [40].

Figure (5.1) shows the different stages for this procedure.

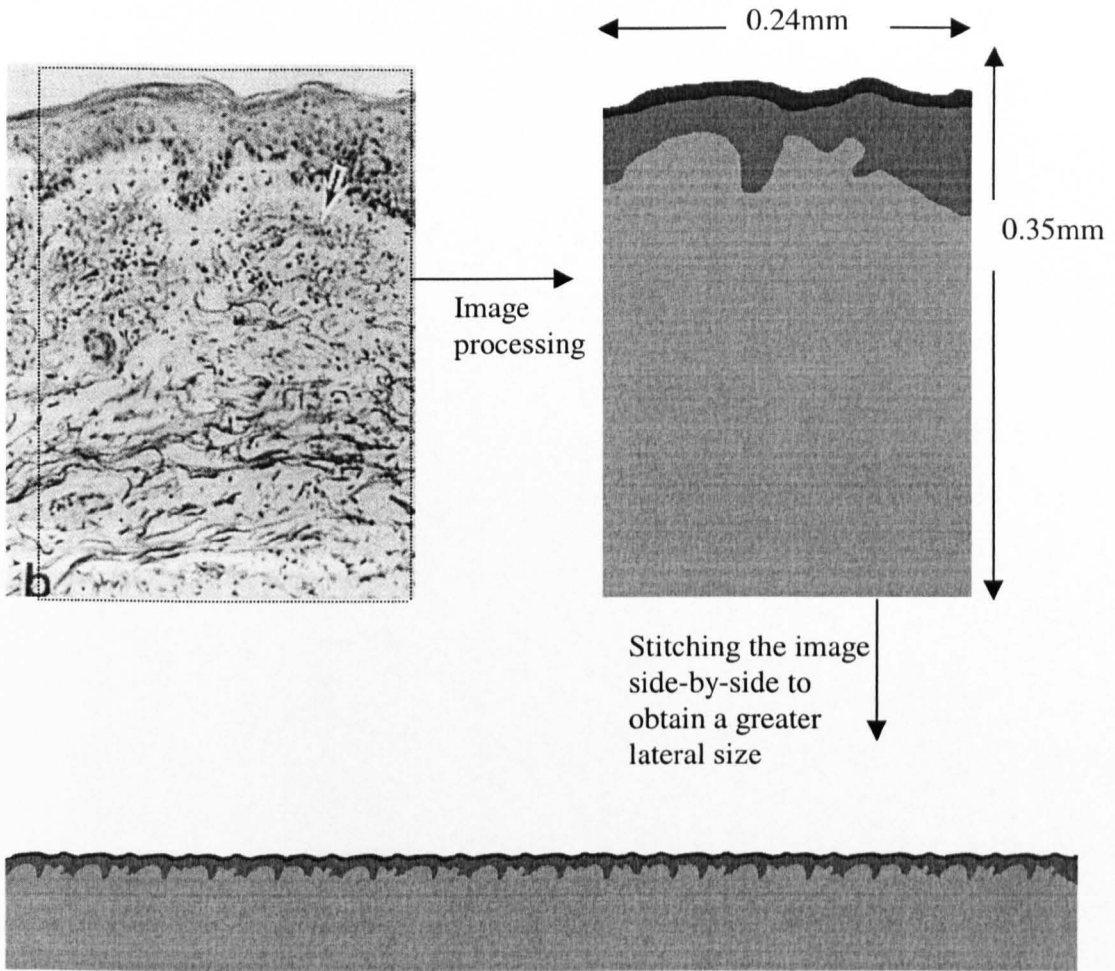


Fig (5.1): The different stages for processing the real micrograph of the skin.

The image processing technique for the skin micrograph was performed using a commercially available package (Adobe Photoshop or Arcsoft Camera Suite).

The FEM mesh was built by superimposing the processed image of the skin micrograph. This was done by writing a table into a file containing the (x, y) coordinates and material properties of each pixel in the image. The file was a text format file created from the processed image using the MATLAB software package (Version 6)

[41]. The MATLAB programme used to create such file from the image is given in Appendix B.

PZFlex can read this table using the TABL command and form the mesh containing the different materials as it is in the real skin structure.

The average thickness of the different layers in the model of the skin and their properties are given in table (5.1).

Table (5.1): The properties of the skin layers.

The skin layer	The density kg/m <sup>3</sup>	The longitudinal velocity m/s	The average thickness, $\mu\text{m}$	The transit time ns	The acoustic impedance MRayl	The ultrasonic wavelength at 80 MHz, $\mu\text{m}$
Stratum Corneum	1500	1550	10	12.9	2.3	19.4
Epidermis	1150	1540	45	58.44	1.77	19.25
Dermis	1116	1580	230	291	1.76	19.75

The attenuation was assumed to be the same as that of the water (0.002 dB/cm) at 1 MHz, increasing linearly with frequency.

## 5.2 Comparison of Planar and Realistic Interfaces:

A normal LiNbO<sub>3</sub> transducer working in thickness mode was modelled at about 80 MHz which is the highest frequency that FE models can use with the current computer facilities. The pulse echo mode performance of this transducer was simulated using the

KLM model (the PiezoCAD software modeling package) [2], with infinite matched backing and water load. The result gave a pulse width of about 26ns, and bandwidth of about 69 MHz at the -6dB. The consequences of this pulse width that the SC of 10 $\mu$ m thickness modeled in the considered skin structure will not be resolved, because the transit time for a 10  $\mu$ m SC is 12.9ns. The required frequency to resolve the SC is even higher than this in some cases where the thickness of the SC is about 7 $\mu$ m in some body sites and the required frequency is about 110 MHz as explained before.

The transducer was modelled with matched backing to produce the shortest time pulse width, and hence the highest resolution. A water column, with an average thickness of approximately 120  $\mu$ m, was used as a coupling medium between the transducer and the skin. This water thickness corresponds to a transit time of about 0.16  $\mu$ s.

Two types of interface between the different layers of the skin structure were investigated; the real interfaces obtained from the micrograph and planar interfaces with the different layers having the average thickness given in table (5.1).

At the nominated frequency of 80 MHz the required speed and memory are very high, and a normal PC is unsuitable. An SGI (Silicon Graphic Incorporated) super computer having 12 processors, each running at 400 MHz, and 6 GB physical memory was used to run the PZFlex program. This program took about 2 hours.

The reflected signals from both these interfaces are shown in Fig (5.2).

The ultrasonic pressure wave propagation in both, the planar skin layer interfaces and the real interfaces is shown in Fig (5.3).

### **5.3 Diffuse Interfaces:**

Although the interface between the epidermis and dermis is structurally abrupt, the collagen fibres in the superficial dermis are such that the transition is more gradual and may represent a diffuse boundary.

The effect of a diffuse planar interface was modelled by interposing one and then three layers with an overall thickness of 15  $\mu\text{m}$  at the interface. The acoustic impedance of these interposed layers decreased linearly from the acoustic impedance of the epidermis to that of the dermis.

The reflected signal from these diffuse interfaces compared to an abrupt interface is shown in Fig (5.4).

## 5.4 Results and Discussion:

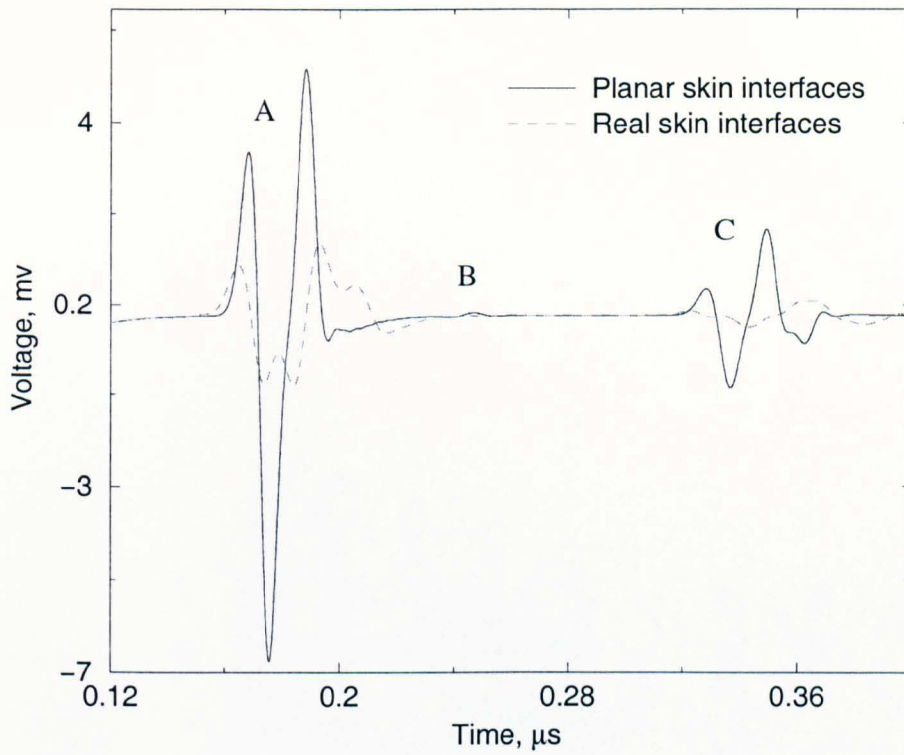


Fig (5.2): Simulated reflection signals from real and planar skin interfaces. A is the reflection from the front face of the SC overlapped with the back face SC reflection. B is the epidermal-dermal interface reflection. C is a multi-path of A.

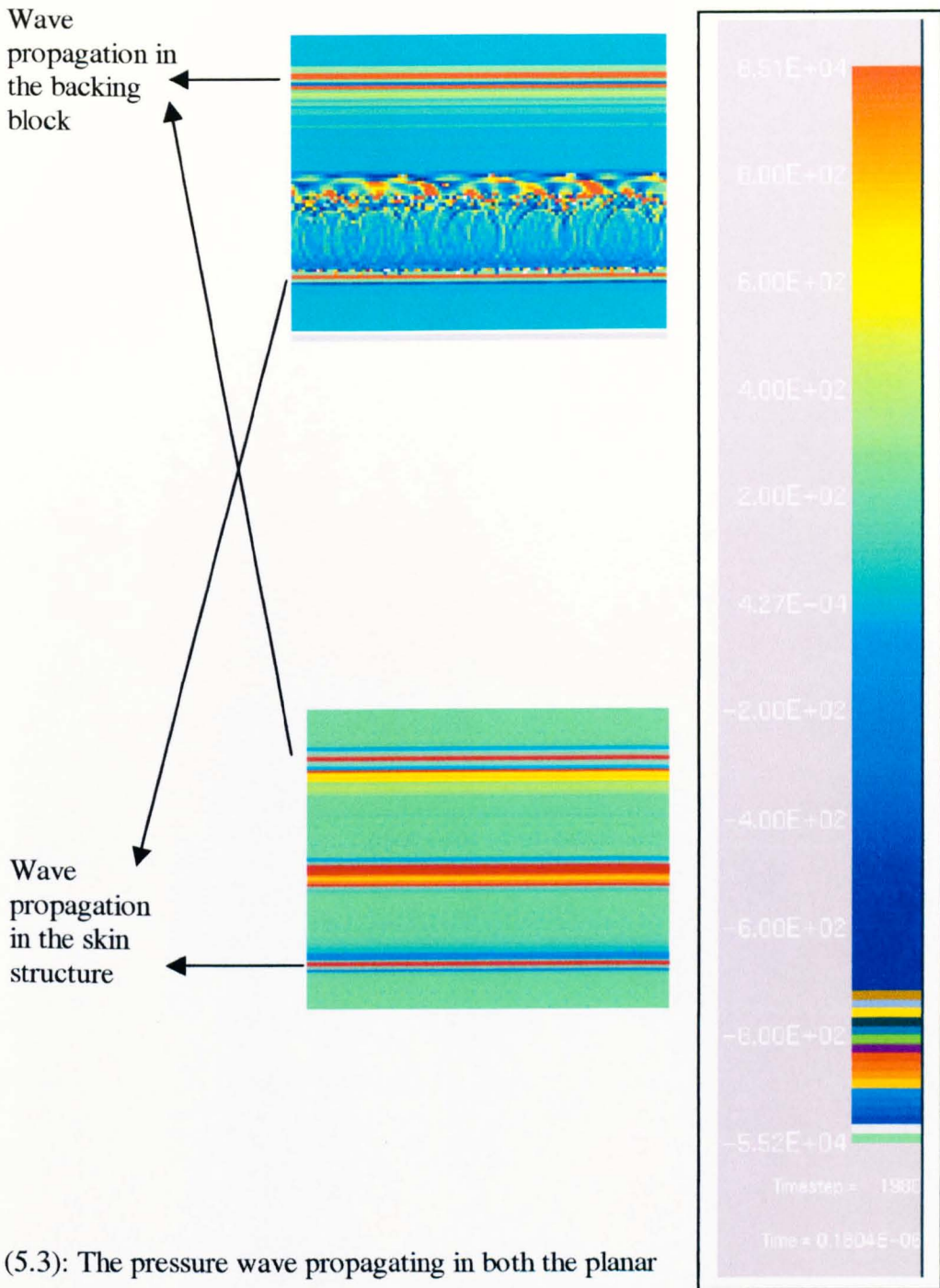


Fig (5.3): The pressure wave propagating in both the planar (lower) and the real (upper) structure of the skin, with the pressure colour code on the right. Both images demonstrate the pressure wave propagation in the transducer-skin structure containing, from the top to the bottom, the backing, the transducer and the skin structure.

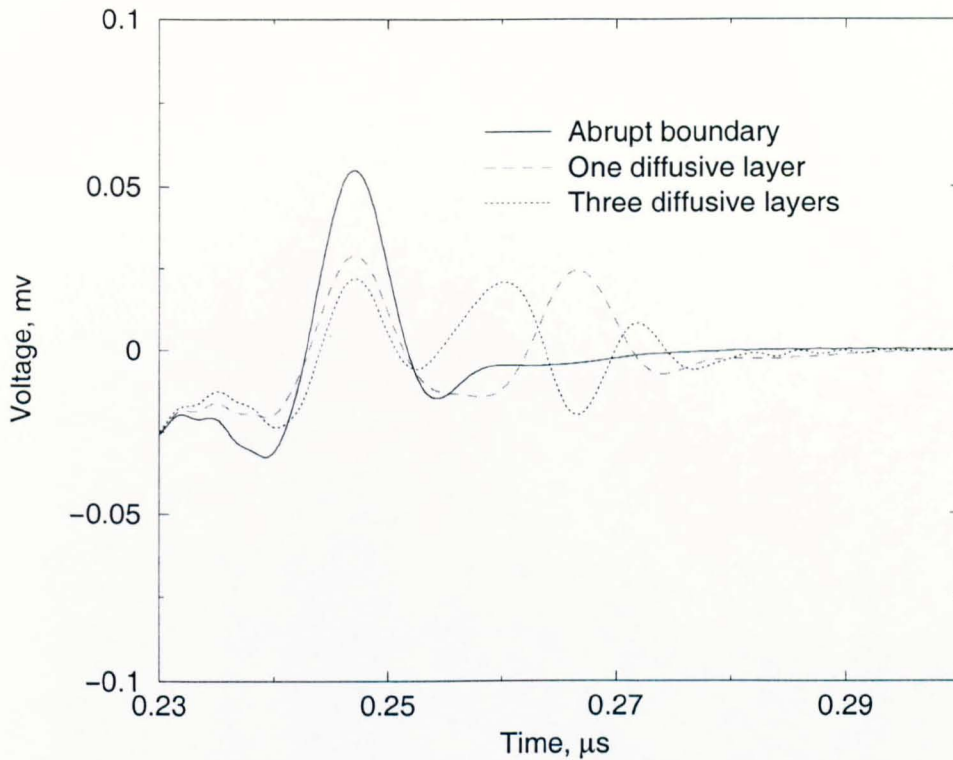


Fig (5.4): The reflection from the epidermal-dermal interface with an abrupt planar boundary, one layer diffusive boundary and three layer diffusive boundaries. The overall thickness of the diffusive boundary is  $15 \mu\text{m}$ .

The output reflected signal from the skin structure in Fig(5.2) shows that an 80 MHz transducer with full damping (matched backing) was not enough to resolve the  $10 \mu\text{m}$  thickness of the SC, as expected. The signal also shows the effect of the real interfaces of the skin on the amplitude of the signal which was reduced compared to the planar interfaces. This means that such interfaces will require a strongly focused transducer to

be resolved more clearly. Also, more reverberations in the reflected signal appear in the case of real skin structure denoting the complex topology of the real skin structure mentioned before.

Therefore, to resolve this structure, both axial and lateral resolution need to be high enough. The lateral resolution, as mentioned in Chapter (3), can be improved by using a focused transducer. The real image of the skin in Fig(5.1) shows that we might need a lateral resolution as small as about  $25\mu\text{m}$  to resolve the different ridge/groove interdigitations of the epidermal-dermal interface and produce a signal that will characterize the complicated pattern. This means that the lateral width of the focal region should be about  $25\mu\text{m}$ . With the transducer having 5mm diameter and considering an average ultrasonic wave velocity of 1550 m/s in the skin structure, from equation 3.7 it can be found that the required radius of curvature is about 6.3mm. For a 100 MHz transducer the radius of curvature will be about 8mm. It is worth mentioning here, that strong focusing will reduce the axial length of the focal area, reducing the depth that can be explored.

It was planned during the progress of this project to model a focused transducer and to compare the output backscattered signal from the skin structure with the output from the unfocused transducer used here. For a focused transducer, a long propagation path exists and unfortunately PZFlex is designed with good accuracy over only a short range of wave propagation (about 10 times the wavelength). Beyond a few 10s of wavelengths this approach becomes burdensome and eventually the meshing required for accuracy, which increases with increasing propagation distance, passes the capability of the hardware.

The axial resolution, as mentioned in Chapter (3), needs to be high enough to resolve the lower thickness of the SC which might be of the order of 7  $\mu\text{m}$  in some body sites, and a transducer of at least about 111 MHz is required in this case. To obtain this frequency using  $\text{LiNbO}_3$  the transducer needs to have a very low thickness of about 33 $\mu\text{m}$ .

One important thing to be noted also from Fig (5.4) that is the very small reflection of the epidermal-dermal interface, because of the approximate matching of the two acoustic impedances as given in table (5.1). When this interface was modelled as a diffuse interface the reflection gets even smaller, increasing the demand for a much more sensitive transducer. This happened as a result of the closely matched acoustic impedance of the adjacent layers. Three layers of diffuse boundary showed more complicated output backscattered signal, compared to one layer, incorporating lower amplitude and more reverberations in the signal.

Fig (5.3) shows clearly the uneven distribution of the acoustic pressure wave when propagating in a real skin structure compared to a planar structure interfaces, creating disturbance in the propagated wave, and this in turn will cause changes in the output-backscattered signal mentioned before in Fig (5.2). The energy was backscattered in different directions and only a small portion of the signal was reflected back to the transducer. More reverberation also appeared in relation to a different depth of the ridge/groove interdigitations. Therefore, as stated previously, a strongly focused transducer is required with spatial averaging of the data.

From this chapter and the previous chapters, the transducer characteristics required for skin measurement can be summarised as follows:

- For the piezoelectric material to work at the required frequency (about 100MHz) the material needs to be lapped down to the required very low thickness. This is difficult for ceramic materials and a single crystal alternative, which is more amenable to lapping, is required. For the LiNbO<sub>3</sub>, for example, chosen in this thesis the thickness will be about 33µm.
- A very short pulse length of about 9ns needs to be achieved to get sufficient axial resolution. This requires a transducer with high frequency of at least 111 MHz and wide bandwidth of about 100MHz.
- A high lateral resolution is required. For a 100 MHz transducer of 5mm diameter, a radius of curvature of about 8mm is required to get lateral resolution of about 25µm.
- The front face configuration design of the transducer needs to be considered carefully. In chapter 4 it was shown that the cylindrical and trapezoidal shape are the best. The rubber needs to be soft to adjust its shape to the surface contour of the skin to allow maximum transmission and reception of ultrasound. The required rubber should have very low attenuation, be relatively thin and to be attached to the transducer by a thin adhesive layer.

The results also show that skin thickness measurement using the current transducer technology is problematic for many reasons that can be summarised as follows:

- The high frequency needed to achieve the very short pulse width required reaching a value of about 9ns is problematic in practice. The piezoelectric material, as stated previously, needs to have a very low thickness of approximately 33 $\mu$ m. During the lapping process to achieve this thickness there is a high potential of rupturing the material. In practice, this is extremely difficult.
- A short pulse width requires a highly damped transducer and this is difficult in practice because the lithium niobate recommended for high frequency applications needs a matched backing material having an acoustic impedance of 34 MRayl which is not achievable experimentally. The bonding line required to bond the backing material to the transducer will increase the reverberations of the output signal from the transducer thus increasing the pulse width and reducing the resolution. Preparing such high acoustic impedance backing block *in situ* without a bonding line is difficult, because the tungsten loaded epoxy material commonly used as a backing block requires a high volume ratio of tungsten and it will be very difficult to mix the material evenly into a paste.
- A strongly focused transducer is required to increase the lateral resolution to resolve the skin structure in the lateral direction. Strong focusing will cause spatial integration and the depth of the focal length (Fig 3.1b) will be small, thus reducing the depth that can be resolved.
- The required front face material needs to be soft with a very low loss at the nominated high frequency of about 100 MHz. The attenuation of most rubbers

increases linearly with frequency, and many commercial rubbers have a high attenuation at this frequency.

- Another very important issue is the ultrasonic properties of the different skin layers. Provided that the appropriate transducer technology can be developed, thickness measurement is possible for all the layers. However, it appears to be too difficult to extract accurate layer properties.
- Due to the nature of the inhomogeneous skin structure, including the layer boundaries which might be diffusive, impedimetry (layer peeling) will be extremely difficult.

The requirements for a highly sensitive transducer possessing a very short pulse width and wide bandwidth needed for skin thickness measurement, are difficult to fulfil and existing technology cannot meet the required specifications. A possible alternative, appearing recently in the literature, is the inversion layer transducers (ILT), incorporating two or more polarisation zones across the device thickness. These devices are expected to have a wider bandwidth and better performance for high frequency applications, than the conventional thickness mode transducers.

ILT may offer a potential way forward in skin measurements, briefly, because of the following benefits over the existing conventional devices:

- Higher frequencies are obtainable at thicker sections, thus eliminating the need to lap the transducer to the very low thickness required in the conventional devices.

- Wider frequency bandwidth may be achieved without the need of the high acoustic impedance matched backing.
- The potential of having increased sensitivity.

ILT devices are discussed in more detail in the next Chapter.

## **5.5 Future Work:**

It is desirable at this stage of modelling, as mentioned, to be able to model the behaviour of focused transducer on a realistic skin structure. This might be possible using another package associated with PZFlex, i.e. SpectralFlex or PSFlex [3, 33] designed for long distance wave propagation through acoustic media with lower contrasts than is seen in PZFlex. It uses different solvers from PZFlex, and at 2 elements per wavelength meshing (the Nyquist limit) is perfectly accurate to infinite propagation distance. But it cannot model solids or piezoelectrics, so three programs are required to obtain the reflection from the real skin structure. The first, in PZFlex, will run with the focused transducer in water for short propagation distance, then the pressure must be imported into another PSFlex program to run for the required propagation distance, and the third, in PZFlex, will import the reflections from the skin structure and apply it as a pressure to be detected by the transducer. This procedure has not been used before and will take some time and more extended research to be familiar with, so it was left for future investigation.

Another issue is the front face material at the high frequency. This involves choosing the suitable rubber material that does not have a very high attenuation at such frequency.

This needs to be investigated more deeply than it was discussed at the low frequency in Chapter 4.

The effect of the real structure of the skin on the backscattered signal discussed here takes into account only the realistic interfaces separating skin layers with uniform properties. Future studies might include a more realistic skin structure in order to investigate the effect of the real inhomogeneous structure of the skin.

## **CHAPTER 6**

### **Heat Treated LiNbO<sub>3</sub> Transducer Design**

## 6.1 Original LiNbO<sub>3</sub>:

Manufacturing of a LiNbO<sub>3</sub> transducer to produce the high frequencies required to resolve the thinnest layer of the skin is a difficult problem. From the manufacturing point of view it was difficult in CUE to reach a frequency higher than 40MHz, because the thickness required of the LiNbO<sub>3</sub> plate is only about 30μm, the plate was often ruptured during the lapping process. Although some authors reported the ability to lap the LiNbO<sub>3</sub> to a very low thickness, suitable for a transducer up to 200 MHz [31], practical devices were not demonstrated.

The pulse width is the main factor that determines the axial resolution of the system (chapter 3). Using a high damping backing block with an acoustic impedance near to that of the lithium niobate decreases the pulse width and hence increases the resolution, but at the same time this will decrease the sensitivity of the system. Using a matching layer(s) enhances the sensitivity, but at the same time can increase the pulse width, so there must be a compromise.

It may be possible to build a relatively thick high frequency transducer using ILT devices. Inversion layer transducers can be made by bonding together two layers of piezoelectric material with reversed polarity, but the bond line thickness at high frequencies, where the thickness of the piezoelectric material is very low, will affect the transducer behavior. An alternative may be the production of a monolithic ILT by reversing the polarity of a surface layer of the piezoelectric material by heat treatment.

Hence, it is possible to build a high frequency transducer avoiding the lapping process which might fracture the piezoelectric material. And as explained before a higher

frequency provides a shorter pulse width and hence higher axial resolution that is required for ultrasonic skin thickness measurement. Such transducers are also expected to have a wider bandwidth which provides a better transducer performance for high frequency applications.

## **6.2 Heat Treated LiNbO<sub>3</sub>:**

Heat treatment of a LiNbO<sub>3</sub> plate, under specific conditions, induces an inverted piezoelectric polarity domain (anti-polarity domain). The new inverted domain is the same as the original except that the piezoelectric constants in the new domain are opposite in sign to those of the un-inverted domain. In this case, even-order thickness-extensional modes as well as odd-order modes can be excited piezoelectrically. Thus, the inversion layer enables the transducer to operate at higher frequencies without thinning the piezoelectric plate. This can be used for building a high frequency transducer with a lower thickness of the piezoelectric material, and the ultrasonic transducer using such a plate is expected to operate over a wide frequency range [42].

The heat treatment and the thickness of the inversion layer depend on many parameters, and can be performed in two ways, either by diffusing a Titanium (Ti) film deposited on the surface of the piezoelectric plate at temperature of about 1070°C (less than, but near to the Curie temperature of the LiNbO<sub>3</sub>, 1160°C), or, alternatively, by placing the LiNbO<sub>3</sub> plate under heat treatment in air at a higher temperatures of approximately 1110°C [43]. The thickness of the inversion layer in the latter case depends on the

temperature at which the material was treated and the treatment time. Heat treatment without Ti diffusion can be performed in a furnace for several hours, either in air or in flowing Argon (Ar) gas containing water vapour so as to suppress out-diffusion of  $\text{Li}_2\text{O}$ . Heat treatment in air usually causes a thicker inversion layer [43].

Generally speaking, the thickness of the inversion layer depends strongly on the conditions of the heat treatment, such as temperature, time, and atmosphere of the treatment.

As the heat treatment temperature increases the inversion layer becomes thicker. The same effect will occur if the heat treatment time is increased.

After treating the plate for the required time at the specified temperature, the temperature is reduced to the ambient temperature. A sample that is rapidly cooled has a thicker inversion layer than one that is cooled slowly [42, 43].

“Any inversion layers thicker than one half of the plate thickness,  $t/2$ , have not been observed yet” [42] and the inversion domain boundary seems to stop at the middle of the plate.

“ The inversion phenomena did not take place in X- and Y- cut plates whose faces are parallel to the spontaneous polarization, but took place in  $36^\circ$ ,  $128^\circ$ , and  $163^\circ$  rotated Y-cut plates which have inclined spontaneous polarizations” [43].

The domain inversion process taking place in the  $\text{LiNbO}_3$  by heat treatment, might arise as a result of the outdiffusion of Li, as was explained by Huang and Jaeger [44]. This outdiffusion will create a large concentration of electrons near the surface, which in turn

will diffuse into the regions of the crystal with lower electron concentration, forming a space-charge region; the electric field resulting from this space-charge region causes the domain inversion.

When such a structure is available, the transducer can be operated not just at the fundamental harmonic, but also at higher harmonics over a wide frequency range for the same thickness, having a wider bandwidth than the conventional devices. This is required for the skin thickness measurements, for which a high frequency transducer with sufficient bandwidth is required.

It is worth pointing out here that no theoretical analyses of ILT's have yet appeared in the literature. The behavior of these devices was modelled using PZFlex to clarify their characteristics.

### **6.3 PZFlex Modelling:**

The only difference between the original  $\text{LiNbO}_3$  and the inverted domain, as explained before, is that the piezoelectric constants are opposite in sign. This was used in the model, in which two matrices characterising the original and inverted layers; i.e. the dielectric and the stiffness constants, are the same, but the third, i.e. the piezoelectric constants, are opposite in sign to the original one.

#### **6.3.1 Thickness:**

The effects of having a single inversion layer on one side of the transducer with specific thicknesses as well as the effect of having two layers, one on each side of the transducer,

or a number of regular opposite polarity layers were modelled using PZFlex for a planar disc, having a thickness of 0.26mm and 10mm diameter.

### 6.3.2 Imperfect Interface:

The effect of non-planar interface between the inverted and the non-inverted domains was also modelled. In this case, two different interfaces, corresponding to a uniform taper and randomly uneven surface, as shown in Fig (6.1), were investigated.

Nakamura [43] and Miyazawa [45] reported the occurrence of random uneven interfaces or 'needlelike' domains, which are more common for specimens heat treated in air than those in which Ti diffusion had been used. But Nakamura et al [42] studied such transducers incorporating inversion layer formed by heat treatment in air and there was no reported effect for such an interface on the transducer behaviour.

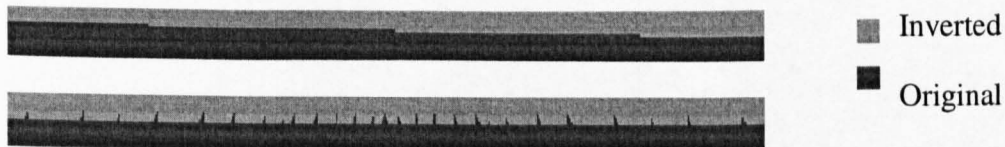


Fig (6.1) : Cross section in the depth direction of the heat treated modelled transducer demonstrating the taper ( $0.5^{\circ}$  slope) and random interfaces (mean 20% of the overall thickness) between the domains.

Fig (6.2) shows an experimental result for a cross section of  $500\mu\text{m}$  thick Z-cut plate of  $\text{LiNbO}_3$  heat treated at  $1110^{\circ}\text{C}$  for 5 hours in air [43].

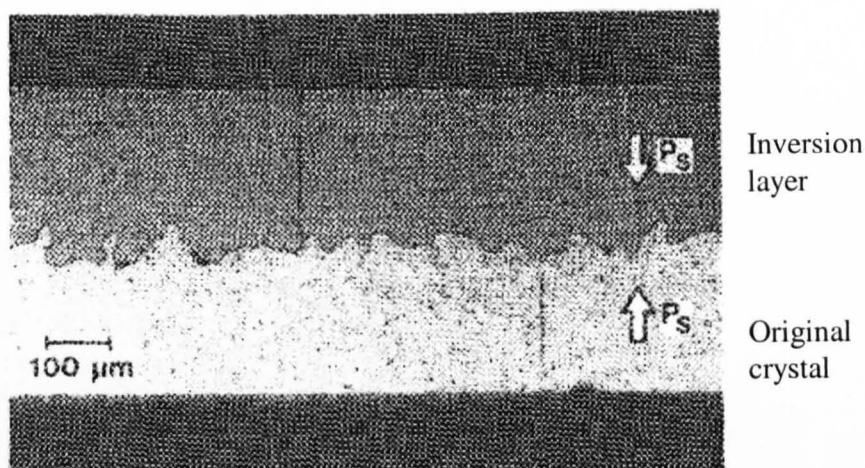


Fig (6.2): Cross section of experimentally heat treated  $\text{LiNbO}_3$  plate [43].

Fig (6.2) shows a needlelike micro-domains with the same polarity of the original crystal penetrating the inversion layer domain. From the shape it can be calculated that the penetration depth of the un-inverted domain into the inverted domain has a mean value of approximately 20% of the overall thickness. A similar interface was generated in the model (Fig 6.1), to represent the randomly uneven interface, where a number of micro triangles were formed projecting from the un-inverted domain into the inverted domain. The overall area of these triangles is approximately 1% of the overall area of the transducer. This is approximately equal to the ratio of the area of the needlelike structures in Fig (6.2), if it is approximated to triangles, to the overall area of the structure.

For the tapered interface the case is different, where the area of the un-inverted domain projecting the inverted domain is approximately 15% of the overall area, and in this case the effect of the interface on the thickness ratio is expected to be much more evident.

### 6.4 Impedance Profile:

A LiNbO<sub>3</sub> transducer, with a varying thickness of the inversion layer was modelled in air and the impedance amplitude profile is reported. One inversion layer with a different thickness ratio of the inverted domain to the overall thickness ( $t_1/t$ ), was modelled to see the effect of this ratio on the impedance. Three different ratios were modelled, i.e. 0, 0.3 and 0.5. The result is shown in Fig (6.3).

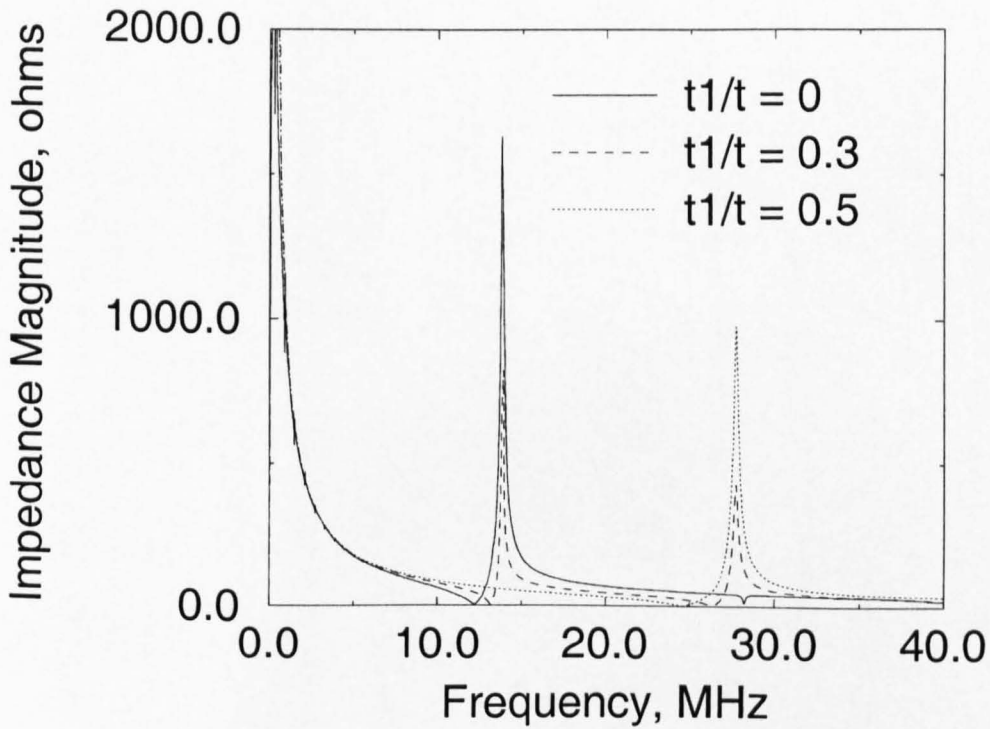


Fig (6.3): The effect of increasing the thickness ratio,  $t_1/t$ , on the transducer impedance magnitude for a transducer in air.

The thickness ratio for one inversion layer affects both the fundamental and the second harmonic. The greater the thickness ratio the lower the fundamental and the higher the second harmonic. When this ratio reaches 0.5, only the second harmonic frequency is evident.

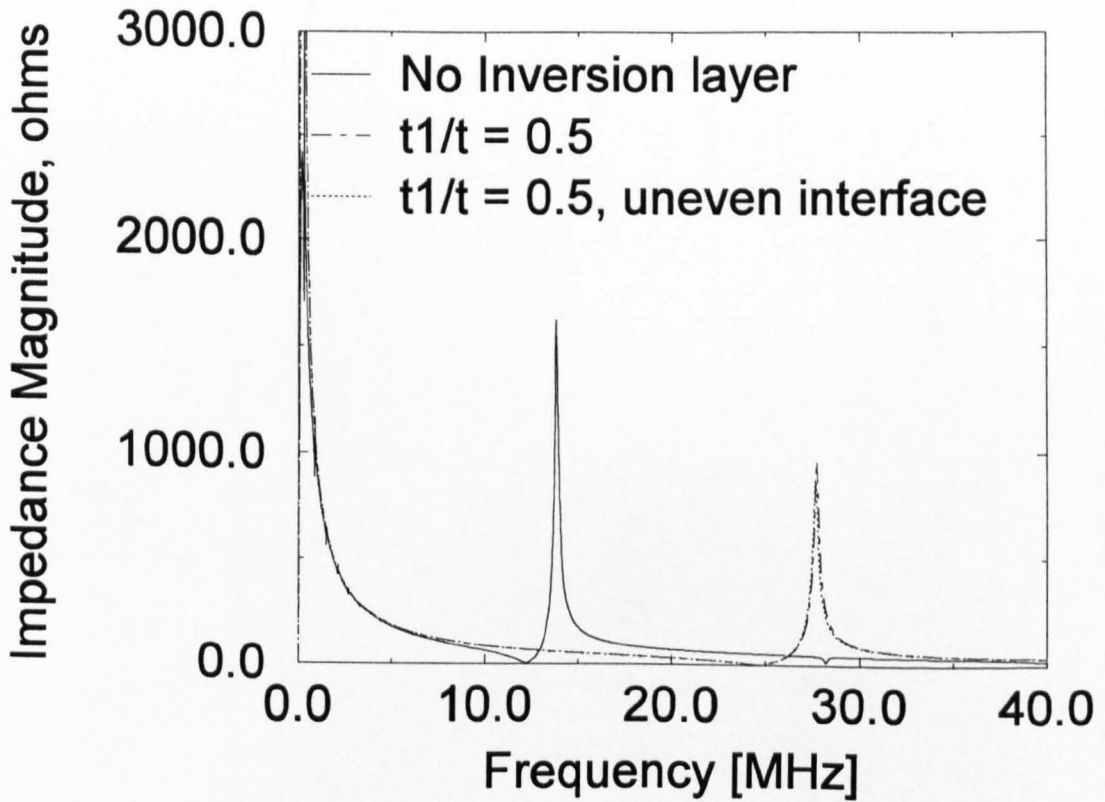


Fig (6.4): the effect of the randomly uneven interface on the transducer impedance magnitude.

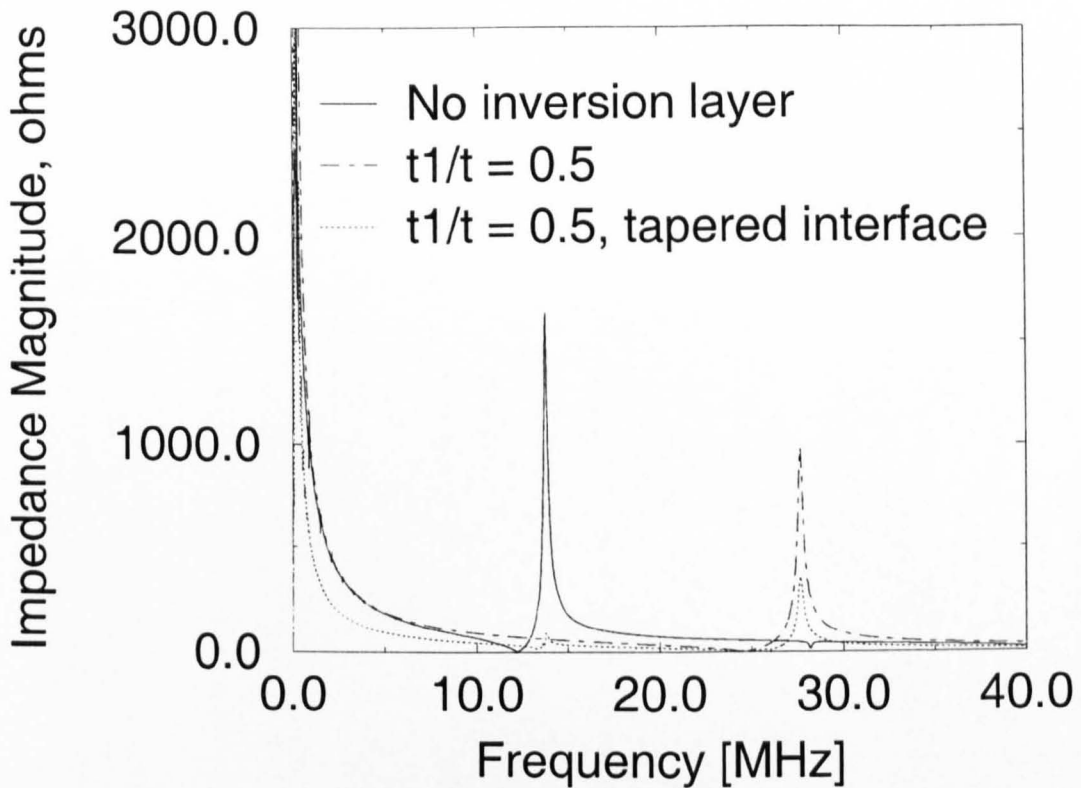


Fig (6.5): The effect of the tapered interface on the transducer impedance magnitude. The fundamental harmonic appear at about 14 MHz, for the tapered interface the amplitude is small as can be seen in the graph.

For the situation under consideration, the influence of the randomly uneven interface on the impedance magnitude is negligible as shown in Fig (6.4), which confirms the findings of Nakamura [42]. The influence of the tapered interface depends on the slope, but for the 0.5 degree slope shown, the effect is small but detectable as shown in Fig (6.5), where the fundamental is evident, since one side of the specimen does not have a full half inversion layer thickness, producing a thickness ratio of less than 0.5.

The effect of having more than one periodic inversion layer in the order inverted-noninverted-inverted...with all the layers having equal thickness in the depth direction was also investigated.

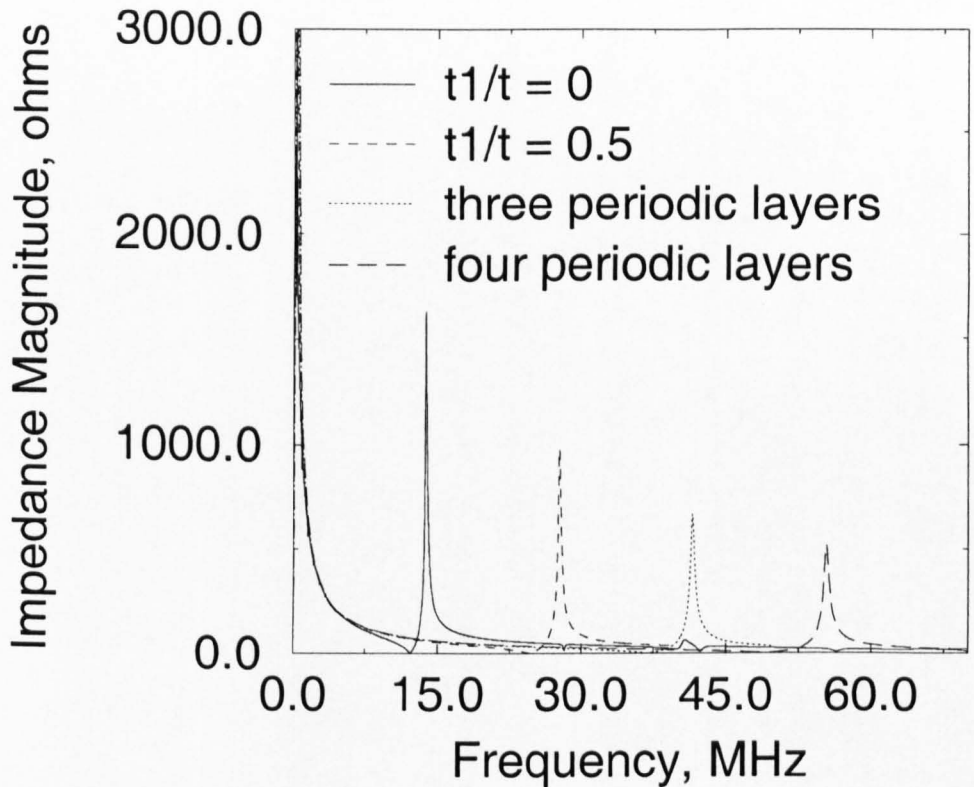


Fig (6.6): the effect of the number of periodic layers in the thickness direction on the transducer impedance.

The result in Fig (6.6) shows that the higher harmonics are induced depending on the number of layers. With two inversion layers of equal thickness (+,-,+), only the third harmonic is evident. With four periodic layers, a strong fourth harmonic is evident and

all lower order modes vanish. This means that the effective thickness of the transducer is halved, divided by three or four depending on the number of the periodic layers. If this structure is achievable experimentally then a relatively thick transducer could be used to generate efficiently the higher harmonic frequencies. However a large number of issues must be resolved such as sensitivity, bandwidth, pulse length and practical manufacture.

### **6.5 The Effect of Backing:**

Two different backing configurations were considered, corresponding to 50% (specific acoustic impedance of 18 MRayl) and matched (34 MRayl) and a water load was assumed. The fundamental frequency of the transducer without the inversion layer was approximately 14 MHz.

The device was excited via a 50 ohm generator, with a pulse width of 3.6 ns, to cover the desired spectral range. The frequency response of the pressure was obtained and used to compare the sensitivity and bandwidth of the different structures. The -3dB fractional bandwidth (FBW) of the output pressure frequency response was calculated.

Different configurations for the inversion layer in the thickness direction were tested with the layer at the front or back face and with multiple inversion layers.

For 50% backing, the pressure spectral responses for the inversion layer positioned at the front or rear faces are shown in Fig (6.7). The widest FBW of 59% was achieved for a front face inversion layer and  $t_1/t = 0.3$ . For the same backing two inversion layers having the same thickness of 0.0866mm, i.e. 1/3 of the overall thickness were modeled.

The peak, as shown in Fig (6.8), was shifted to higher frequency as expected but the FBW decreases to 46%.

More than one peak in the pressure spectral response will usually appear when one or more inversion layers present. With one inversion layer peaks occur at the fundamental, the second harmonic and the odd harmonics, with the second harmonic peak dominating. With two inversion layers peaks appear at higher harmonics, mainly the third and its odd harmonics.

In the case of matched backing, the FBW increases to 69% for one front face inversion layer, having  $t_1/t = 0.3$ . The best FBW reaching a value of 165% was achieved with the normal transducer with no inversion layer. The FBW was reduced by the presence of an inversion layer. A back face inversion layer with  $t_1/t = 0.3$  gave the best FBW reaching a value of 132%.

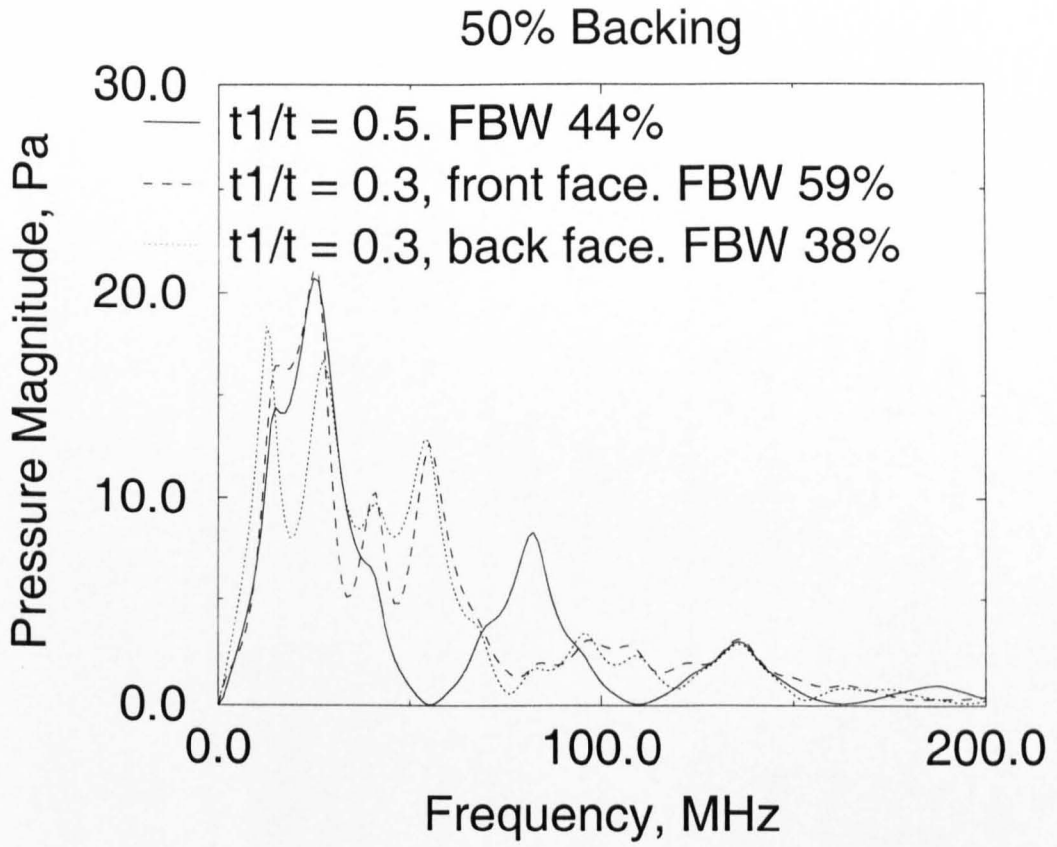


Fig (6.7): The effect of front or back face inversion layer and the thickness ratio on the pressure response.

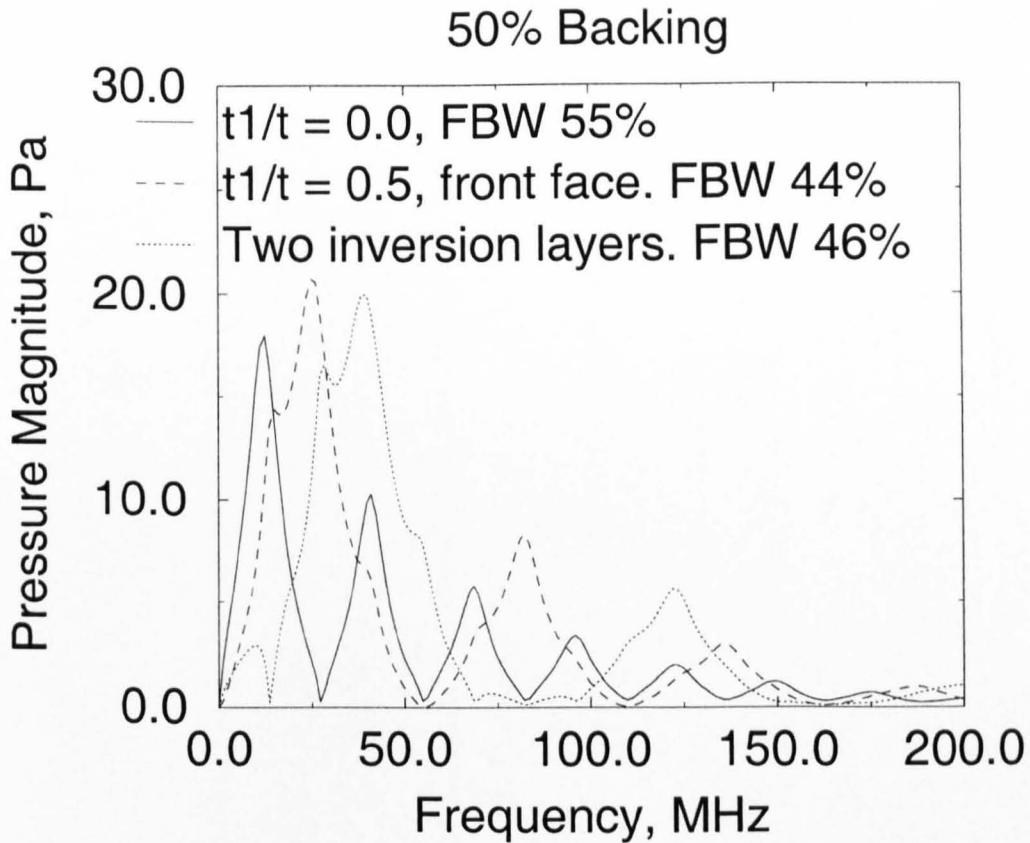


Fig (6.8): The effect of the number of periodic layers in the thickness direction on the pressure response.

Fig (6.9) indicates that the FBW is slightly higher (47%) with two inversion layers and matched backing, compared to 50% backing. However, the peak is shifted to a lower frequency at an intermediate point between the first and second harmonic for the case of one inversion layer and between the second and the third harmonic for two inversion layers. Although matched backing reduces the peak pressure in normal lithium niobate to about half of that with 50% backing, the corresponding decrease is very small in the inversion layer devices. It is interesting to note that the sensitivity of the higher

harmonics is very high for those cases where all layers are of the same thickness. However, the relationships between the individual cause and effect are difficult to determine from this modelling approach.

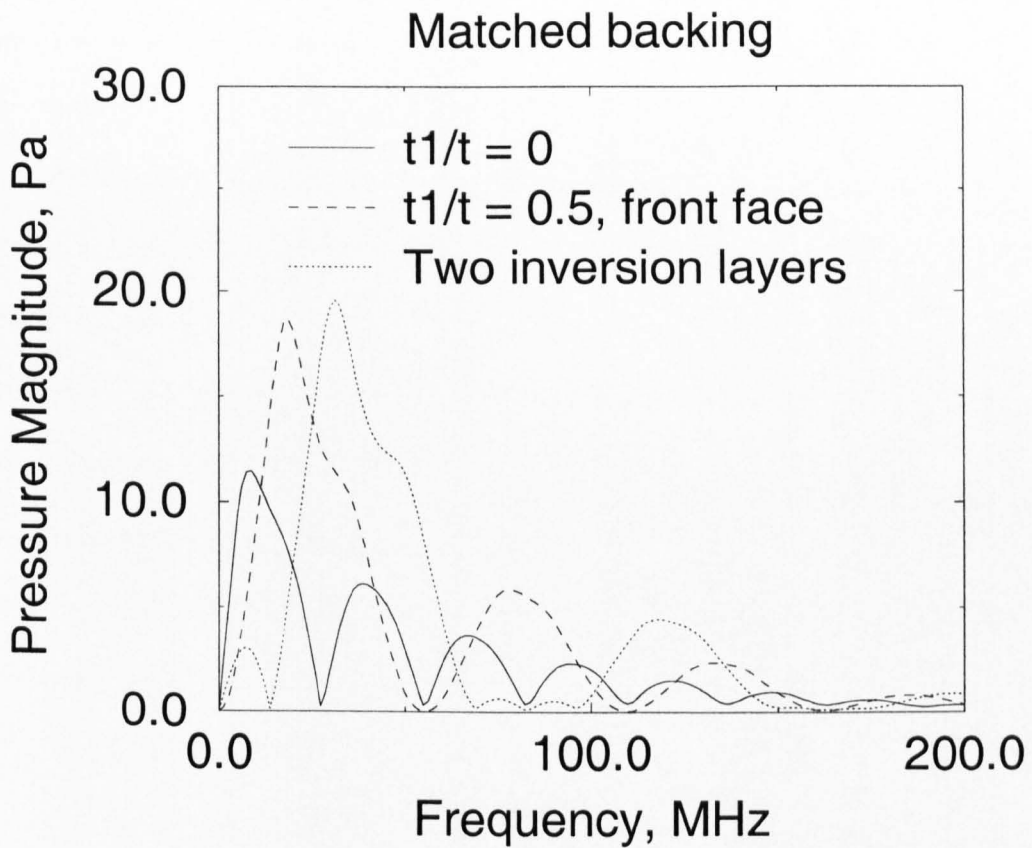


Fig (6.9): The effect of the number of periodic layers in the thickness direction on the pressure response.

## **6.6 The Influence of a Front Face Matching Layer:**

One matching layer was modelled at three different thicknesses. The matching layer was added to the case of the matched backed transducer. The matching layer was of quarter wavelength thickness, simulated at frequencies corresponding to the fundamental, the second and the third harmonics, depending on the number of the inversion layers used in the transducer. A water load was assumed, with matching layer of silver epoxy having a specific acoustic impedance of 7.33 MRayl. The required specific acoustic impedance of 7.107 MRayl between  $\text{LiNbO}_3$  and water was calculated using equation 3.7a, section 3.3.4. Silver epoxy with 7.33 MRayl was chosen as the nearest available value. The efficiency improved significantly when the matching layer was added to the front face of the transducer, as shown in Fig (6.10). The matching layer was designed for the fundamental frequency when there was no inversion layer. For one front face inversion layer and  $t_1/t=0.5$ , the transducer was matched to the second harmonic, and for two inversion layers at the third harmonic. However no bandwidth improvements were obtained in these cases.

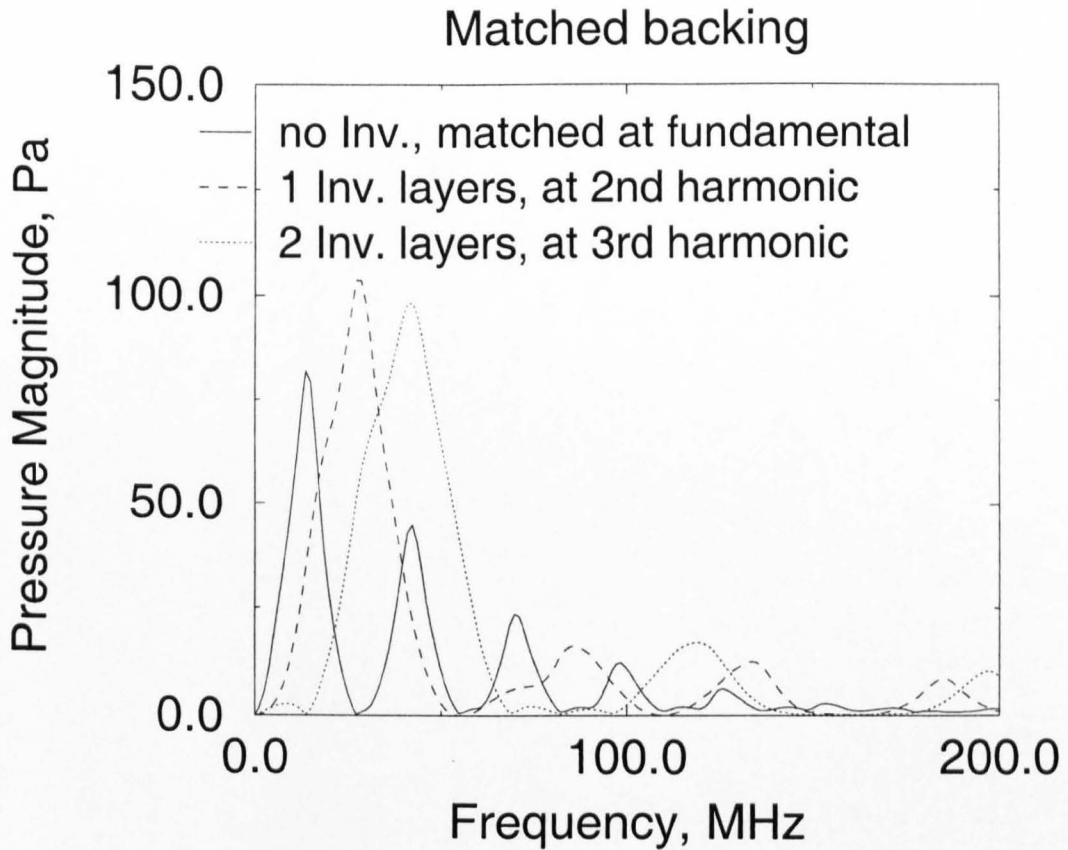


Fig (6.10): The effect of adding a matching layer between the transducer and water on the pressure frequency response.

### 6.6.1 The Fractional Bandwidth (FBW):

The influence on FBW of inversion layers and the different backings and matchings are summarised in tables 6.1 and 6.2.

Table (6.1): The bandwidth of the different cases modelled without a matching layer.

		No Inversion layer	One Inversion Layer			Three periodic layers (two Inversion layers)
			Front face $t1/t = 0.5$	$t1/t = 0.3$	Back face $t1/t = 0.3$	
<b>The Fractional Bandwidth % (FBW)</b>	50% backing	55.84	43.49	58.62	37.53	46
	matched backing	165	71.72	68.95	132	47.12

Table (6.2): The FBW of the matched backing transducers after adding the matching layer.

	No Inversion layer	One front face inversion layer $t1/t = 0.5$	Three periodic layers (two inversion layers)
<b>FBW %</b>	41.23	39.55	39.93

The time domain pulse width is of major significance in the design of transducers for skin thickness measurement (see Section 3.5). The pulse width for the output pressure from the transducer is summarised in table 6.3.

Table (6.3): The time pulse width for the pressure wave at the front face of the transducer in water.

		No Inversion layer	One Inversion Layer			Three periodic layers (two Inversion layers)
			Front face $t_1/t = 0.5$	$t_1/t = 0.3$	Back face $t_1/t = 0.3$	
The Time Pulse Width [ $\mu$ s]	50% backing	0.116	0.096	0.09	0.107	0.102
	matched backing	0.08	0.065	0.055	0.042	0.058

The above table shows that the time pulse width for the pressure wave decreases when the inversion layer exists. Matched backing provided a shorter pulse width and hence better resolution in all the cases, but as was stated previously matched backing is impractical.

All the above cases are for a transducer in transmission. In medical imaging the pulse echo mode is used and the same transducer is used for transmission and then reception. The pulse width in this case is for the impulse pulse-echo response. In the previous modelling, each programme including or excluding the inversion layer, at the specified fundamental frequency of approximately 14MHz, took about 17 hours to run on a SUN workstation having 1GB memory and 300 MHz speed using PZFlex. It would be impractical to run the same program for transmission and then reception, since this will

require a huge memory and a very long run times. Clearly, an alternative approach is required.

The result obtained from the models considered showed that the sensitivity of the transducer in transmission mode increased with the inversion layer. This is desirable for skin thickness measurement, but more analysis is required for both transmission and receptions modes to understand the behaviour of ILT devices and the effect of the inversion layer on both the pulse width and the sensitivity. In any case, the results appear to indicate only marginal improvements in resolution where there is a very small variations in the pulse width whether the inversion layer is presence or absent, but overall, the gain–resolution product appears to increase.

More analysis regarding the behaviour of these devices was required. This was carried out in the next Chapter.

## **6.7 Experimental Result:**

As a starting point a disc of lithium niobate having a diameter of 10mm and thickness of 0.21mm was heat treated for two hours in air at a temperature of about 1110° C in a muffle furnace in the metallurgy department in Strathclyde University. After two hours the furnace was opened and the sample was taken out to allow cooling to the room temperature; this fast cooling as mentioned before should result in higher thickness of the inversion layer.

The sample was then tested in the impedance analyser to see the effect on the impedance profile. The results are displayed in Fig 6.11.

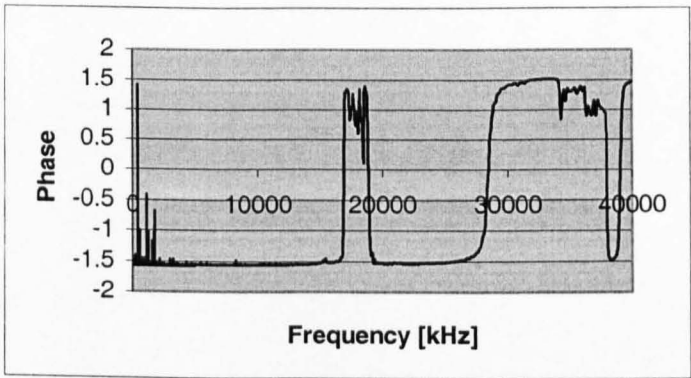
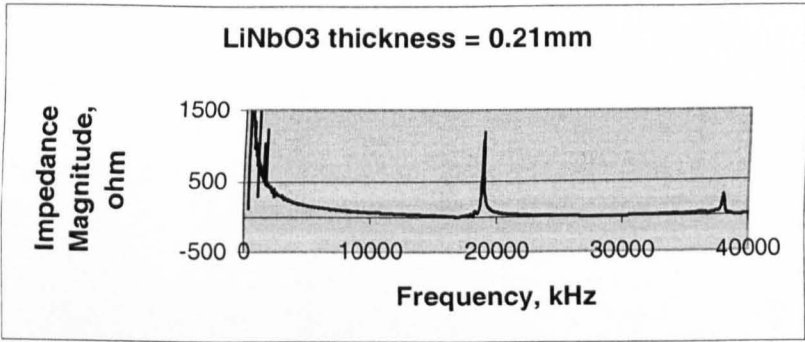


Fig (6.11): The experimental impedance response of the heat treated lithium niobate disc.

Fig 6.11 shows the presence of a second harmonic, which clearly confirmed the effect of heat treatment on the lithium niobate plate.

The same furnace became unavailable because of malfunction and further experiments were not possible using this furnace. Additional specimens were treated in an alternative furnace, but none showed any effect of treatment. This may be due to a different furnace environment or set-up procedures.

## **6.8 Concluding Remarks and Discussion:**

Transducers incorporating inversion layer(s) in their structure will have different features depending on the number of these layers and the thickness ratio.

Incorporating a number of periodic layers allows the transducer to be used at higher frequencies, with a wider bandwidth and good efficiency. Changing the thickness ratio or the placing of the inversion layer at the front or back face of the transducer will alter the bandwidth and sensitivity. By applying higher damping to the transducer the bandwidth will improve, but the efficiency will decrease slightly compared to a transducer without any inversion layer. Using a matching layer in front of the transducer will improve the sensitivity of the transducer and high bandwidths might be possible, depending on the selection of frequency.

The limitation of FEM is that the solutions are specific to the model being analysed and generalisation is often difficult. Run times may also be extremely long, limiting the number of models that can be analysed.

In order to have better understanding of both the transmission and reception mode of the inversion layer transducers and also to have a physical insight into their behaviour a new mathematical model was developed.

The result showed that the higher the damping applied to the transducer the better the FBW, but with the case of  $\text{LiNbO}_3$  matched damping is not possible, because the material required must have high acoustic impedance reaching a value of 34 MRayl. As explained by Kerr [2] this is not achievable using the tungsten loaded epoxy widely used

as backing block, because the high volume ratio of tungsten required makes it difficult to mix the material evenly into a paste.

The modelling procedure has allowed the investigation of a potential transducer configuration. The best bandwidth is obtained with one front face inversion layer and 0.3 thickness ratio, using the medium damping which might be achievable experimentally. Further improvement to produce the wider bandwidth and shorter pulse width needed to resolve the different skin structures will require the exploration of additional structures and damping.

Further experiments are required to have clear and better knowledge and control about the furnace, the temperature and the time required to achieve the desired heat treatment effect.

More experiments on heat treated specimens are required to confirm the predictions of the modelling.

## **CHAPTER 7**

### **Mathematical Model**

## **7.1 Introduction:**

As was shown before, the FEM approach provided useful information, that was, however, limited to the specific cases modelled. To obtain a more general physical insight into the behaviour of inversion layer transducers a fundamental theoretical investigation was carried out. Several issues need to be resolved, such as, bandwidth, receiver operation, electrical interfacing and mechanical backing and matching. These issues need to be understood before a proper design assessment can be undertaken.

A mathematical model was developed using the Laplace domain to investigate the transfer function of both the transmitting and receiving modes of such transducers. For simplicity, the case of one front face inversion layer was investigated. In the future this may be extended to more than one inversion layer in the front or back face of the transducer.

## **7.2 The Thickness Mode Receiver:**

In this section a transfer function of the transducer as receiver of ultrasound was developed. The theory used here follows the pattern used by Hayward [35], which, in turn, relied initially on the method adopted by Redwood [46]. The main difference here is that an inversion layer was added to the front face of the transducer to see the effect of that layer on the transducer behaviour. The transducer is subjected to an arbitrary electrical and mechanical loading, in order to obtain the general transfer function. The transducer was a disc, thickness  $L$ , vibrating in the thickness mode. For simplicity of the mathematical computation, the following assumptions were made:

- 1- The diameter of the transducer is of the order by 20 times its thickness to allow the neglect of the effect of the radial waves and study only the effect of the plane waves.
- 2- The transducer is vibrating only in the normal direction to the plane surface. Thus the mathematical and electrical quantities exist only in the x-direction, implying that the transducer is only vibrating in its thickness mode.
- 3- The attenuation in the transducer and the surrounding media are neglected, thus these media are considered to be loss-free.
- 4- The effect of irregular modes of vibration and the effect due to aging or thermal changes are all neglected.

### 7.2.1 Basic Equations for Piezoelectric Resonator:

To start this analysis we need to have the basic equations describing the behaviour of the piezoelectric resonator. These equations were proposed by Mason [47].

$$\Gamma_x = \hat{Y}_x^D S_x - h_{33} D_x \quad \text{Indirect Piezoelectric effect.}$$

$$E_x = -h_{33} S_x + D_x / \epsilon_x^S \quad \text{Direct effect.}$$

Where:

$\Gamma_x$  The tensile or compressive stress, [newtons / m<sup>2</sup>]

$\hat{Y}_x^D$  The elastic constant measured under constant electrical displacement (open circuit), [newtons / m<sup>2</sup>]

$S_x$  The strain, or fractional change in length

$h_{33}$  The piezoelectric constant relating the stress and charge or the electrical field and mechanical strain, measured under constant electrical displacement

$D_x$  The electrical displacement, [coulombs / m<sup>2</sup>]

$E_x$  The electrical field strength, [volts / m]

$\epsilon_x^S$  The absolute permittivity of the transducer material measured under constant strain, [farad / m]

The suffix  $_{33}$  indicates that it is applicable to the thickness direction

The suffix  $_x$  in all the above equations indicates the x or the thickness direction

We also have :

$$S_x = \frac{\partial \xi_x}{\partial x}$$

Where:  $\xi_x$  is the mechanical displacement in any point x within the transducer.

If the suffixes in the previous indirect and direct piezoelectric effect equations are dropped (considering a 1-D case), for convenience, and by substituting  $S_x$  these equations can be rewritten as follows:

$$\Gamma = \hat{Y} \frac{\partial \xi}{\partial x} - h D$$

$$E = -h \frac{\partial \xi}{\partial x} + D / \epsilon$$

If we assume that there is no net free charge within the transducer, then by applying Gauss law, it can be found that:

$$\frac{\partial D}{\partial x} = 0$$

And hence:

$$\begin{aligned} \frac{\partial \Gamma}{\partial x} &= \hat{Y} \frac{\partial}{\partial x} \left[ \frac{\partial \xi}{\partial x} \right] - \frac{h \partial D}{\partial x} \Rightarrow \\ \frac{\partial \Gamma}{\partial x} &= \frac{\hat{Y} \partial^2 \xi}{\partial x^2} \end{aligned} \quad \text{7.1}$$

Applying Newton's law relating force to acceleration, to a very small element within the transducer we obtain:

$$\frac{\partial \Gamma}{\partial x} = \rho \frac{\partial^2 \xi}{\partial t^2} \quad \text{7.2}$$

Where:  $\rho$  is the material density.

From equations 7.1 and 7.2, the equation describing the mechanical propagation in the transducer can be obtained:

$$\frac{\partial^2 \xi}{\partial t^2} = v^2 \frac{\partial^2 \xi}{\partial x^2} \quad \text{7.3}$$

Where  $v$  is the longitudinal wave velocity measured in [m / s],  $v^2 = \hat{Y} / \rho$ .

It is worth noting, as explained by Redwood [46], that the wave equation is the same for piezoelectric or non piezoelectric material.

Let us now introduce the Laplace transform  $G[f(t)]$  which is defined by the following formula:

$$G[f(t)] = \int_0^{\infty} e^{-st} f(t) dt$$

Here  $s$  is a complex variable,  $G$  is the transformation symbol and  $f(t)$  is the time domain function.

Equation 7.3 is a differential equation, the transform of the solution of which can be expressed in the following form:

$$\xi(s) = A e^{-s(x/v)} + B e^{s(x/v)} \quad \text{-----} \quad 7.4$$

Equation 7.4 represents two waves travelling within the transducer, in the positive and negative  $x$  direction.  $A$  and  $B$  are constants related to the boundary conditions at  $x = 0$  and  $x = L$ , defining the two faces of the transducer.

Because there is no net free charge within the transducer, all the charge resides on the transducer surface; hence the electrical displacement  $D$  can be defined as follows:

$$D = \frac{Q}{A'} \quad \text{C/m}^2$$

Where:  $A' = \pi r^2$ , the area of the transducer surface

$Q$  is the net charge residing on either of the surfaces

From the above equation and the equation of the indirect effect it can be found that:

$$\frac{F}{A'} + \frac{hQ}{A'} = \hat{Y} \frac{\partial \xi}{\partial x}, \quad F \text{ is the force in the } x \text{ direction.}$$

Hence:

$$F + hQ = A' \hat{Y} \frac{\partial \xi}{\partial x}$$

Substituting equation 7.4 into the above equation, the relationship between the force and mechanical displacement within the transducer is obtained:

$$F(s) + hQ(s) = sZc \{ -A e^{-s(x/vc)} + B e^{s(x/vc)} \} \quad \text{-----} \quad 7.5$$

Where:  $v_c$ , the longitudinal acoustic velocity of the transducer material.

$$Z_c = \rho v_c A', \text{ the acoustic impedance of the transducer.}$$

In the same way the force in a non piezoelectric medium can be obtained from equations 7.2 and 7.4 yielding:

$$F(s) = s Z_m \{ - A e^{-s(x/v_m)} + B e^{s(x/v_m)} \} \text{ ————— 7.6}$$

Where:  $v_m$  is the longitudinal acoustic velocity of the medium.

$Z_m$  is the acoustic impedance of the medium.

Now let us go back to the direct piezoelectric effect where:

$$E = -h \frac{\partial \xi}{\partial x} + D / \epsilon$$

By integrating this equation, i.e. the electric field, the voltage across the transducer thickness  $L$  is obtained as follows:

$$\begin{aligned} V &= \int_0^L E dx = \int_0^L \left[ \frac{-h \partial \xi}{\partial x} + \frac{Q}{A' \epsilon} \right] dx \\ &= -h \{ \xi_{(x=L)} - \xi_{(x=0)} \} + \frac{QL}{A' \epsilon} \end{aligned}$$

$$\text{Therefore: } V = -h \{ \xi_{(x=L)} - \xi_{(x=0)} \} + Q / C_0 \text{ ————— 7.7}$$

Where:  $C_0$  is the bulk static capacitance of the transducer, i.e. the capacitance in the absence of the piezoelectric action.

The difference  $\xi_{(x=L)} - \xi_{(x=0)}$  indicates the mechanical displacement difference between the front and the rear face of the transducer, i.e. the net strain on the device.

All the above equations describe a normal transducer in thickness mode. Now if the transducer incorporates an inversion layer at the front face as shown in Fig 7.1. The

same equations will apply, except that the transducer can be considered of two parts, i.e. the normal part extending from  $l'$  to  $L$  and the inversion layer part extending from  $0$  to  $l'$ . In this case, the voltage on the transducer is the sum of the voltage across the normal and the inverted layer. The only difference between the inverted and the non inverted layer, as mentioned before, is that  $h$  will be of opposite sign.

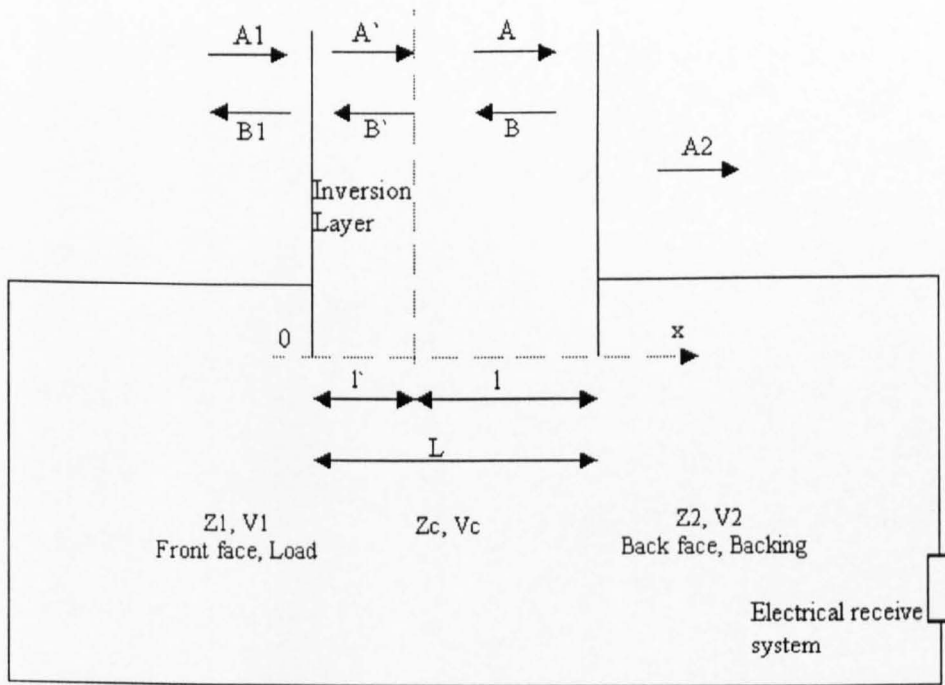


Fig (7.1): The structure of the transducer incorporating front face inversion layer in reception mode.

The overall voltage across the transducer with an inversion layer is thus:

$$V = V_{\text{normal}} + V_{\text{Inverted}}$$

$$= -h \{ \xi_{c(x=L)} - \xi_{c(x=l')} \} + \frac{Ql}{A'\epsilon} + h \{ \xi_{c'(x=l')} - \xi_{c'(x=0)} \} + \frac{Ql'}{A'\epsilon}$$

$$= -h \{ \xi_{c(x=L)} - \xi_{c(x=l)} \} + h \{ \xi_{c'(x=l)} - \xi_{c'(x=0)} \} + \frac{QL}{A\epsilon}$$

$$V = -h \{ \xi_{c(x=L)} - \xi_{c(x=l)} - \xi_{c'(x=l)} + \xi_{c'(x=0)} \} + Q / C_0$$

Where:  $\xi_c$  and  $\xi_{c'}$  denotes the displacement of the normal and the inverted layer respectively.

$V_{normal}$  and  $V_{Inverted}$  are the voltage across the un-inverted and the inverted layer respectively

The continuity conditions at the interface of two layers gives:

$$\xi_{c(x=l)} = \xi_{c'(x=l)}$$

Therefore:

$$V = -h \{ \xi_{c(x=L)} - 2 \xi_{c(x=l)} + \xi_{c'(x=0)} \} + Q / C_0 \quad \text{————— 7.7}$$

The application of a force to the surface of the transducer will produce a charge because of the direct piezoelectric effect. Electrically connecting an arbitrary loading impedance,  $Z_E$ , across its terminals will cause a current  $I(t)$  to flow through the loading impedance. This will produce a voltage  $V(t)$  across the transducer. The current  $I(t)$  is related to the charge  $Q$  as follows:

$$I(t) = dQ / dt$$

Taking the Laplace transformation of this formula, assuming zero initial conditions:

$$I(s) = -s Q(s)$$

Hence:

$$V(s) = -s Q(s) Z_E(s) \text{ or}$$

$$Q(s) = \frac{-V(s)}{sZ_E(s)}$$

Substituting this in equation 7.7` for the transducer with inversion layer, gives the voltage across the transducer:

$$V(s) = -h \{ \xi c_{(x=L)} - 2 \xi c_{(x=l')} + \xi c_{(x=0)} \} (s) - \frac{V(s)}{sC_0 Z_E(s)}$$

Defining the term  $C_0 Z_E(s)$  as  $\tau(s)$ , the following equation is obtained for the voltage across the transducer with an inversion layer.

$$V(s) = -h \{ \xi c_{(x=L)} - 2 \xi c_{(x=l')} + \xi c_{(x=0)} \} (s) \cdot \frac{s\tau(s)}{1 + s\tau(s)} \quad \text{7.8}$$

## 7.2.2 Boundary Conditions and Equation Development:

Taking the case of a piezoelectric transducer positioned between two non piezoelectric elastic media as shown in Fig 7.1 and assuming an infinite extension of the two media away from the transducer.

The constants  $A_1, B_1, A', B', A, B$  and  $A_2$  represent the constants  $A$  and  $B$  mentioned in equation 7.4 for the boundary conditions at  $x = 0, l'$  and  $L$  for the load medium, the inversion layer, the normal layer, i.e. the non inverted layer, and the backing medium respectively.  $A$  is an amplitude factor related to the incident wave, and  $B$  is an amplitude factor related to reflected wave in each medium at the boundary. The constants  $Z_c, v_c, Z_1, v_1$  and  $Z_2, v_2$  are the acoustic impedance and the longitudinal wave velocity for the transducer, the load medium and the backing medium respectively. The load medium is at the front face of the transducer and the backing medium is at the rear face of the

transducer. Note that the acoustic impedance and the longitudinal velocity is the same for a normal or inverted layer. The acoustic impedances here are assumed real and equal to the product of the material density and its longitudinal velocity per unit area.

The mechanical boundary conditions at the interface between two media have continuity of both displacement and normal stress. The continuity of displacement at both faces of the transducer and at the interface between the un-inverted and the inverted piezoelectric layer gives the following:

$$\xi_1 (x=0) = \xi_{c'} (x=0)$$

$$\xi_{c'} (x=l') = \xi_c (x=l')$$

$$\xi_c (x=L) = \xi_2 (x=L)$$

Where:  $\xi_1$  and  $\xi_2$  are the displacements in medium 1 (the load) and 2 (the backing) respectively.

From equation 7.4 it can be found that:

$$\xi_1 (s) = A_1 e^{-s(x/v_1)} + B_1 e^{s(x/v_1)}$$

$$\xi_2 (s) = A_2 e^{-s(x/v_2)}$$

$$\xi_c (s) = A e^{-s(x/v_c)} + B e^{s(x/v_c)}$$

$$\xi_{c'} (s) = A' e^{-s(x/v_{c'})} + B' e^{s(x/v_{c'})}$$

In the same way the continuity of the normal stress at the same boundaries gives:

$$F_1 (x=0) = F_{c'} (x=0)$$

$$F_{c'} (x=l') = F_c (x=l')$$

$$F_c (x=L) = F_2 (x=L)$$

Again from equations 7.5 and 7.6 for piezoelectric and non piezoelectric media we can get:

$$F1(s) = s Z1 \{ - A1 e^{-s(x/v1)} + B1 e^{s(x/v1)} \}$$

$$F2(s) = s Z2 \{ - A2 e^{-s(x/v2)} \}$$

$$Fc(s) + h Q(s) = s Zc \{ - A e^{-s(x/vc)} + B e^{s(x/vc)} \}$$

$$Fc'(s) - h Q(s) = s Zc \{ - A' e^{-s(x/vc)} + B' e^{s(x/vc)} \}$$

Where F1, F2, Fc, Fc' are the normal stresses or forces for the loading medium, the backing medium, the un-inverted and the inverted layer respectively.

It is worth noting here that the only difference between Fc and Fc' is the opposite sign of h as mentioned before.

Applying these boundaries to the equations will give rise to the following set of formulae containing A, B, A1, B1, A', and B':

$$A1 + B1 = A' + B'$$

$$A' e^{-s(l'/vc)} + B' e^{s(l'/vc)} = A e^{-s(l'/vc)} + B e^{s(l'/vc)}$$

$$A e^{-s(L/vc)} + B e^{s(L/vc)} = A2 e^{-s(L/v2)}$$

$$s Z1 [ - A1 + B1 ] = h Q(s) + s Zc [ - A' + B' ] \quad \text{—————} \quad 7.9$$

$$h Q(s) + s Zc [ - A' e^{-s(l'/vc)} + B' e^{s(l'/vc)} ] =$$

$$- h Q(s) + s Zc [ - A e^{-s(l'/vc)} + B e^{s(l'/vc)} ]$$

$$- h Q(s) + s Zc [ - A e^{-s(L/vc)} + B e^{s(L/vc)} ] =$$

$$s Z2 [ - A2 e^{-s(L/v2)} ]$$

As we have seen before, the voltage across the transducer incorporating an inversion layer on the front face is given in equation 7.8 as follows:

$$V(s) = - h \{ \xi c_{(x=L)} - 2 \xi c_{(x=l')} + \xi c'_{(x=0)} \} (s) \cdot \frac{s\tau(s)}{1 + s\tau(s)}$$

By substituting  $\xi c$  and  $\xi c'$  in the above equation we get:

$$V(s) = -h \{ A e^{-s(L/vc)} + B e^{s(L/vc)} - 2 A e^{-s(l'/vc)} - 2 B e^{s(l'/vc)} + A' + B' \} \cdot \frac{s\tau(s)}{1 + s\tau(s)} \quad \text{7.10}$$

Now we need to express A, B, A', and B' in terms of A1, the incident wave, that is the input in the receiver case.

From the first and the fourth equation in the set of equations 7.9 it is possible to obtain the following:

$$s Z_1 [-2A_1 + A' + B'] = h Q(s) + s Z_c [-A' + B'] \quad \text{7.10a}$$

From the third and the sixth equation in the set of equations 7.9 it is possible to obtain the following:

$$s Z_c [-A e^{-sT} + B e^{sT}] - h Q(s) = -s Z_2 [A e^{-sT} + B e^{sT}] \quad \text{7.10b}$$

Where:

$T = L / vc$ , the time taken for the acoustic wave to cross the transducer.

From the second equation in the set of equations 7.9 it is possible to obtain the following:

$$A' - A = (B - B') e^{2s(l'/vc)}$$

$$B - B' = (A' - A) e^{-2s(l'/vc)}$$

From the fifth equation in the set of equation 7.9 it is possible to obtain the following:

$$\frac{2hQ(s)}{sZ_c} = (A' - A) e^{-s(l'/vc)} + (B - B') e^{s(l'/vc)}$$

Substituting  $(A' - A)$  and  $(B - B')$  in turn in the above equation yields:

$$\frac{2hQ(s)}{sZc} = (A' - A) e^{-s(l'/vc)} + (A' - A) e^{-s(l'/vc)}$$

$$\frac{2hQ(s)}{sZc} = (B - B') e^{s(l'/vc)} + (B - B') e^{s(l'/vc)}$$

From the above two equations in turn we get:

$$A' = \frac{hQ(s)}{sZc} \cdot e^{s(l'/vc)} + A$$

————— 7.10c

$$B' = -\frac{hQ(s)}{sZc} \cdot e^{-s(l'/vc)} + B$$

Substituting both  $A'$  and  $B'$  in terms of  $A$  and  $B$  in equation 7.10a yields:

$$sZl \left[ -2A1 + \frac{hQ(s)}{sZc} e^{s(l'/vc)} + A - \frac{hQ(s)}{sZc} e^{-s(l'/vc)} + B \right] =$$

$$hQ(s) + sZc \left[ -\frac{hQ(s)}{sZc} e^{s(l'/vc)} - A - \frac{hQ(s)}{sZc} e^{-s(l'/vc)} + B \right]$$

Rearranging the above equation yields:

$$A - B R_F = A1 (1 - R_F) - \frac{hQ(s)}{s(Zc + Zl)} \cdot X \quad \text{————— 7.11a}$$

Where:

$$R_F = \frac{Zc - Zl}{Zc + Zl}$$

$$X = \left[ \frac{Zl}{Zc} e^{s(l'/vc)} - \frac{Zl}{Zc} e^{-s(l'/vc)} - 1 + e^{s(l'/vc)} + e^{-s(l'/vc)} \right]$$

Rearranging equation 7.10b yields:

$$-sZc A e^{-sT} + sZc B e^{sT} - hQ(s) + sZ2 A e^{-sT} + sZ2 B e^{sT} = 0$$

Rearranging the above equation yields:

$$A R_B e^{-2sT} - B = - \frac{hQ(s)}{s(Zc + Z2)} e^{-sT} \quad \text{————— 7.11b}$$

Where:  $R_B = \frac{Zc - Z2}{Zc + Z2}$

From equations 7.11a and 7.11b the following matrix equation can be obtained:

$$\begin{bmatrix} 1 & -R_F \\ R_B e^{-2sT} & -1 \end{bmatrix} \cdot \begin{bmatrix} A \\ B \end{bmatrix} = \begin{bmatrix} A1(1 - R_F) - \frac{hQ(s)}{s(Zc + Z1)} X \\ - \frac{hQ(s)}{s(Zc + Z2)} e^{-sT} \end{bmatrix}$$

Solving the previous matrix equation yields for A and B:

$$\begin{bmatrix} A \\ B \end{bmatrix} = \frac{1}{\Delta} \begin{bmatrix} 1 & -R_F \\ R_B e^{-2sT} & -1 \end{bmatrix} \begin{bmatrix} A1(1 - R_F) - \frac{hQ(s)}{s(Zc + Z1)} X \\ - \frac{hQ(s)}{s(Zc + Z2)} e^{-sT} \end{bmatrix}$$

Where:  $\Delta = 1 - R_F R_B e^{-2sT}$

From the above equation, for A and B, it can be found that:

$$A = \frac{(J1)(L)}{\Delta} \quad \text{————— 7.12}$$

$$B = \frac{(J2)(L)}{\Delta}$$

Where J1, J2 and L are the following matrices:

$$J1 = \begin{bmatrix} 1 & -R_F e^{-sT} \end{bmatrix}$$

$$J2 = e^{-sT} \begin{bmatrix} R_B e^{-sT} & -1 \end{bmatrix}$$

$$L = \begin{bmatrix} A1(1 - R_F) - \frac{hQ(s)}{s(Zc + Z1)} X \\ -\frac{hQ(s)}{s(Zc + Z2)} \end{bmatrix}$$

Substituting A` and B` in terms of A and B, from equation 7.10c, in the voltage equation 7.10 yields:

$$V(s) = -h \{ A (e^{-sT} - 2e^{-st'} + 1) + B (e^{sT} - 2e^{st'} + 1) + \frac{hQ(s)}{sZc} (e^{st'} - e^{-st'}) \} \cdot U(s)$$

Where:

$t' = l' / vc$ , The time taken for the acoustic wave to cross the inversion layer.

$$U(s) = \frac{s\tau(s)}{1 + s\tau(s)}$$

Substituting equation 7.12 for A and B in the above voltage equation gives:

$$V(s) = -h U(s) \left\{ \frac{(J1)(L)}{\Delta} (e^{-sT} - 2e^{-st'} + 1) + \frac{(J2)(L)}{\Delta} (e^{sT} - 2e^{st'} + 1) + \frac{hQ(s)}{sZc} (e^{st'} - e^{-st'}) \right\} \quad \text{7.13}$$

This equation describes the response of a transducer incorporating one front face inversion layer when it is loaded under arbitrary electrical conditions in the receiving mode.

Substituting J1, J2, and L in the above equation and rearranging the terms yields:

$$V(s) = h U(s) \left\{ A1 (1 - R_F) K_{FI}(s) - \frac{hQ(s)}{s(Zc + Z1)} X K_{FI}(s) - \frac{hQ(s)}{s(Zc + Z2)} K_{BI}(s) - \frac{hQ(s)}{sZc} (e^{st'} - e^{-st'}) \right\} \quad \text{7.14}$$

$$\text{Where: } K_{FI}(s) = \frac{-e^{-sT} + 2e^{-st'} - 1 - R_B e^{-sT} + 2R_B e^{-2sT} e^{st'} - R_B e^{-2sT}}{\Delta}$$

————— 7.15

$$K_{BI}(s) = \frac{e^{-sT} - 2e^{-sT} e^{st'} + 1 + R_F e^{-sT} - 2R_F e^{-sT} e^{-st'} + R_F e^{-2sT}}{\Delta}$$

A1 is the amplitude factor denoting the incident mechanical wave, which is assumed to be planar. Following Redwood [46], the incident wave is required to be described in terms of pressure or force. The initial force striking the transducer is given in the following equation:

$$F1(s) = sZ1 (-A1 e^{-s(x/v1)} + B1 e^{s(x/v1)})$$

If only the incident wave was considered at x=0:

$$A1 = -\frac{F1(s)}{sZ1} \quad \text{————— 7.16}$$

$$\text{Also } R_F = \frac{Zc - Z1}{Zc + Z1} \Rightarrow 1 - R_F = \frac{2Z1}{Zc + Z1}$$

$$\text{Let } T_F = \frac{2Zc}{Zc + Z1}$$

Substituting A1 and taking in account  $T_F$  and  $(1 - R_F)$  in the above voltage equation 7.14 yields:

$$V(s) = h U(s) \left\{ -\frac{F1(s)T_F K_{FI}(s)}{sZc} - \frac{hQ(s)}{s(Zc + Z1)} \times K_{FI}(s) \right. \\ \left. - \frac{hQ(s)}{s(Zc + Z2)} K_{BI}(s) - \frac{hQ(s)}{sZc} (e^{st'} - e^{-st'}) \right\}$$

Substituting  $Q(s) = \frac{-V(s)}{sZ_E(s)}$  in the above equation yields:

$$V(s) = -\frac{hU(s)F1(s)T_F K_{F1}(s)}{sZc} + \frac{h^2U(s)V(s)}{s^2(Zc + Z1)Z_E(s)} \times K_{F1}(s) \\ + \frac{h^2U(s)V(s)}{s^2(Zc + Z2)Z_E(s)} K_{B1}(s) + \frac{h^2U(s)V(s)}{s^2ZcZ_E(s)} (e^{st} - e^{-st})$$

Rearranging this equation to get  $V(s)$  in terms of  $F1(s)$  yields:

$$V(s) = \frac{-hU(s)F1(s)T_F K_{F1}(s)}{sZc} \\ 1 - \frac{h^2U(s)}{s^2Z_E(s)} \left[ \frac{XK_{F1}(s)}{Zc + Z1} + \frac{K_{B1}(s)}{Zc + Z2} + \frac{e^{st} - e^{-st}}{Zc} \right]$$

$$\text{Let } T_B = \frac{2Zc}{Zc + Z2}$$

Rearranging the above equation to include  $T_B$  and  $T_F$  gives:

$$V(s) = \frac{-hU(s)F1(s)T_F K_{F1}(s)}{sZc} \\ 1 - \frac{h^2U(s)}{s^2ZcZ_E(s)} \left[ XK_{F1}(s) \frac{T_F}{2} + K_{B1}(s) \frac{T_B}{2} + e^{st} - e^{-st} \right] \quad \text{--- 7.17}$$

Therefore:

$$\frac{V(s)}{F1(s)} = \frac{-hU(s)T_F K_{F1}(s)}{sZc} \\ 1 - \frac{h^2U(s)}{s^2ZcZ_E(s)} \left[ XK_{F1}(s) \frac{T_F}{2} + K_{B1}(s) \frac{T_B}{2} + e^{st} - e^{-st} \right] \quad \text{--- 7.17a}$$

Equation 7.17a gives the transfer function of the transducer incorporating the inversion layer as a receiver. The input is the incident force  $F1$  on the front face of the transducer and the output is the voltage across the transducer under arbitrary electrical load  $Z_E$ .

To compare this equation with that for a transducer without an inversion layer, the thickness of the inversion layer  $t'$  in equation 7.17a is set to zero yielding:

$$\frac{V(s)}{F1(s)} = \frac{\frac{-hU(s)T_F K_F(s)}{sZc}}{1 - \frac{h^2 U(s)}{s^2 Zc Z_E(s)} \left[ K_F(s) \frac{T_F}{2} + K_B(s) \frac{T_B}{2} \right]} \quad \text{--- 7.18}$$

Where in this case when  $t'=0$  (no inversion layer):

$$X = 1$$

$$K_F(s) = \frac{-e^{-sT} + 1 - R_B e^{-sT} + R_B e^{-2sT}}{\Delta}$$

$$K_B(s) = \frac{-e^{-sT} + 1 - R_F e^{-sT} + R_F e^{-2sT}}{\Delta}$$

This is the same as the transfer function found by Hayward [35].

Hayward defined  $K_F$  as the front face reverberation factor of the transducer representing the difference in displacement between the front and rear faces when an ideal impulse function of displacement is incident on the front face. In the same manner he defined  $K_B$  as the rear face reverberation factor of the transducer representing the difference in displacement between the front and rear faces when an impulse of displacement is incident on the rear face.

The case when the transducer incorporates a front face inversion layer is more complex as equation 7.17 shows. In this case the effect of both the normal and the inverted layer, having a piezoelectric boundary in between because of the different polarities, added more terms to the transfer function. Here we see the term  $X$  related to  $t'$ ,  $vc$ ,  $Z1$  and  $Zc$ .

Also  $K_{FI}$  and  $K_{BI}$  both have terms related to  $t'$ . And an extra term,  $(e^{st'} - e^{-st'})$ , also appears.

### 7.2.3 Some Specific Conditions of Electrical and Mechanical Loading:

Considering an open circuit across the transducer, i.e.  $Z_E = \infty$ , equation 7.17a gives:

$$\frac{V(s)}{F1(s)} = \frac{-hT_F K_{FI}(s)}{sZc} \quad \text{7.19}$$

This equation represents the Laplace transfer function of the receiver device incorporating a front face inversion layer under the open circuit condition.

In this equation  $K_{FI}$  is the only term related to  $t'$  which is related to  $l'$ , the thickness of the inversion layer. For no inversion layer,  $t' = 0$ ,  $K_{FI}$  in equation 7.15 gives:

$$K_F(s) = \frac{-e^{-sT} + 1 - R_B e^{-sT} + R_B e^{-2sT}}{\Delta}$$

For all the device having an inversion layer,  $t' = T$ ,  $K_{FI}$  gives:

$$K_{FI}(s) = \frac{+e^{-sT} - 1 + R_B e^{-sT} - R_B e^{-2sT}}{\Delta}$$

This is opposite in sign to the previous  $K_F$  confirming the opposite electrical polarity.

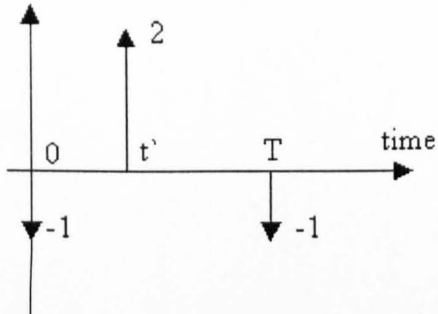
For  $t'$  having a general value, rearranging  $K_{FI}$  in equation 7.15 for the delay terms and substituting  $\Delta$  gives:

$$K_{FI}(s) = \frac{-e^{-sT}(1 + R_B) + 2e^{-st'} - 1 + 2R_B e^{-s(2T-t')} - R_B e^{-2sT}}{1 - R_F R_B e^{-2sT}} \quad \text{7.20}$$

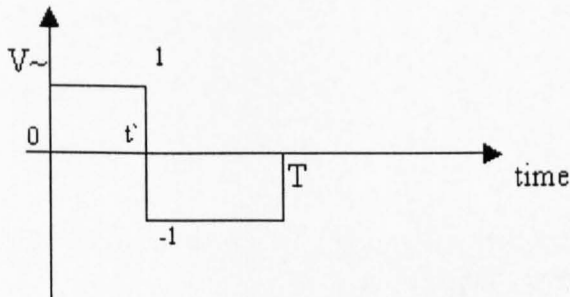
For a transducer with matched backing  $R_B = 0$  and  $K_{FI}$  becomes:

$$K_{FI}(s) = -e^{-sT} + 2e^{-st'} - 1 \quad \text{—————} \quad 7.21$$

Representing this in the time domain gives:



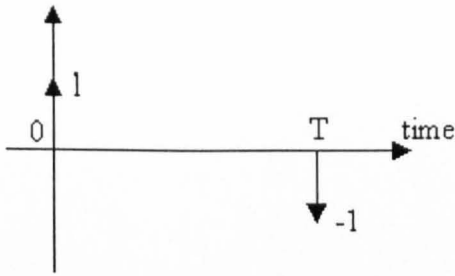
From equation 7.19 when a dirac Delta function is applied as the force, i.e.  $F1(s) = 1$ , the voltage across the transducer will be proportional (but of negative sign) to the integral of the above time function giving:



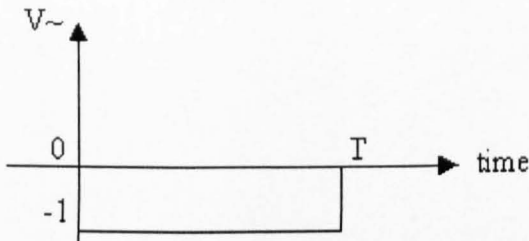
For no inversion layer,  $t' = 0$ , equation 7.21 gives:

$$K_F(s) = -e^{-sT} + 1$$

This can be represented in the time domain as follows:



The integration of this as mentioned before is proportional to the voltage yielding:

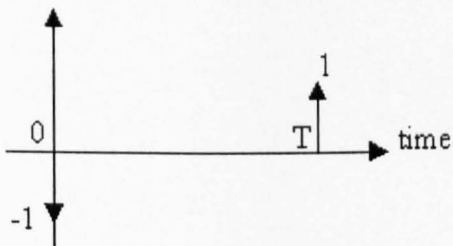


This represents the response of normal receiver without an inversion layer under conditions of open circuit and matched backing.

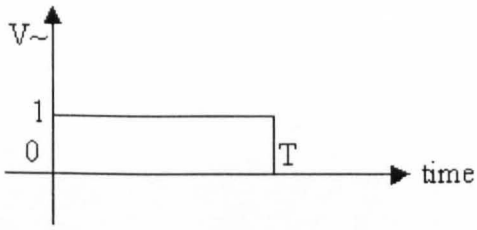
In the case when all the device is inversion layer,  $t' = T$ , from equation 7.21 we get:

$$K_{FI}(s) = e^{-sT} - 1$$

Representing this in the time domain gives:



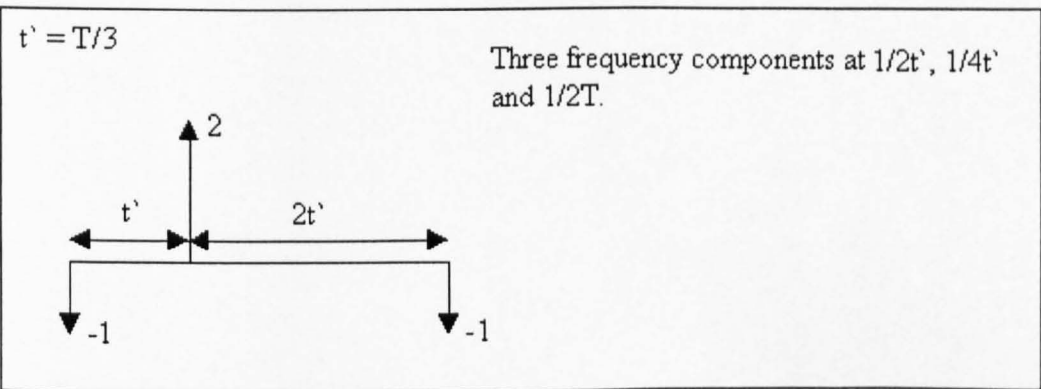
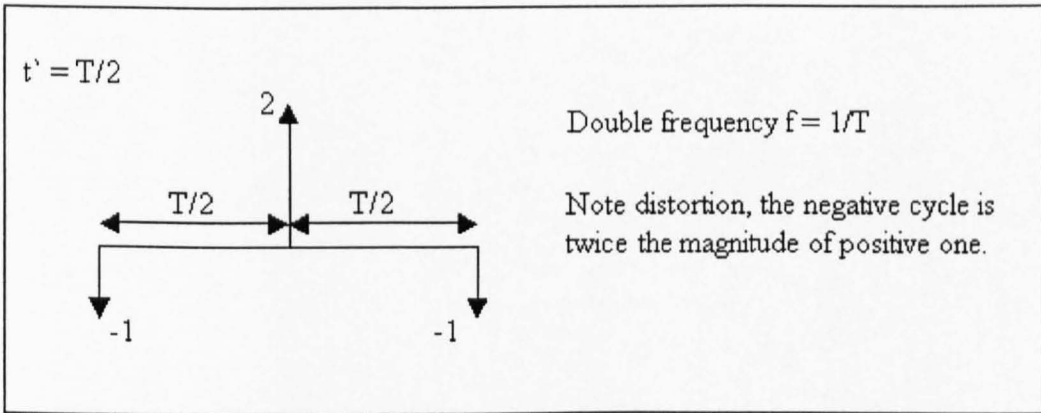
The voltage in this case will be proportional to the following:



This is opposite in sign to the case with no inversion layer confirming the results.

The energy is the same in each case, as expected.

The frequency content, in the presence of the inversion layer, is related to  $t'$  and this can be illustrated as follows:



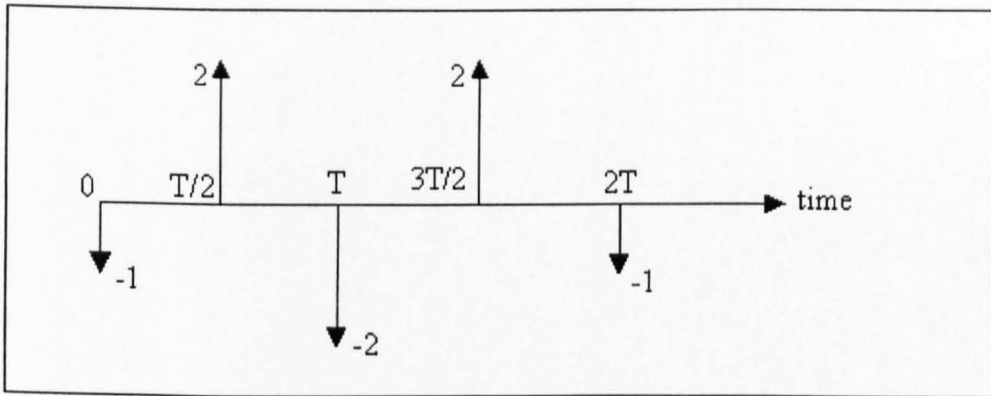
For  $t = T/2$ , i.e. the inversion layer occupying half the transducer thickness equation 7.20 gives:

$$K_{FI}(s) = \frac{-e^{-sT}(1 + R_B) + 2e^{-\frac{sT}{2}} - 1 + 2R_B e^{-\frac{3sT}{2}} - R_B e^{-2sT}}{1 - R_F R_B e^{-2sT}}$$

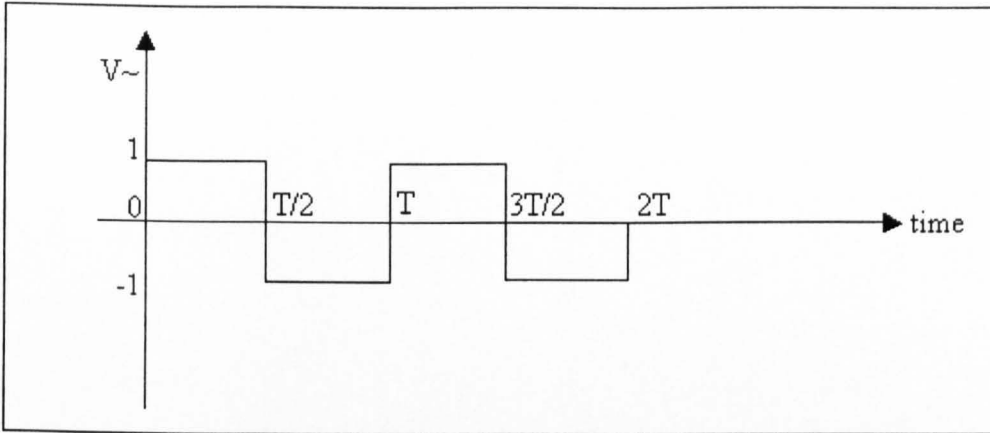
For the case of air backed transducer ( $R_B = 1$ ) and the load is ideally matched with the transducer ( $R_F = 0$ ) the above equation yields:

$$K_{FI}(s) = -2e^{-sT} + 2e^{-\frac{sT}{2}} - 1 + 2e^{-\frac{3sT}{2}} - e^{-2sT}$$

This can be represented in time domain as follows:



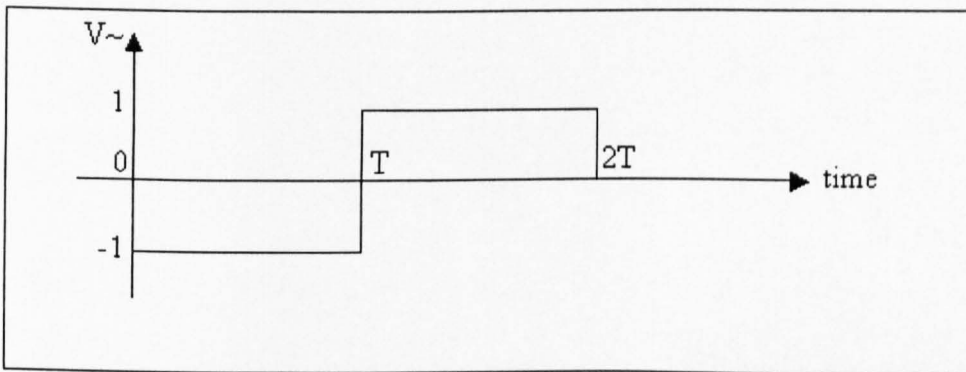
Again from equation 7.19 the voltage is proportional, but of negative sign, to the integral of the above result yielding:



This shows two cycles. If the same conditions were compared to a transducer with no inversion layer, i.e.  $\tau = 0$ , equation 7.20 gives:

$$K_F(s) = -2 e^{-sT} + 1 + e^{-2sT}$$

This can be represented for the voltage in the time domain as follows:



Comparing this to the previous case we can see only one cycle and the polarity is opposite due to the presence of the inversion layer, but the frequency is doubled.

## 7.2.4 The Pulse Width in Reception Mode:

All the previous cases considered show that the pulse width of the output signal in reception mode; i.e. the pulse width of the output voltage, of the transducer incorporating a front face inversion layer will be equal to that of the normal transducer without the inversion layer, but more cycles or reverberations will appear in the presence of the inversion layer. The number of these cycles or reverberations is related to the mechanical matching and backing applied on the transducer, while the frequency content of the signal depends on the thickness ratio or the thickness of the inversion layer.

For the general case when  $Z_E$  is not infinity, for example  $Z_E = 50$  ohm, it is possible to code the normalized voltage magnitude of equation 7.17 for the Delta function applied as the force on the transducer front face, i.e.  $F1(s) = 1$ . The parameters described in table 7.1 for  $36^\circ$  Y-cut lithium niobate transducer gives the graphs shown in Fig 7.2.

The code was built using MATLAB to plot the output voltage given in equation 7.17 as a function of the frequency  $f$ , where  $s = j\omega = 2\pi f$ .

Table (7.1): The Lithium niobate transducer parameters for the receiver.

$Z_E$ ohm	$Z1$ MRayl	$Z2$ MRayl	$Zc$ MRayl	$vc$ m/s	$h$ V/m	$\Gamma$ mm	$L$ mm	$C_o$ pF
50.	1.5	34.	34.	7340	1.34 $*10^{+10}$	0	0.26	133
	Water	Matched				0.078		
	Load	Backing				0.13		

The Acoustic impedance is per unit area (The area is the transducer surface). The transducer has a radius of 5mm.

Repeating the plot of  $V(s)$  magnitude, but with 50% backing, i.e.  $Z_2 = 18 \text{ MRayl}$ , gives the graphs shown in Fig 7.3.

These graphs show that the bandwidth for the voltage across the transducer varies with the thickness ratio or the thickness of the inversion layer.

The peak output for a transducer without an inversion layer is less for a matched backing than for a 50% backing. The effect is less for a transducer having an inversion layer. Hence the inversion layer appears to promote the efficiency of the transducer. The fractional bandwidth for the different cases is given in Table 7.2, for both -3dB and -6dB.

Table (7.2): The fractional bandwidth of the different cases for 50 ohm loading.

thickness ratio	50% Backing		Matched Backing	
	-3dB	-6dB	-3dB	-6dB
0	69.7%	108.61%	172.%	250.8%
0.3	59.%	73.%	66.5%	117.%
0.5	69.72%	89.25%	69.%	151.3%

The graphs also show that for a 50% backing, in the presence of the inversion layer, different peaks appear and the dominant one is at the second harmonic. The value of these peaks are related to the thickness ratio. For matched backing these peaks emerged together at one peak the value of which is related to the thickness ratio, but in all cases it was shifted down.

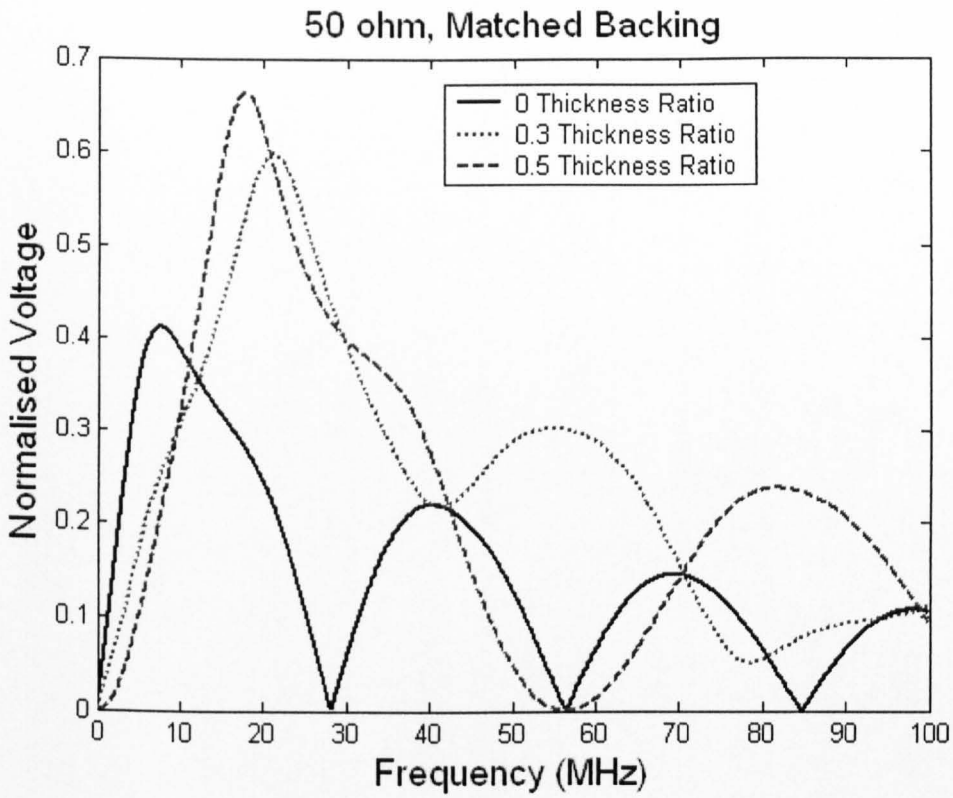


Fig (7.2): The normalised voltage magnitude for the receiver for matched backing. The graphs show that increasing the thickness ratio shifts the peaks to higher frequencies.

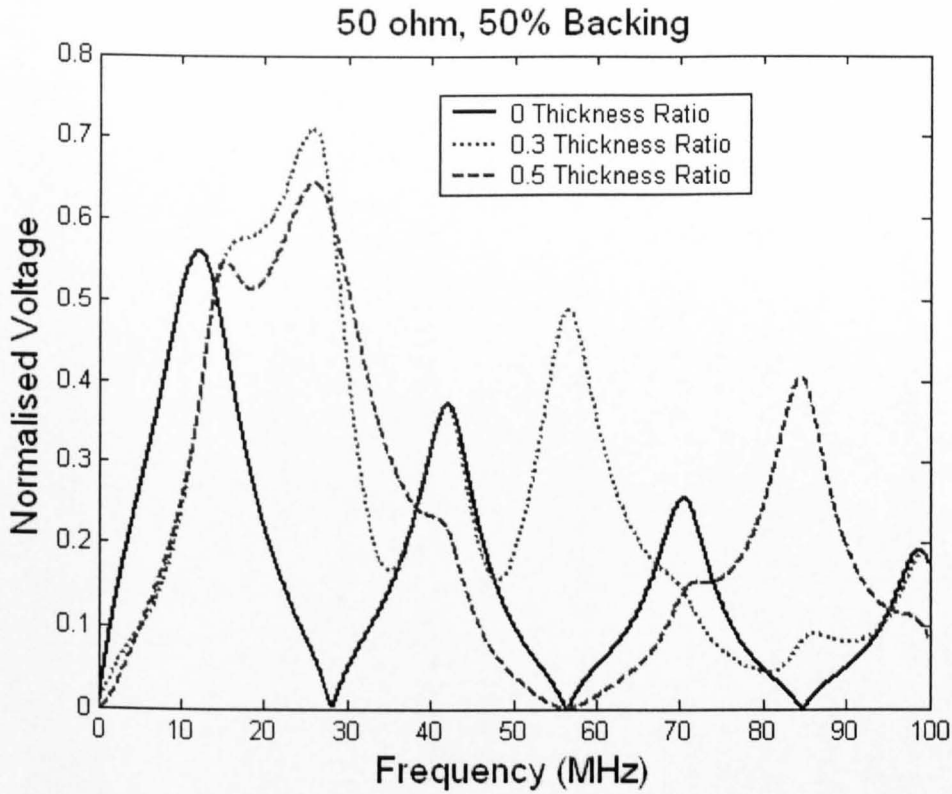


Fig (7.3): The normalised voltage magnitude for the receiver for 50% backing. More peaks appeared at higher frequencies depending on the thickness ratio.

Table 7.2 shows that the fractional bandwidth is higher in the  $\text{LiNbO}_3$  transducer without the inversion layer, but in the case of 0.5 thickness ratio and 50% backing the -3dB fractional bandwidth shows the highest value reaching to 69.72%.

To clarify the issue of the time pulse width the IFFT (Inverse Fast Fourier Transform) was performed on the previous frequency domain results for the voltage to get the time response and the results are shown in Fig 7.3a.

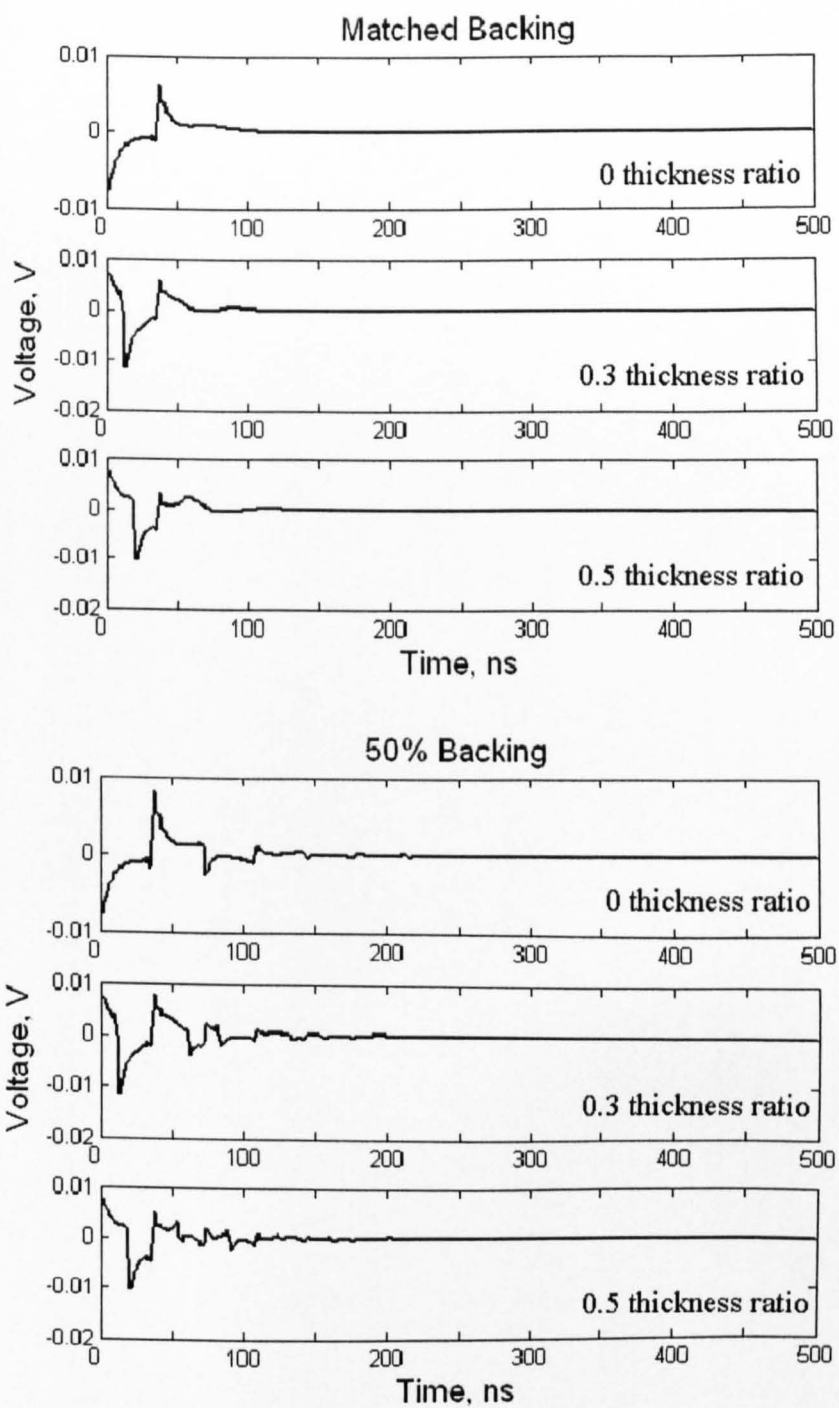


Fig (7.3a): The voltage time response for the receiver for matched and 50% backing and different thickness ratio.

From the results in Figs 7.3a the time pulse width was calculated. It was found that the pulse width is the same whether the inversion layer is present or absent and equal to 70 and 110ns for matched and 50% backing respectively. At the same time the efficiency was better with the presence of the inversion layer showing higher voltage amplitude.

To have clearer understanding of the effect of electrical loading,  $Z_E$  was changed from 50 to 150 ohm and the normalized voltage magnitude plotted. The results are shown in Figs 7.4 and 7.5, and the fractional bandwidths are given in table 7.3.

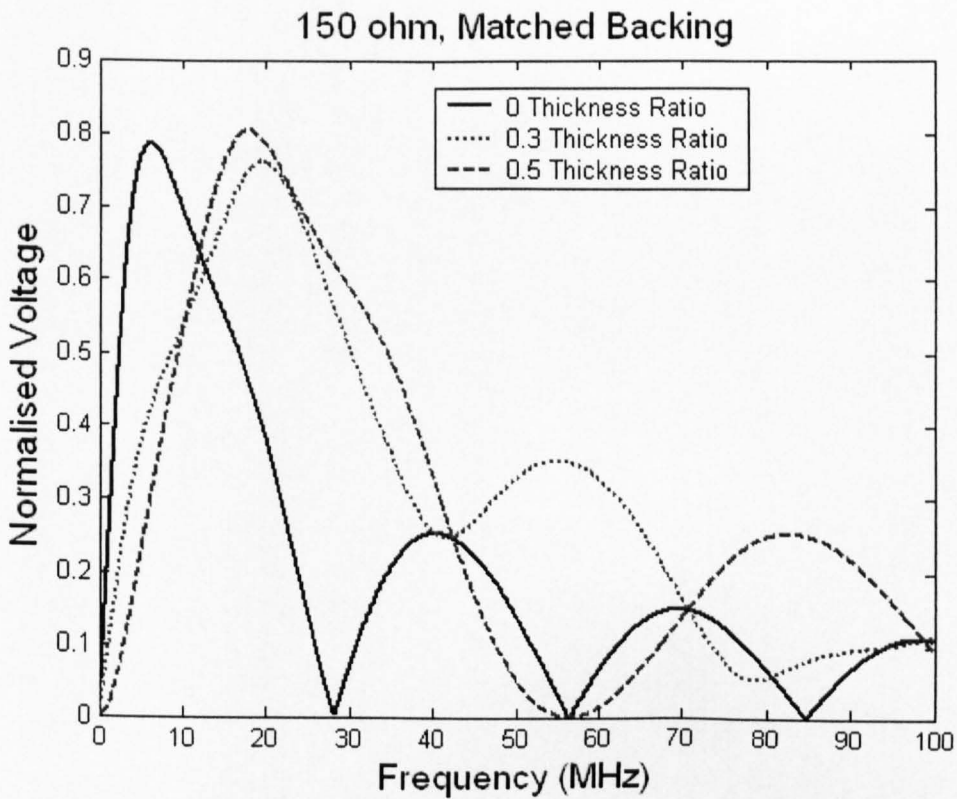


Fig (7.4): The normalised voltage magnitude for the receiver for matched backing and 150 ohm electrical load.

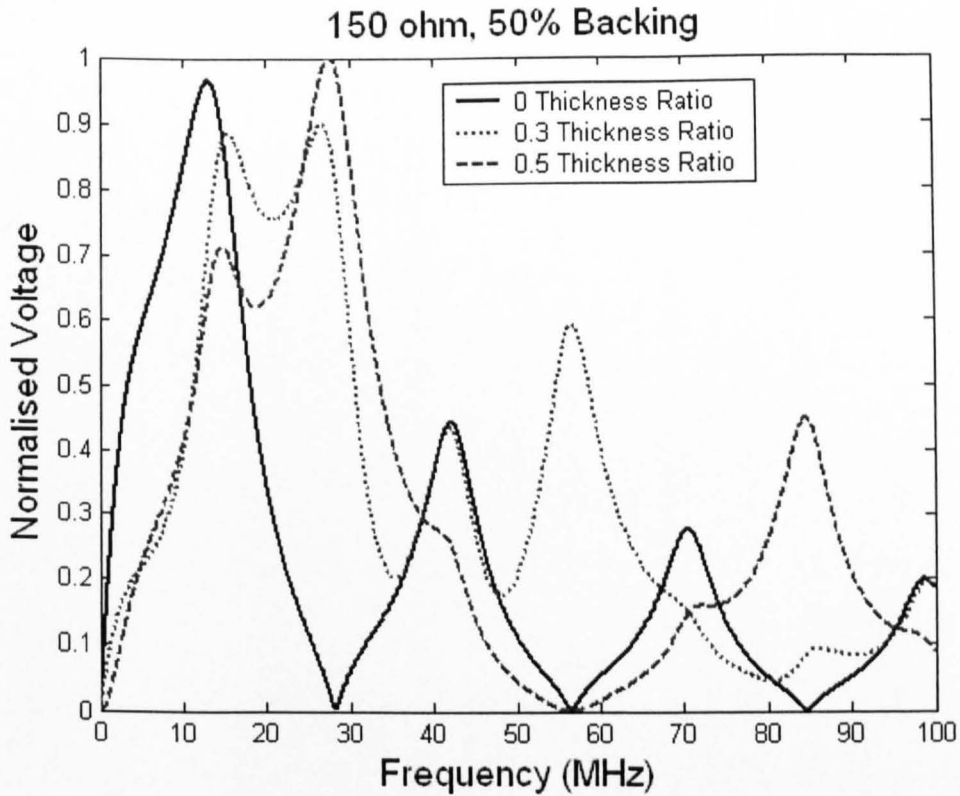


Fig (7.5): The normalised voltage magnitude for the receiver for 50% backing and 150 ohm electrical load.

Figs 7.4 and 7.5 show that with 150 ohm electrical load the peaks are shifted to higher values compared to 50 ohm. The decrement of the peaks when the backing is changed from 50% to matched backing is approximately same for all the cases whether the inversion layer is presence or not.

Table (7.3): The fractional bandwidth of the different cases for 150 ohm loading.

thickness ratio	50% Backing		Matched Backing	
	-3dB	-6dB	-3dB	-6dB
0	71.9%	115.9%	196.3%	289.96%
0.3	64.37%	75.73%	96.9%	149.16%
0.5	61.9%	80.23%	114.9%	168.76%

Table 7.3 shows that for 150 ohm electrical load the fractional bandwidth is higher if there is no inversion layer for all the cases.

The previous results show that the pulse width and hence the axial resolution was not improved with the presence of the inversion layer. In this case, although we have higher frequency components demonstrated by a wider bandwidth than the typical thickness mode devices, more cycles appeared in the output voltage giving approximately the same pulse width resulting from the normal thickness mode device without the inversion layer. However, the sensitivity was better with the presence of the inversion layer which is one of the requirements for skin thickness measurement giving preference of the inversion layer devices over conventional transducers.

### 7.3 The Device as a Transmitter:

Taking the same case as the receiver where the transducer is positioned between two non-piezoelectric elastic media that extend infinitely away from the transducer surfaces. The transducer as a transmitter is excited electrically causing stress waves to propagate

away from the transducer into both media at the front and rear faces. Waves also will be generated within the transducer towards its centre. This situation is illustrated in Fig 7.6.

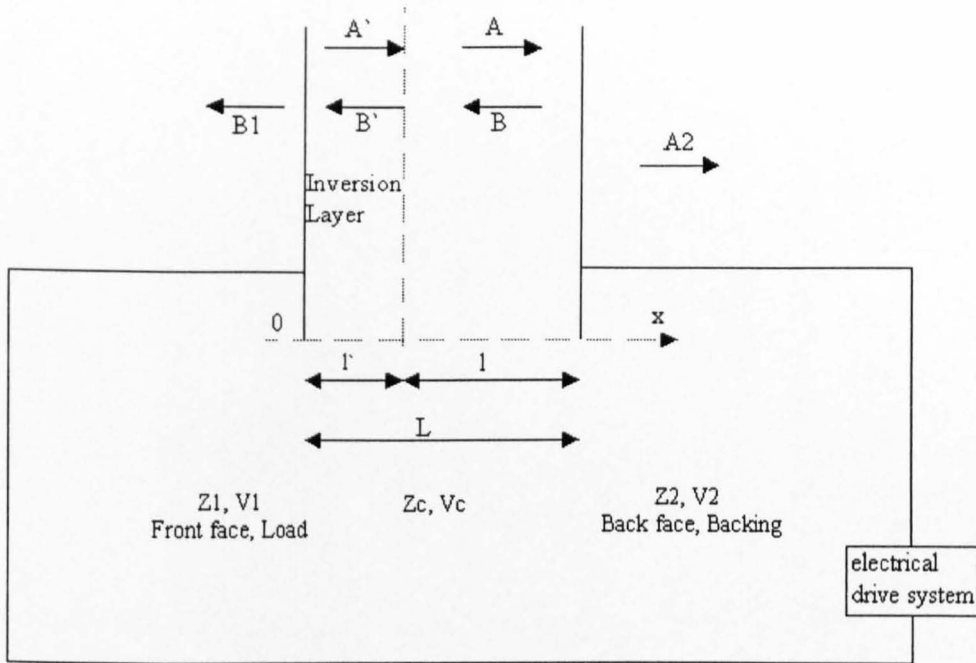


Fig (7.6): The device incorporating the inversion layer as transmitter of ultrasound.

This situation is similar to the case when the device is working as a receiver except there is no incident wave of force, i.e.  $A_1 = 0$  and the analysis will be the same as the receiver with  $A_1$  set to zero.

Therefore, equation 7.12 can be used to express the amplitude factors  $A$  and  $B$  inside the transducer as follows:

$$A = \frac{(J1)(L')}{\Delta}, \quad B = \frac{(J2)(L')}{\Delta}$$

Where:

$$J1 = [1 \quad -R_F e^{-sT}]$$

$$J2 = e^{-sT} [R_B e^{-sT} \quad -1]$$

$$L' = \begin{bmatrix} -\frac{hQ(s)}{s(Zc + Z1)} X \\ -\frac{hQ(s)}{s(Zc + Z2)} \end{bmatrix} = \frac{-hQ(s)}{2sZc} \begin{bmatrix} T_F \cdot X \\ T_B \end{bmatrix}$$

$$\Delta = 1 - R_F R_B e^{-2sT}$$

$$X = \left[ \frac{Z1}{Zc} e^{st'} - \frac{Z1}{Zc} e^{-st'} - 1 + e^{st'} + e^{-st'} \right]$$

### 7.3.1 Relationship Between Force and Charge for Transmitter:

The equation relating the force created at each face of the transducer to the charge deposited on the transducers electrodes is developed here.

As was found before the force in any point x within the transducer is given by the equation 7.5:

$$F_x(s) + h Q(s) = s Zc \{ -A e^{-s(x/vc)} + B e^{s(x/vc)} \} \quad \text{Normal layer}$$

$$F_x(s) - h Q(s) = s Zc \{ -A' e^{-s(x/vc)} + B' e^{s(x/vc)} \} \quad \text{Inversion layer}$$

Substituting A', B' in terms of A and B as in equation 7.10c and then substituting A and B yields:

$$F_x(s) + h Q(s) = s Zc \left\{ -\frac{(J1)(L')}{\Delta} e^{-s(x/vc)} + \frac{(J2)(L')}{\Delta} e^{s(x/vc)} \right\}$$

$$F_x(s) - h Q(s) = s Zc \left\{ \left( -\frac{hQ(s)}{sZc} e^{st} - \frac{(J1)(L)}{\Delta} \right) e^{-s(x/vc)} + \left( -\frac{hQ(s)}{sZc} e^{-st} + \frac{(J2)(L)}{\Delta} \right) e^{s(x/vc)} \right\}$$

Substituting  $L$  and rearranging the terms gives:

$$F_x(s) = -h Q(s) \left\{ 1 - \frac{(J1) \begin{bmatrix} T_F \cdot X \\ T_B \end{bmatrix}}{2\Delta} e^{-s(x/vc)} + \frac{(J2) \begin{bmatrix} T_F \cdot X \\ T_B \end{bmatrix}}{2\Delta} e^{s(x/vc)} \right\}$$

————— 7.22

$$F_x(s) = h Q(s) \left\{ 1 - \left\{ \left( e^{st} - \frac{(J1) \begin{bmatrix} T_F \cdot X \\ T_B \end{bmatrix}}{2\Delta} \right) e^{-s(x/vc)} + \left( e^{-st} + \frac{(J2) \begin{bmatrix} T_F \cdot X \\ T_B \end{bmatrix}}{2\Delta} \right) e^{s(x/vc)} \right\} \right\}$$

Equation 7.22 gives the general Laplace transform relationship between the force at any position  $x$  within the transducer, in both the inverted and the un-inverted domains, and the charge developed on the transducer electrodes.

In the case of a device as transmitter, the forces at both the front and the rear faces of the transducer are the most important, i.e. at  $x = 0$  and  $x = L$  respectively. Where  $x = 0$  is for the inversion layer while  $x = L$  is for the un-inverted layer.

Substituting for  $x = 0$  in the inversion layer in equation 7.22 ( $F_{x=0}(s)$ ), gives the transform equation for the force at the front face of the transducer as follows:

$$\begin{aligned} F_F(s) &= h Q(s) \left\{ 1 - \left\{ \left( e^{st} - \frac{(J1) \begin{bmatrix} T_F \cdot X \\ T_B \end{bmatrix}}{2\Delta} \right) + \left( e^{-st} + \frac{(J2) \begin{bmatrix} T_F \cdot X \\ T_B \end{bmatrix}}{2\Delta} \right) \right\} \right\} \\ &= \frac{-hQ(s)}{2\Delta} \left\{ -2\Delta + 2\Delta (e^{st} + e^{-st}) - T_F \cdot X + R_F e^{-sT} T_B \right. \\ &\quad \left. + R_B e^{-2sT} T_F \cdot X - e^{-sT} T_B \right\} \end{aligned}$$

Substituting for  $\Delta$  and  $X$ , and noting that  $T_F = 1 + R_F$ ,  $T_B = 1 + R_B$  the previous equation gives:

$$F_F(s) = -h Q(s) \frac{(1 - R_F)}{2} K_{FI}(s) \Rightarrow$$

$$F_F(s) = -h Q(s) \frac{Z_1}{Z_C + Z_1} K_{FI}(s) \quad \text{————— 7.23}$$

Equation 7.23 gives the Laplace transform of the stress wave generated at the front face of the transducer.

Substituting for  $x = L$  in the un-inverted layer in equation 7.22 ( $F_{x=L}(s)$ ), gives the transform equation for the force at the rear face of the transducer as follows:

$$F_B(s) = -h Q(s) \left\{ 1 - \frac{(J1) \begin{bmatrix} T_F \cdot X \\ T_B \end{bmatrix}}{2\Delta} e^{-sT} + \frac{(J2) \begin{bmatrix} T_F \cdot X \\ T_B \end{bmatrix}}{2\Delta} e^{sT} \right\}$$

$$= \frac{-hQ(s)}{2\Delta} \left\{ 2\Delta - T_F \cdot X e^{-sT} + R_F e^{-2sT} T_B + R_B e^{-sT} T_F \cdot X - T_B \right\}$$

Substituting for  $\Delta$  and  $X$ , and noting that  $T_F = 1 + R_F$ ,  $T_B = 1 + R_B$  the above equation gives:

$$F_B(s) = -h Q(s) \frac{Z_2}{Z_C + Z_2} K_{BI}(s) \quad \text{————— 7.24}$$

Equation 7.24 gives the transform of the stress wave generated at the rear face of the transducer.

Where  $K_{FI}(s)$  and  $K_{BI}(s)$  have the same value given in equation 7.15 as follows:

$$K_{FI}(s) = \frac{-e^{-sT} + 2e^{-st} - 1 - R_B e^{-sT} + 2R_B e^{-2sT} e^{st} - R_B e^{-2sT}}{\Delta}$$

$$K_{BI}(s) = \frac{e^{-sT} - 2e^{-sT}e^{st} + 1 + R_F e^{-sT} - 2R_F e^{-sT}e^{-st} + R_F e^{-2sT}}{\Delta}$$

Equations 7.23 and 7.24 give the Laplace transforms of the waves of force radiating into the surrounding media when the transducer is stimulated electrically by a charge whose Laplace transform is  $Q(s)$ .

When the device works as a receiver  $K_{FI}$  and  $K_{BI}$  are related to the difference in displacement produced at opposite faces of the transducer under conditions of external mechanical stress. When the device is a transmitter,  $K_{FI}$  and  $K_{BI}$  describes the stress behaviour for both the transducer faces when the latter are displaced due to the inverse piezoelectric effect by applying a function of charge to the electrodes.

### 7.3.2 Relationship Between Voltage and Charge for Transmitter:

To develop the transfer function relating the applied voltage to the output forces of the transducer as a transmitter we need to substitute for  $Q(s)$  in terms of the voltage  $V(s)$  in equations 7.23 and 7.24.

From equation 7.7 the following may be written:

$$V(s) = -h \{ \xi c_{(x=L)} - 2 \xi c_{(x=r)} + \xi c_{(x=0)} \} + Q(s) / C_0$$

Substituting for the different displacement at the boundaries yields:

$$V(s) = -h \{ A e^{-sT} + B e^{sT} - 2 A e^{-st} - 2 B e^{st} + A' + B' \} + Q(s) / C_0$$

Substituting for  $A'$  and  $B'$  in terms of  $A$  and  $B$  from equation 7.10c and arranging the terms gives:

$$V(s) = -h \left\{ A (e^{-sT} - 2 e^{-st} + 1) + B (e^{sT} - 2 e^{st} + 1) + \frac{hQ(s)}{sZc} (e^{st} - e^{-st}) \right\} + \frac{Q(s)}{C_0}$$

Substituting for A and B yields:

$$\begin{aligned}
 V(s) &= -h \left\{ \frac{(J1)(L')}{\Delta} (e^{-sT} - 2e^{-st'} + 1) + \frac{(J2)(L')}{\Delta} (e^{sT} - 2e^{st'} + 1) \right. \\
 &\quad \left. + \frac{hQ(s)}{sZc} (e^{st'} - e^{-st'}) \right\} + \frac{Q(s)}{C_0} \\
 &= + \frac{h^2 Q(s)}{2sZc\Delta} \left\{ (J1) \begin{bmatrix} T_F \cdot X \\ T_B \end{bmatrix} (e^{-sT} - 2e^{-st'} + 1) + \right. \\
 &\quad \left. (J2) \begin{bmatrix} T_F \cdot X \\ T_B \end{bmatrix} (e^{sT} - 2e^{st'} + 1) - 2\Delta (e^{st'} - e^{-st'}) \right\} + \frac{Q(s)}{C_0}
 \end{aligned}$$

Hence:

$$\begin{aligned}
 V(s) &= + \frac{h^2 Q(s)}{2sZc\Delta} \left\{ (T_F \cdot X - R_F e^{-sT} T_B) (e^{-sT} - 2e^{-st'} + 1) + \right. \\
 &\quad \left. (R_B e^{-2sT} T_F \cdot X - T_B e^{-sT}) (e^{sT} - 2e^{st'} + 1) - 2\Delta (e^{st'} - e^{-st'}) \right\} + \frac{Q(s)}{C_0} \\
 &= + \frac{h^2 Q(s)}{2sZc\Delta} \left\{ T_F \cdot X (e^{-sT} - 2e^{-st'} + 1 + R_B e^{-sT} - 2R_B e^{-2sT} e^{st'} + R_B e^{-2sT}) \right. \\
 &\quad \left. + T_B (-R_F e^{-2sT} + 2R_F e^{-sT} e^{-st'} - R_F e^{-sT} - 1 + 2e^{-sT} e^{st'} - e^{-sT}) \right. \\
 &\quad \left. - 2\Delta (e^{st'} - e^{-st'}) \right\} + \frac{Q(s)}{C_0} \\
 V(s) &= - \frac{h^2 Q(s)}{s} \left\{ \frac{K_{FI}(s)}{Zc + Z1} \cdot X + \frac{K_{BI}(s)}{Zc + Z2} + \frac{e^{st'} - e^{-st'}}{Zc} \right\} + \frac{Q(s)}{C_0}
 \end{aligned}$$

or:

$$V(s) = \frac{Q(s)}{C_0} \left\{ 1 - \frac{h^2 C_0}{sZc} \left[ K_{FI}(s) \cdot X \frac{T_F}{2} + K_{BI}(s) \cdot \frac{T_B}{2} + e^{st'} - e^{-st'} \right] \right\} \quad \text{--- 7.25}$$

Equation 7.25 gives the relationship, in the Laplace domain, between the voltage across the transducer and the charge developed on its electrodes.

For a transducer without an inversion layer,  $t' = 0$ , equation 7.25 yields:

$$V(s) = \frac{Q(s)}{C_0} \left\{ 1 - \frac{h^2 C_0}{sZc} \left[ K_F(s) \frac{T_F}{2} + K_B(s) \cdot \frac{T_B}{2} \right] \right\}$$

This is the same equation that was found by Hayward [35] for a normal transducer without an inversion layer.

From equation 7.25 it is easy to obtain the electrical impedance of the transducer defined as:

$$Z_T(s) = \frac{V(s)}{I(s)} = \frac{V(s)}{sQ(s)}$$

Therefore from equation 7.25 we may write:

$$Z_T(s) = \frac{1}{sC_0} \left\{ 1 - \frac{h^2 C_0}{sZc} \left[ K_{FI}(s) \cdot X \frac{T_F}{2} + K_{BI}(s) \cdot \frac{T_B}{2} + e^{st'} - e^{-st'} \right] \right\} \quad \text{--- 7.26}$$

### 7.3.3 Developing the Transfer Function of the Transmitter:

Considering the electrical circuit configuration outlined in Fig 7.7; where the transducer is connected to a non-ideal voltage source having an output impedance  $Z_0$ , and an arbitrary electrical load  $Z_E$ .

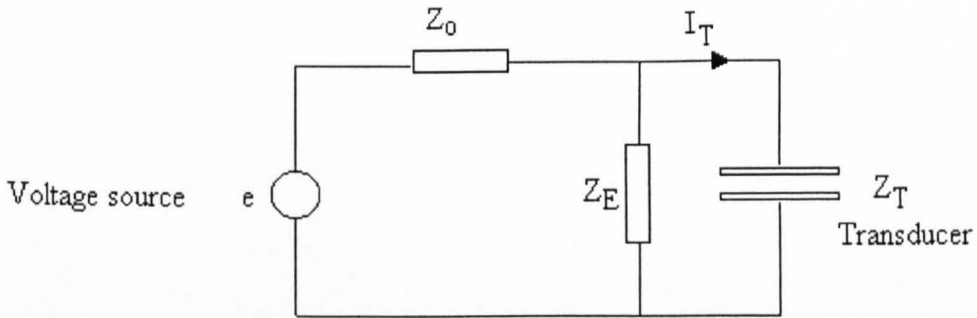


Fig (7.7): Transmitter circuit configuration.

For the electrical configuration in Fig 7.7, the voltage-current relationship of the voltage source  $e(s)$  and the current across the transducer  $I_T(s)$  is given as follows:

$$\frac{I_T(s)}{e(s)} = \frac{Z_E}{Z_T(Z_0 + Z_E) + Z_0 Z_E}$$

Where all the impedances  $Z_E$ ,  $Z_0$  and  $Z_T$  are functions of  $s$ .

Rearranging the above equation yields:

$$\frac{I_T(s)}{e(s)} = \frac{\frac{Z_E}{Z_0 + Z_E}}{Z_T + \frac{Z_0 Z_E}{Z_0 + Z_E}} = \frac{a(s)}{Z_T(s) + b(s)}$$

Therefore:

$$I_T(s) = \frac{a(s)e(s)}{Z_T(s) + b(s)}$$

Hence:

$$Q(s) = \frac{a(s)e(s)}{s\{Z_T(s) + b(s)\}} \quad \text{—————} \quad 7.27$$

Equations 7.23 and 7.24 may be rewritten as:

$$F_F(s) = -h Q(s) \frac{A_F}{2} K_{FI}(s)$$

$$F_B(s) = -h Q(s) \frac{A_B}{2} K_{BI}(s)$$

Where:

$$\frac{A_F}{2} = \frac{Z1}{Zc + Z1}, \quad \frac{A_B}{2} = \frac{Z2}{Zc + Z2}$$

Substituting Q(s) from equation 7.27 for F<sub>F</sub>(s) yields:

$$\frac{F_F(s)}{e(s)} = \frac{-ha(s)}{s\{Z_T(s) + b(s)\}} \frac{A_F}{2} K_{FI}(s)$$

Substituting Z<sub>T</sub> from equation 7.26 yields:

$$\begin{aligned} \frac{F_F(s)}{e(s)} &= \frac{-ha(s) \frac{A_F}{2} K_{FI}(s)}{s\left\{\frac{1}{sC_o} - \frac{h^2}{s^2 Zc} (K_{FI}(s).X \frac{T_F}{2} + K_{BI}(s) \frac{T_B}{2} + e^{st'} - e^{-st'}) + b(s)\right\}} \\ &= \frac{-ha(s) \frac{A_F}{2} K_{FI}(s)}{\left\{\frac{1 + b(s)C_o s}{C_o}\right\} - \frac{h^2}{sZc} \left\{K_{FI}(s).X \frac{T_F}{2} + K_{BI}(s) \frac{T_B}{2} + e^{st'} - e^{-st'}\right\}} \end{aligned}$$

$$\text{Let } Y(s) = \frac{C_o}{1 + b(s)C_o s} \Rightarrow$$

$$\frac{F_F(s)}{e(s)} = \frac{-ha(s) \frac{A_F}{2} Y(s) K_{FI}(s)}{1 - \frac{h^2}{sZc} Y(s) \{ K_{FI}(s) \cdot X \frac{T_F}{2} + K_{BI}(s) \frac{T_B}{2} + e^{st} - e^{-st} \}} \quad \text{--- 7.28}$$

This equation gives the transfer function relating the stress wave generated into the load medium to the input voltage for a transmitter incorporating a front face inversion layer.

Substituting  $s = j\omega$ , where  $\omega = 2\pi f$  in equation 7.28 gives the force as a function of the frequency  $f$ . Dividing the result by the area of the transducer gives the pressure on the front face of the transducer. Plotting the normalized pressure magnitude of the front face using MATLAB for the parameters given in table 7.4 for a  $\text{LiNbO}_3$  transducer having 0, 0.3 and 0.5 inversion layer thickness ratios and for input voltage as a pulse having a width 3.6ns (the same input used for the FEM analysis), gives the graphs shown in Fig 7.8.

The device was electrically excited via a 50 ohm generator, as can be seen from table 7.4.

Plotting the normalized pressure magnitude again for  $\text{LiNbO}_3$  transducer for the same parameters given in table 7.4 but in this case for  $Z_2 = 18 \text{ MRayl}$ , i.e. 50% backing; gives the graphs shown in Fig 7.9.

Table (7.4): The Lithium niobate transducer parameters for the transmitter.

$Z_E$	$Z_o$	$Z_1$	$Z_2$	$Z_c$	$v_c$	$h$	$\Gamma$	$L$	$C_o$
Ohm	Ohm	MRayl	MRayl	MRayl	m/s	V/m	mm	mm	PF
$\infty$		1.5	34.				0		
Open	50.	Water	Matched	34.	7340	1.34	0.078	0.26	133
Circuit		Load	Backing			$* 10^{+10}$	0.13		

The Acoustic impedance is per unit area (The area is the transducer surface). The transducer has a radius of 5mm.

In the same way, the transfer function relating the stress wave generated into the backing medium,  $F_B(S)$ , to the input voltage can be found to be:

$$\frac{F_B(s)}{e(s)} = \frac{-ha(s) \frac{A_B}{2} Y(s) K_{BI}(s)}{1 - \frac{h^2}{sZ_c} Y(s) \{ K_{FI}(s) \cdot X \frac{T_F}{2} + K_{BI}(s) \frac{T_B}{2} + e^{st} - e^{-st} \}} \quad \text{--- 7.29}$$

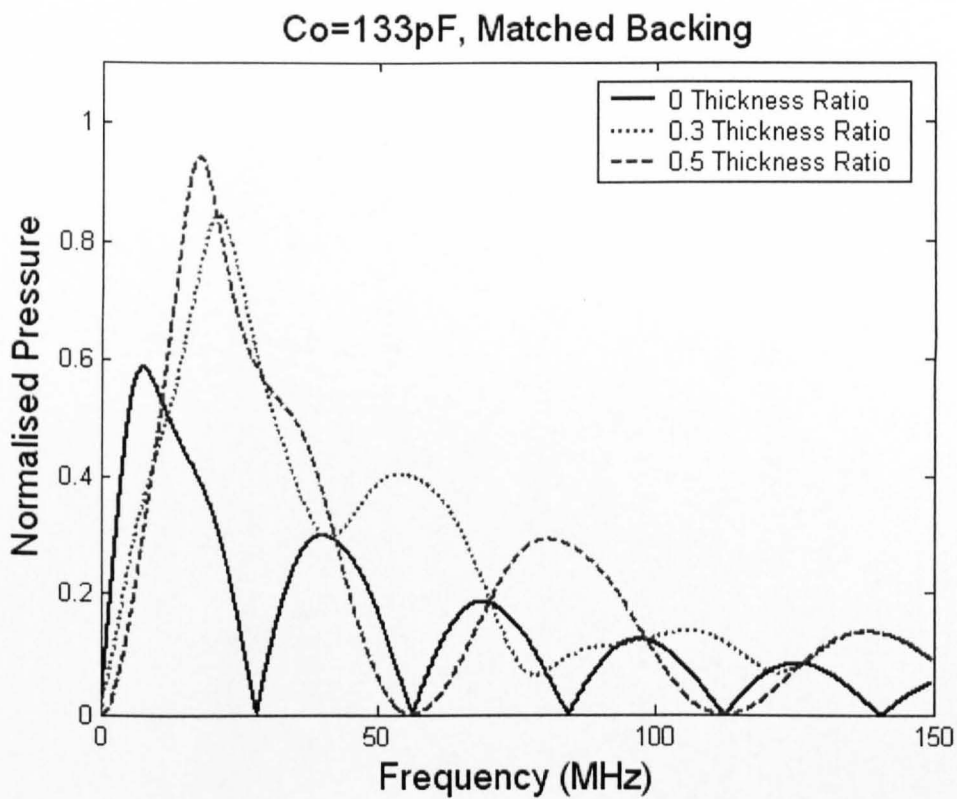


Fig (7.8): The normalised pressure magnitude on the front face of the transducer incorporating front face inversion layer for different thickness ratios and matched backing.

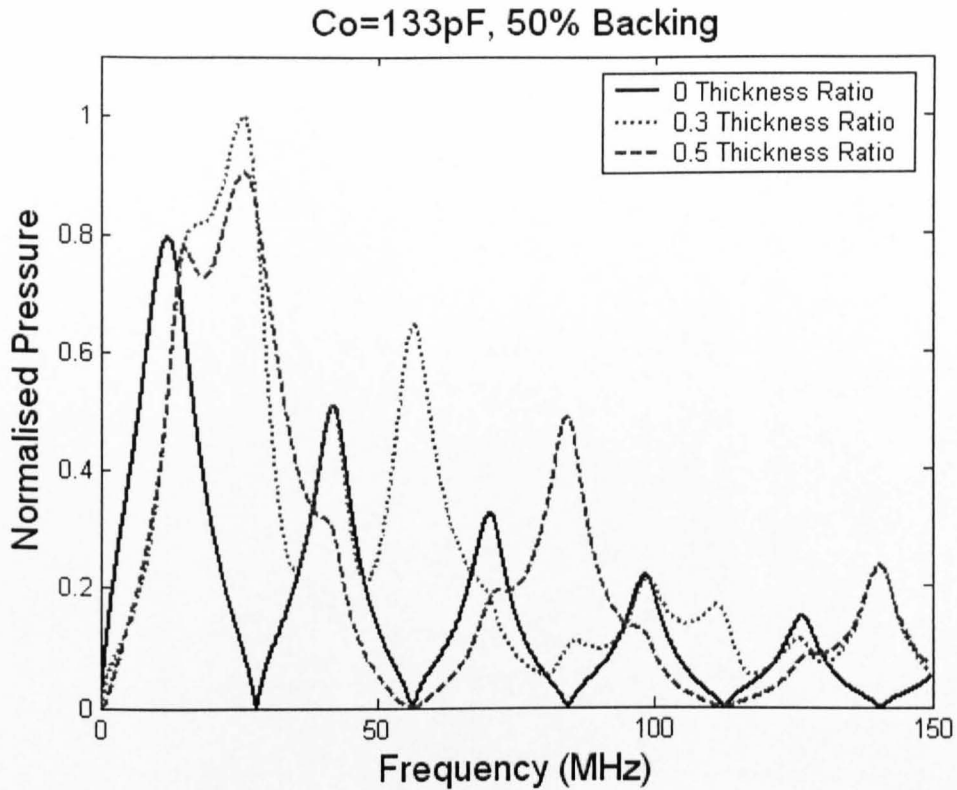


Fig (7.9): The normalised pressure magnitude on the front face of the transducer incorporating front face inversion layer for different thickness ratios and 50% backing.

Figures 7.8 and 7.9 show the same results described in the FEM result for the different harmonics. For 50% backing the peaks of the fundamental the second and the third harmonic are more clearly separated compared to the case of matched backing. The position of the different peaks is related to the thickness ratio. As was noted in the FEM results, the matched backing will significantly reduce the higher peak for the case of no inversion layer, while this decrease is much less in the presence of an inversion layer. The results of both the FEA modelling and the mathematical model are plotted together for the different thickness ratios in Figs 7.10-7.15.

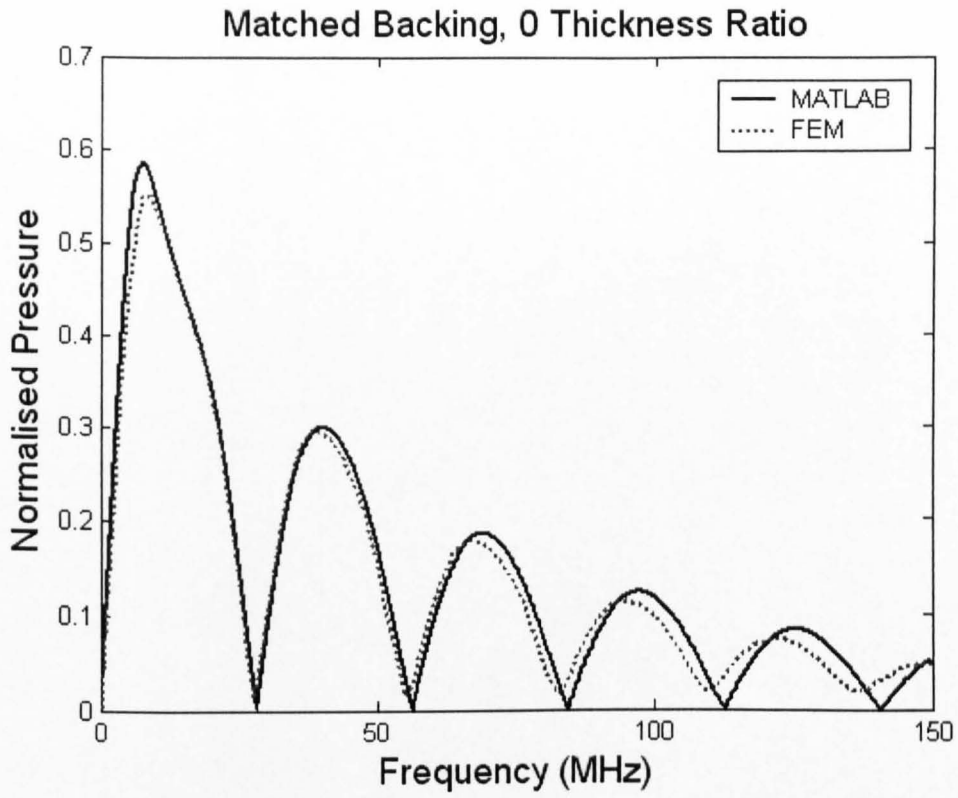


Fig (7.10): The normalised pressure magnitude in the front face of LiNbO<sub>3</sub> transducer for both the FEM Analysis and the mathematical model (simulated using MATLAB).

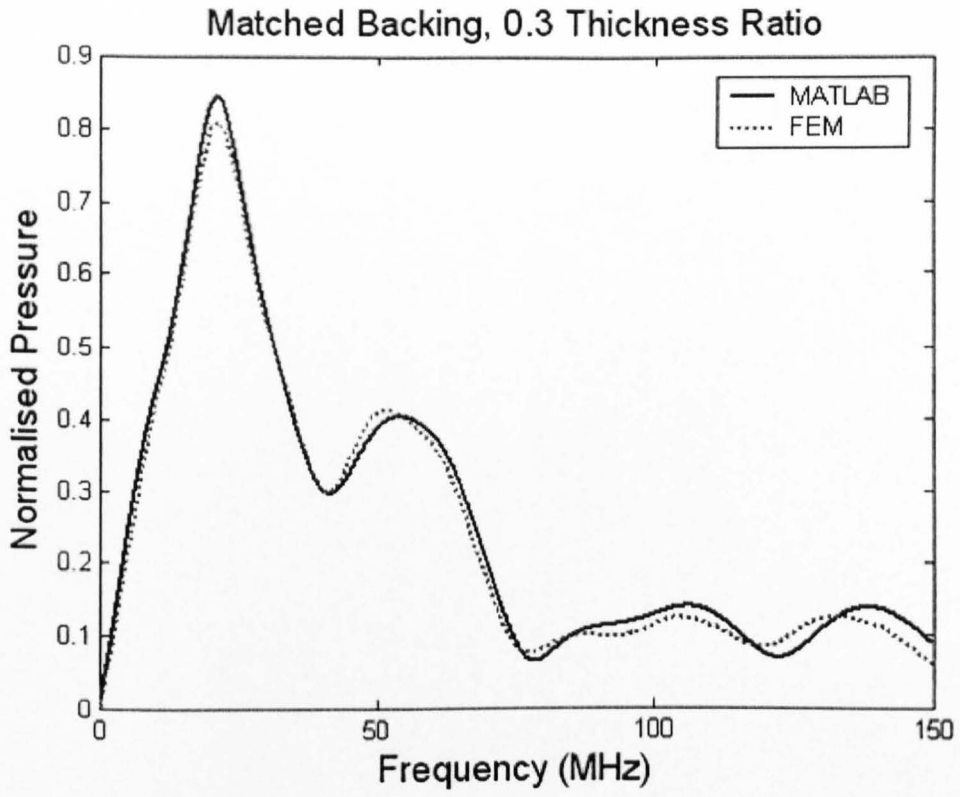


Fig (7.11): The normalised pressure magnitude in the front face of LiNbO<sub>3</sub> transducer for both the FEM analysis and the mathematical model (simulated using MATLAB).

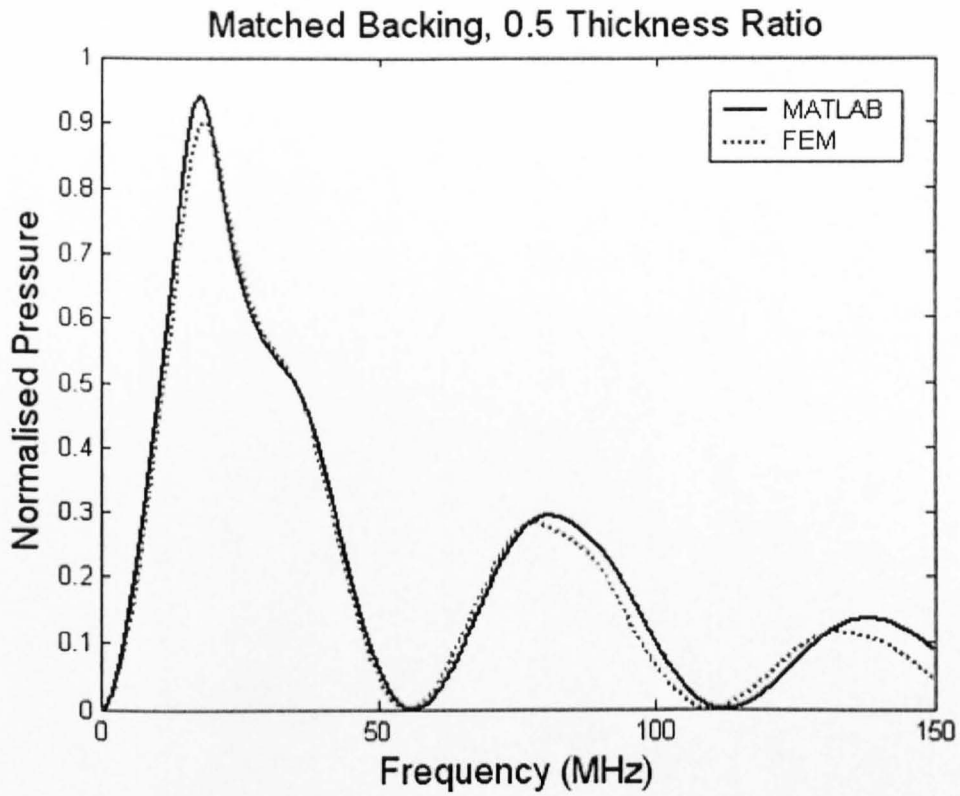


Fig (7.12): The normalised pressure magnitude in the front face of LiNbO<sub>3</sub> transducer for both the FEM analysis and the mathematical model (simulated using MATLAB).

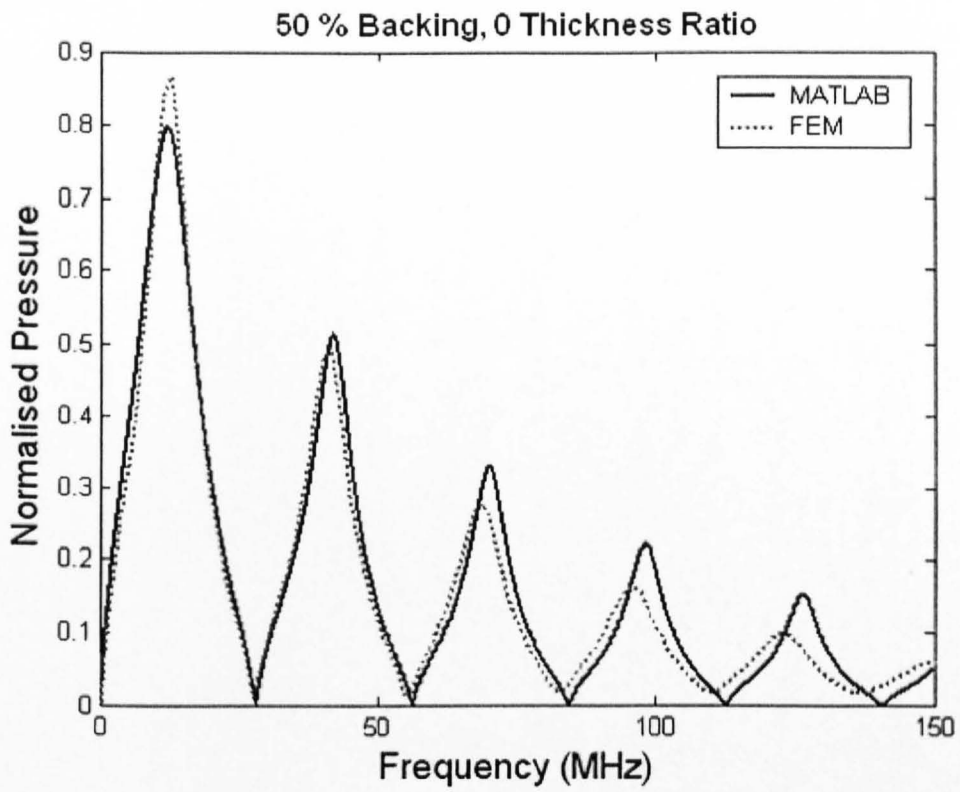


Fig (7.13): The normalised pressure magnitude in the front face of LiNbO<sub>3</sub> transducer for both the FEM analysis and the mathematical model (simulated using MATLAB).

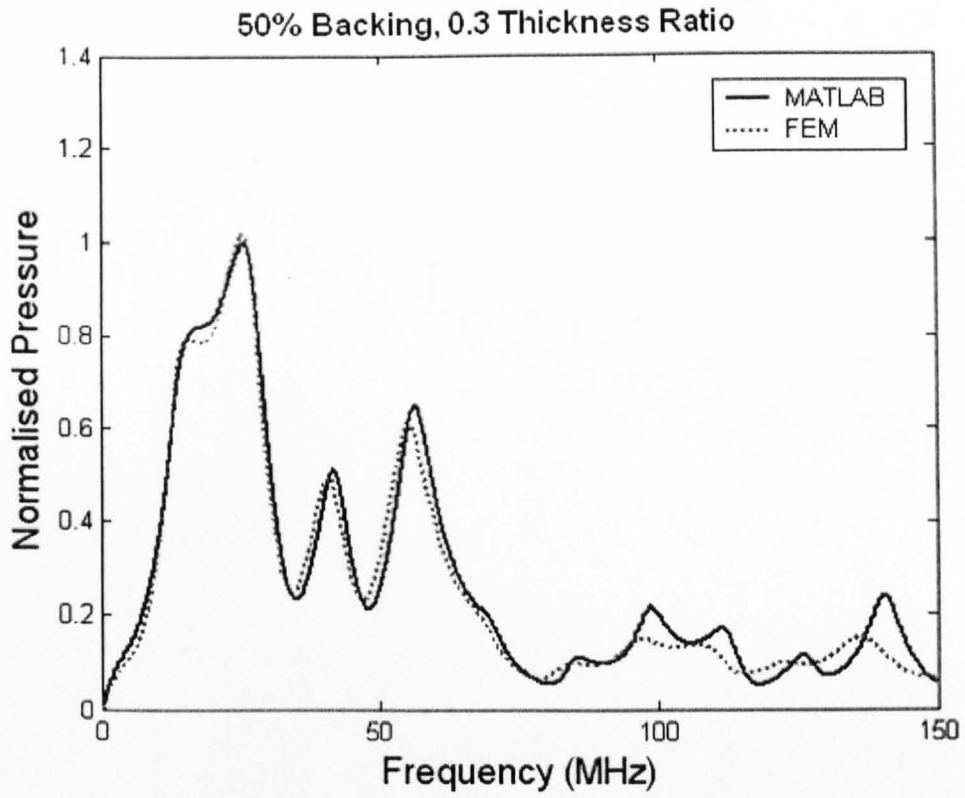


Fig (7.14): The normalised pressure magnitude in the front face of LiNbO<sub>3</sub> transducer for both the FEM analysis and the mathematical model (simulated using MATLAB).

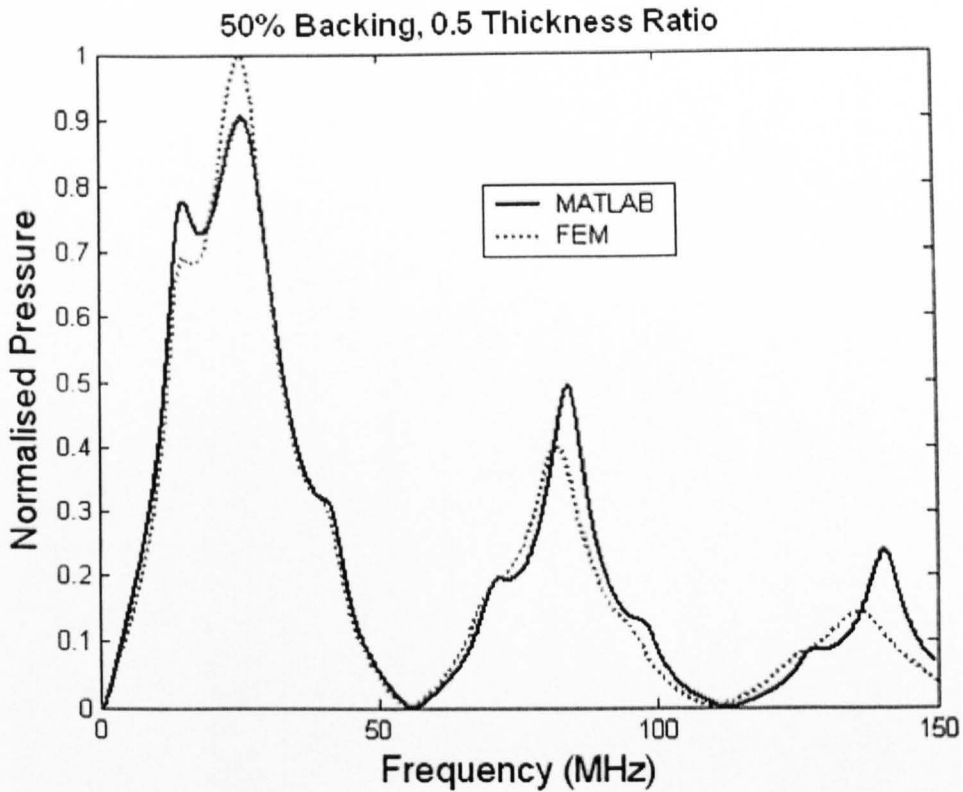


Fig (7.15): The normalised pressure magnitude in the front face of  $\text{LiNbO}_3$  transducer for both the FEM analysis and the mathematical model (simulated using MATLAB).

All the previous graphs show good agreement between the FEM analysis and the mathematical model. Slight differences can be seen between the two approaches. This might be due to the fact that assumptions were made in the linear systems model to simplify the analysis, as mentioned at the beginning of this Chapter. However, the close agreement between the two data sets in all cases seems to confirm the validity of the linear systems model theory.

To check the effect of the electrical load on the output force or pressure, the impedance  $Z_o$  was changed from 50 to 150 ohm. The resulted normalised pressure magnitudes are shown in Figs 7.16 and 7.17.

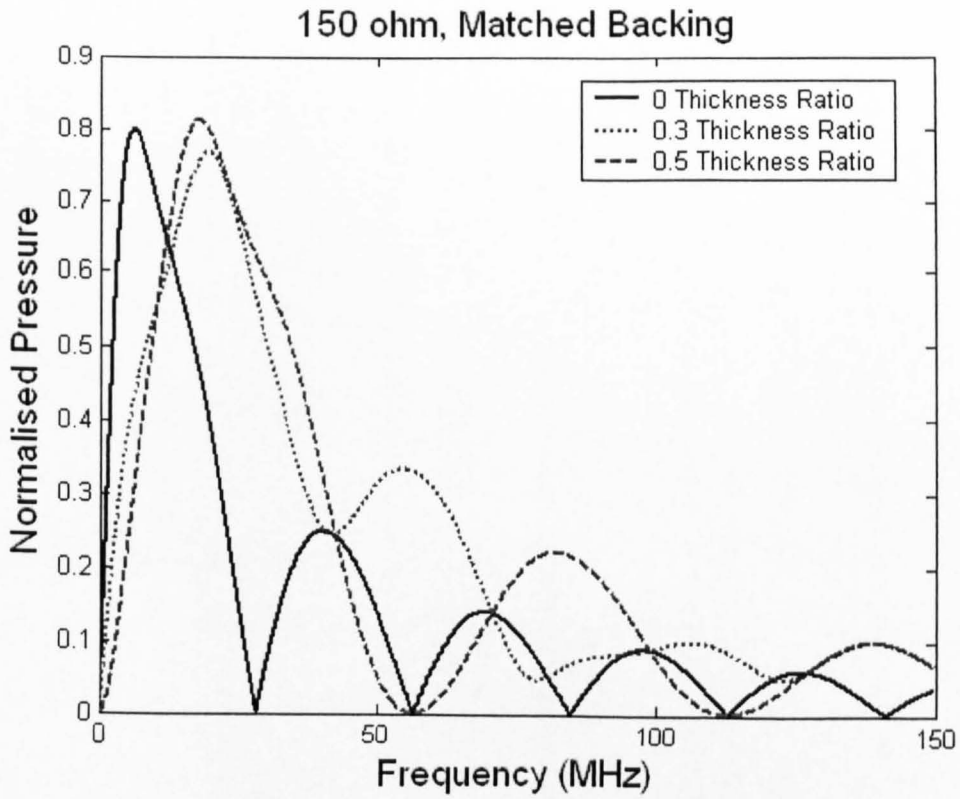


Fig (7.16): The normalised pressure magnitude for  $Z_o = 150$  ohm.

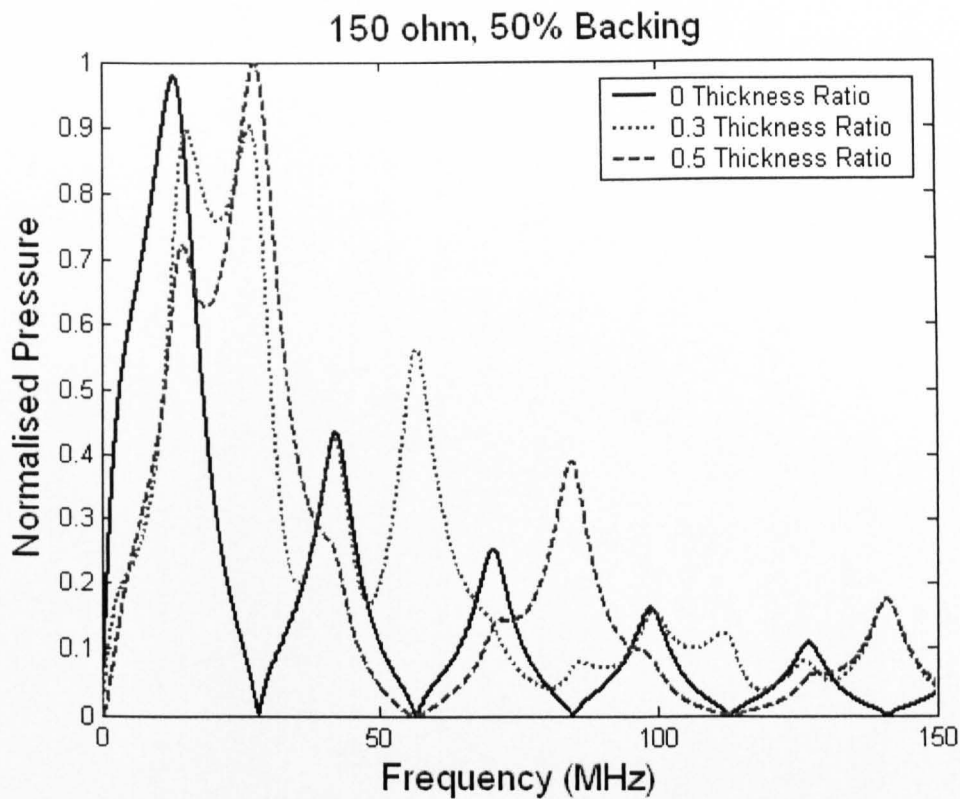


Fig (7.17): The normalised pressure magnitude for  $Z_0 = 150$  ohm.

The previous two graphs, when compared to the previous cases with  $Z_0 = 50$  ohm, show that changing the electrical circuit connected to the transmitter will alter the peak values. In this case it is also clear that the decrease of the peaks values when the backing was changed from 50% to matched backing, will be approximately the same for all the cases whether the inversion layer is absent or presence.

The presence of the inversion layer improved the sensitivity of the transmitter as was the case for the receiver.

### **7.3.4 The Pulse-Echo Mode:**

In the pulse echo mode the same transducer is used for transmission and then reception. The transfer function in this case is the product of the transfer function of the transmitter and the receiver, i.e. the product of equations 7.28 and 7.17a. To check the pulse width for the pulse-echo mode, the IFFT was performed to obtain the time domain using the parameters in table 7.4. The pulse widths were calculated for both matched and 50% backing and are shown in Fig (7.17a). The pulse width was approximately the same whether the inversion layer was present or absent, giving a value of 80 and 190ns for matched and 50% backing respectively.

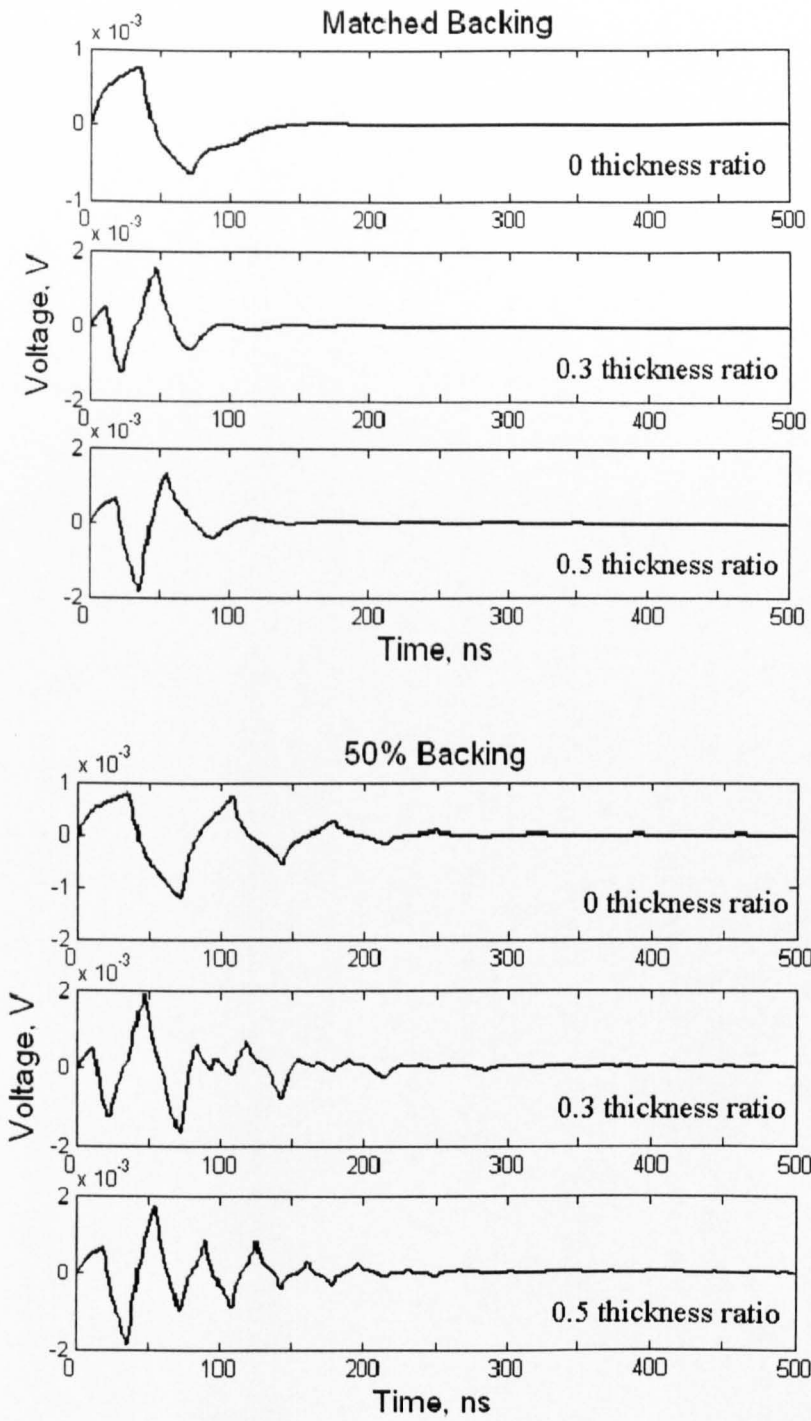


Fig (7.17a): The time response for the pulse-echo mode for matched and 50% backing and different thickness ratio.

## 7.4 Electrical Impedance Analysis:

The expression giving the electrical impedance of the transducer in equation 7.26 was found to be:

$$Z_T(s) = \frac{1}{sC_0} \left\{ 1 - \frac{h^2 C_0}{sZ_c} \left[ K_{FI}(s) \cdot X \frac{T_F}{2} + K_{BI}(s) \cdot \frac{T_B}{2} + e^{st} - e^{-st} \right] \right\}$$

This expression gives the transfer function of the relation between the voltage across the transducer and the current.

The electro mechanical coupling coefficient,  $k$ , for a piezoelectric material is a measure of the efficiency of the device when converting the electrical voltage to mechanical displacement and vice versa; and is defined as:

$$k = h_{33} \left[ \frac{\epsilon_{33}^S}{\hat{Y}_{33}^D} \right]^{1/2}$$

All the suffixes have been defined previously.

Rewriting the above formula after dropping the suffixes yields:

$$k^2 = h^2 \left[ \frac{\epsilon}{\hat{Y}} \right]$$

The permittivity,  $\epsilon$ , is related to the capacity  $C_0$  as follows:

$$\epsilon = \frac{LC_0}{A}$$

And the elastic constant,  $\hat{Y}$ , is related to the longitudinal velocity  $vc$  as follows:

$$\hat{Y} = vc^2 \rho$$

Using these relationships and noting that  $L/vc = T$ ,  $Z_c = A \cdot vc \rho$ , we obtain:

$$h^2 C_o = \frac{k^2 Z_c}{T} \quad \text{—————} \quad 7.30$$

Substituting equation 7.30 into the equation defining  $Z_T$  we may write:

$$Z_T(s) = \frac{1}{sC_o} \left\{ 1 - \frac{k^2}{sT} \left[ K_{FI}(s) \cdot X \frac{Z_c}{Z_c + Z_1} + K_{BI}(s) \cdot \frac{Z_c}{Z_c + Z_2} + e^{st} - e^{-st} \right] \right\} \quad \text{————} \quad 7.31$$

Consider the device to be operating in the mechanically free state. This situation is approximated by an air medium surrounding the transducer, i.e. air backing and air load. In this case both  $R_F$  and  $R_B$  are equal to unity and  $Z_1 = Z_2 \approx 0$ . Consequently, equation 7.31 for the transducer impedance incorporating a front face inversion layer may be rewritten as follows:

$$Z_T(s) = \frac{1}{sC_o} \left\{ 1 - \frac{k^2}{sT} \left[ K_{F0}(s) \cdot X_0 + K_{B0}(s) \cdot + e^{st} - e^{-st} \right] \right\} \quad \text{————} \quad 7.32$$

Where:

$$X_0 = -1 + e^{st} + e^{-st}$$

$$\Delta = 1 - e^{-2sT}$$

$$K_{F0}(s) = \frac{-2e^{-sT} + 2e^{-st} - 1 + 2e^{-2sT}e^{st} - e^{-2sT}}{1 - e^{-2sT}}$$

$$K_{B0}(s) = \frac{2e^{-sT} - 2e^{-sT}e^{st} + 1 - 2e^{-sT}e^{-st} + e^{-2sT}}{1 - e^{-2sT}}$$

Substituting for  $t = 0$  for no inversion layer in equation 7.32 yields:

$$Z_T(s) = \frac{1}{sC_0} \left\{ 1 - \frac{k^2}{sT} \left[ \frac{1 - 2e^{-sT} + e^{-2sT}}{1 - e^{-2sT}} + \frac{1 - 2e^{-sT} + e^{-2sT}}{1 - e^{-2sT}} \right] \right\}$$

Rearranging the above equation gives:

$$Z_T(s) = \frac{1}{sC_0} \left\{ 1 - \frac{2k^2}{sT} \left[ \frac{1 - e^{-sT}}{1 + e^{-sT}} \right] \right\} \quad \text{————— 7.33}$$

This is the same equation found by Hayward [35], for a normal transducer with no inversion layer.

Substituting  $s = j 2\pi f$  in equation 7.32 and plotting the magnitude of the impedance for different thickness ratios, gives the graphs shown in Fig 7.18. The parameters used are listed in table 7.5.

Table (7.5): The Lithium niobate transducer parameters for the impedance simulation.

Z1 MRayl	Z2 MRayl	k	vc m/s	l' mm	L mm	C <sub>o</sub> PF
≈ 0 (Air)	≈ 0 (Air)	0.48	7340.	0 0.078 0.13	0.26	133.

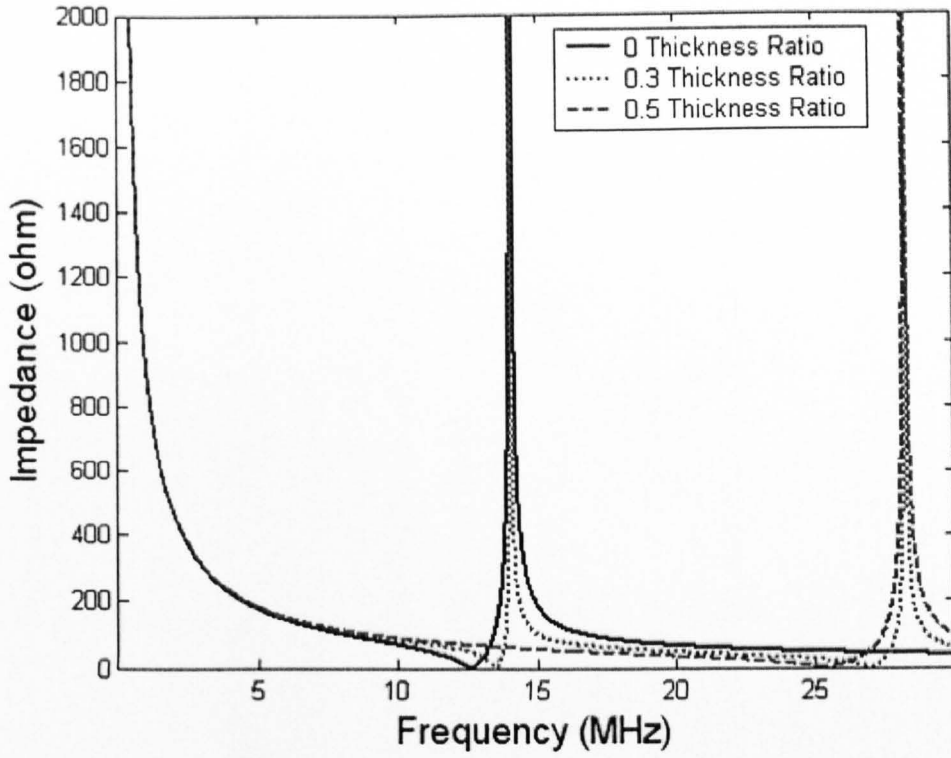


Fig (7.18): The impedance plot for different thickness ratios.

The results in Fig 7.18 are similar to those obtained by the FEA (Fig 6.3).

Plotting the impedance magnitude obtained from the FEM analysis and the mathematical model for the different thickness ratios gives the results shown in Figs 7.19-7.21.

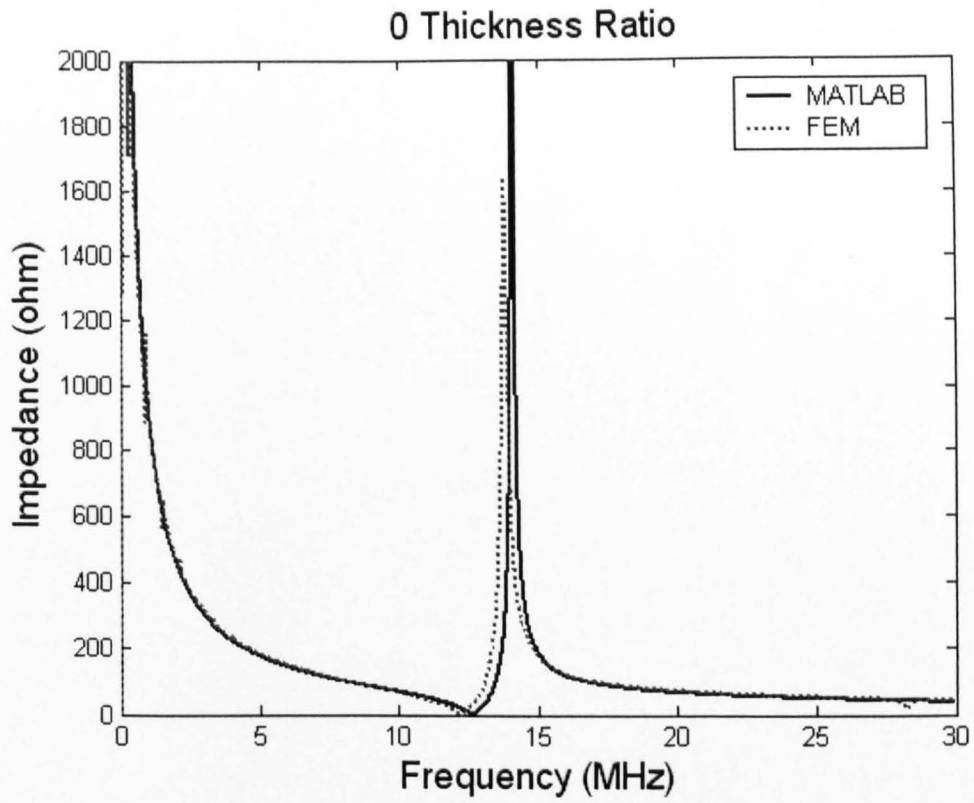


Fig (7.19): The impedance magnitude of both the FEM and the mathematical analysis (simulated using MATLAB) for 0 thickness ratio.

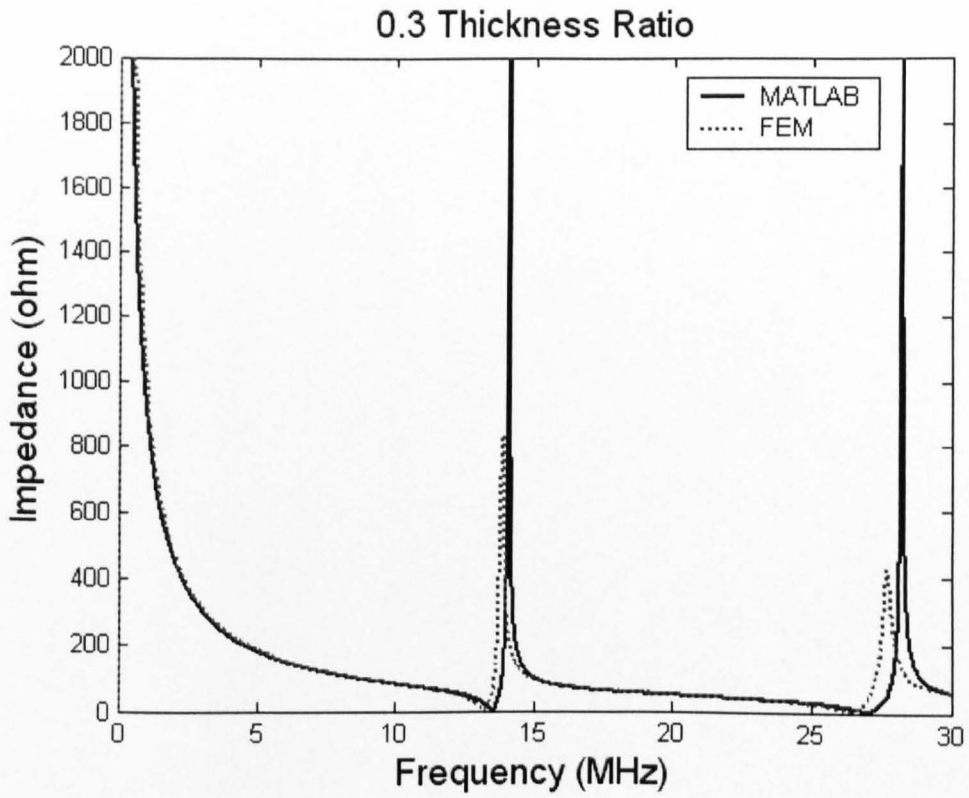


Fig (7.20): The impedance magnitude of both the FEM and the mathematical analysis (simulated using MATLAB) for 0.3 thickness ratio.

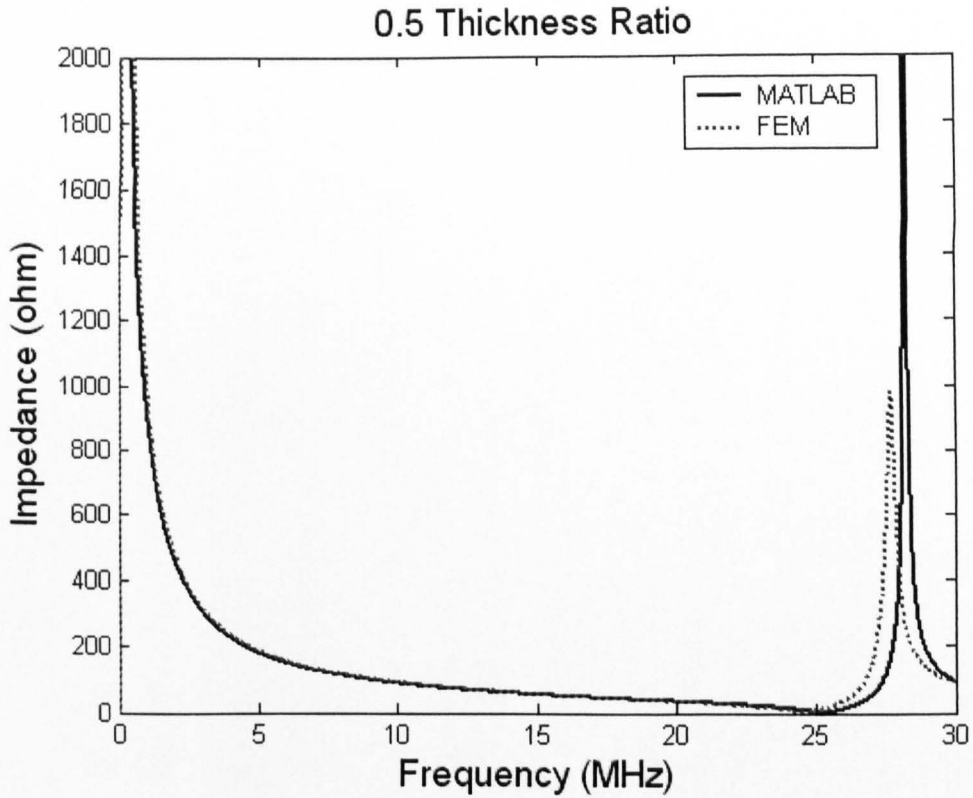


Fig (7.21): The impedance magnitude of both the FEM and the mathematical analysis (simulated using MATLAB) for 0.5 thickness ratio.

There is good matching between the results of the FEA and the mathematical model developed in this thesis. The higher peaks resulting from the mathematical model compared to the FEM might be due to the assumptions considered and also PZFlex used for the FE model is a more complete package.

Substituting  $X_0$ ,  $K_{F0}$  and  $K_{B0}$  in equation 7.32 and rearranging the terms yields:

$$Z_T(s) = \frac{1}{sC_0} \left\{ 1 - \frac{2k^2}{sT} \left[ \frac{1 - e^{-sT}}{1 + e^{-sT}} \right] \right\} - \frac{1}{sC_0} \left\{ \frac{2k^2}{sT} \left[ \frac{e^{-2sT} + 4e^{-sT} - 2e^{-2sT}e^{st'} + e^{-2sT}e^{2st'} - 2e^{-sT}e^{st'} - 2e^{-sT}e^{-st'} + 1 - 2e^{-st'} + e^{-2st'}}{1 - e^{-2sT}} \right] \right\}$$

This equation is composed of two parts and can be expressed as follows:

$$Z_T(s) = Z_{NIL} - \frac{1}{sC_0} \left\{ \frac{2k^2}{sT} \left[ \frac{e^{-2sT} + 4e^{-sT} - 2e^{-2sT}e^{st'} + e^{-2sT}e^{2st'} - 2e^{-sT}e^{st'} - 2e^{-sT}e^{-st'} + 1 - 2e^{-st'} + e^{-2st'}}{1 - e^{-2sT}} \right] \right\}$$

————— 7.34

Where:

$Z_{NIL}$  is the same value given in equation 7.33 for a normal transducer without inversion layer.

The second part of equation 7.34 expresses the effect of the inversion layer on the transducer impedance.

## 7.5 The Feedback System Block Diagrams and Physical Insight:

### 7.5.1 The Receiver Transfer Function Feedback System:

Equation 7.17a giving the transfer function of the receiver incorporating a front face inversion layer, can be represented as the feedback system shown in the block diagram in Fig 7.22.

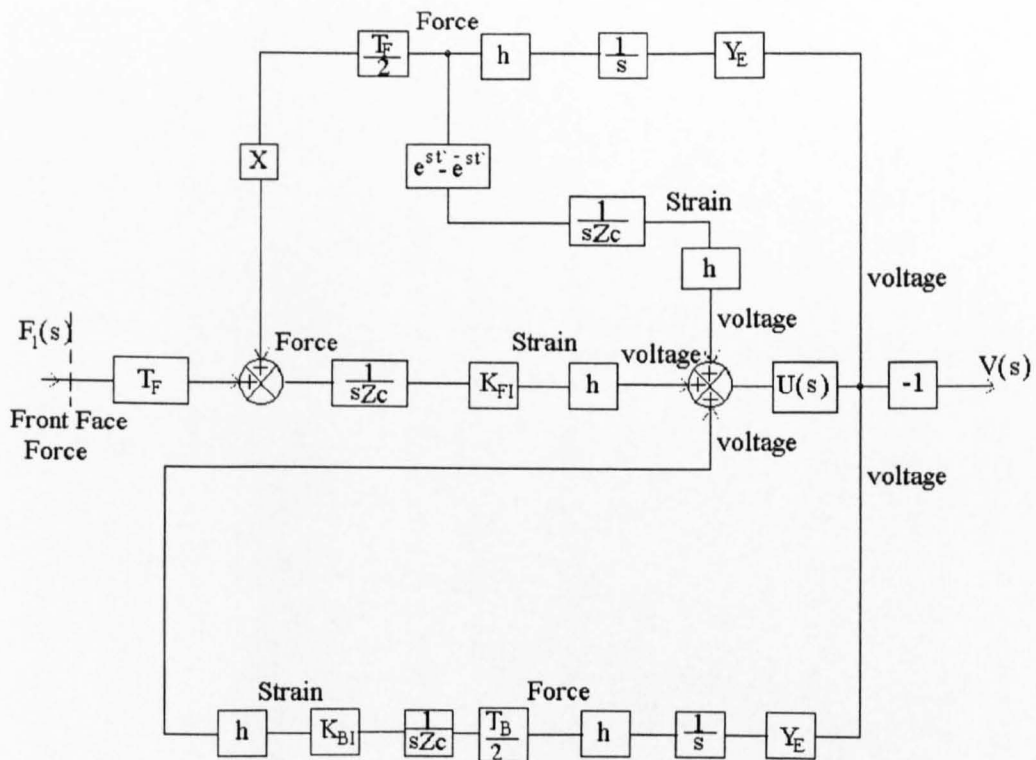


Fig (7.22): The block diagram of the feedback system for the transducer as a receiver.

A force applied to the transducer front face will reverberate forward and backward between the front and the back face of the transducer. This in turn will create particle

displacement in the transducer and the surrounding media. The term  $\frac{1}{sZc}$ , as was explained by Hayward [35], converts the pressure function inside the transducer to one of particle displacement. This particle displacement will propagate into the transducer and reverberate forward and backward between the front and the back face of the transducer, as is shown in Fig 7.23. Bearing in mind that the reflection coefficients for particle displacements are 180 degree out of phase with those of the pressure [48].

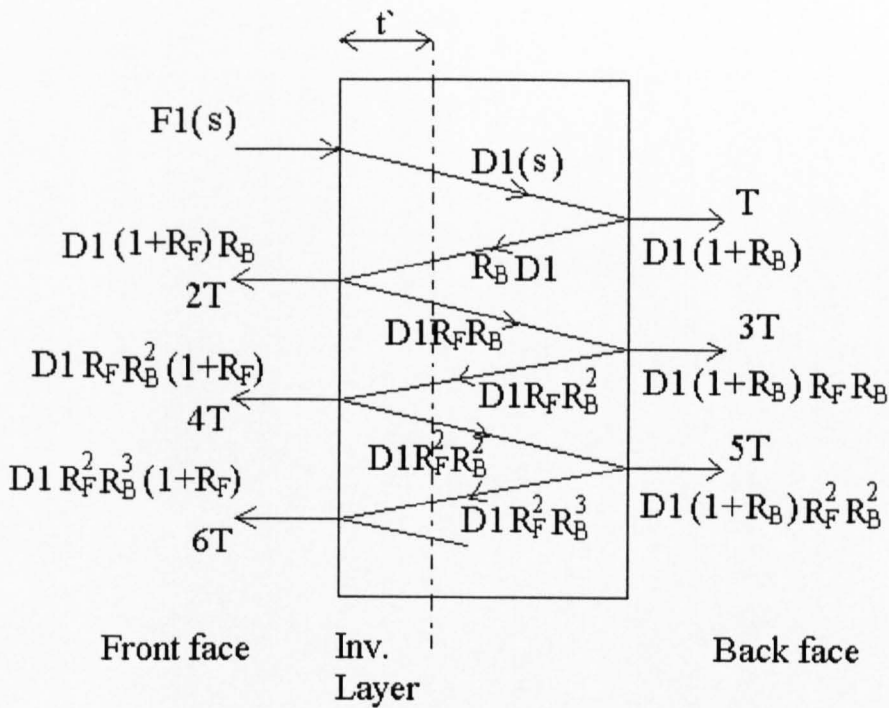


Fig (7.23): The reverberation of the particle displacement between the front and the back face.

From the figure above, the total displacement at the front face can be calculated as follows:

$$\begin{aligned}
\xi_F(s) &= D1(s) + D1(s) (1+R_F) R_B e^{-2sT} + D1(s) (1+R_F) R_F R_B^2 e^{-4sT} + \\
&\quad D1(s) (1+R_F) R_F^2 R_B^3 e^{-6sT} + \dots \\
&= D1(s) + D1(s) (1 + R_F) R_B e^{-2sT} \{ 1 + R_F R_B e^{-2sT} + R_F^2 R_B^2 e^{-4sT} + \dots \} \\
&= D1(s) + D1(s) (1 + R_F) R_B e^{-2sT} \sum_{n=0}^{\infty} (R_F R_B)^n e^{-2nsT}
\end{aligned}$$

The series given in the equation above is a geometric progression whose sum to infinity is expressed in the following formula:

$$\sum_{n=0}^{\infty} (R_F R_B)^n e^{-2nsT} = \frac{1}{1 - R_F R_B e^{-2sT}}$$

Therefore:

$$\xi_F(s) = D1(s) + D1(s) (1 + R_F) R_B e^{-2sT} \cdot \frac{1}{1 - R_F R_B e^{-2sT}}$$

$$\xi_F(s) = D1(s) \left\{ \frac{1 + R_B e^{-2sT}}{1 - R_F R_B e^{-2sT}} \right\} \quad \text{————— 7.35}$$

In the same way it can be found that the displacement on the back face is given by the formula:

$$\xi_B(s) = D1(s) \left\{ \frac{(1 + R_B) e^{-sT}}{1 - R_F R_B e^{-2sT}} \right\} \quad \text{————— 7.36}$$

The displacement  $\xi_{c'}$  at the border between the inversion and the original layer can also be calculated in the same way, where the delay term in this case is  $e^{-st'}$  from the front face. Hence the displacement can be calculated as follows:

$$\begin{aligned}
\xi_{c'} &= D1(s) e^{-st'} + D1(s) R_B e^{-s(2T+t')} + D1(s) R_F R_B e^{-s(2T+t')} + \\
&\quad D1(s) R_F R_B^2 e^{-s(4T+t')} + D1(s) R_F^2 R_B^2 e^{-s(4T+t')} \dots
\end{aligned}$$

$$\begin{aligned}
&= D1(s) \{ e^{-st'} + R_B e^{-2sT} e^{st'} + R_F R_B e^{-2sT} e^{-st'} + R_F R_B^2 e^{-4sT} e^{st'} \\
&\quad + R_F^2 R_B^2 e^{-4sT} e^{-st'} \dots \} \\
&= D1(s) \{ e^{-st'} (1 + R_F R_B e^{-2sT} + R_F^2 R_B^2 e^{-4sT} \dots) + \\
&\quad e^{st'} R_B e^{-2sT} (1 + R_F R_B e^{-2sT} + R_F^2 R_B^2 e^{-4sT} \dots) \} \\
&= D1(s) \left\{ e^{-st'} \left( \frac{1}{1 - R_F R_B e^{-2sT}} \right) + e^{st'} R_B e^{-2sT} \left( \frac{1}{1 - R_F R_B e^{-2sT}} \right) \right\} \\
\xi c' &= D1(s) \left\{ \frac{e^{-st'} + R_B e^{st'} e^{-2sT}}{1 - R_F R_B e^{-2sT}} \right\} \quad \text{-----} \quad 7.37
\end{aligned}$$

None of the previous equations take in account the secondary piezoelectric action included in the front and back face feedback loops in the block diagrams.

The voltage developed across the transducer is given in equation 7.8 as follows:

$$V(s) = -h \{ \xi c_{(x=L)} - 2 \xi c_{(x=l')} + \xi c'_{(x=0)} \} (s) \cdot \frac{s\tau(s)}{1 + s\tau(s)}$$

The voltage is proportional to the term:

$$V(s) \sim h \{ 2 \xi c_{(x=l')} - \xi c_{(x=L)} - \xi c'_{(x=0)} \} (s)$$

At the border between the inversion layer and the original layer  $\xi c_{(x=l')} = \xi c'_{(x=l')}$ ,

hence:

$$V(s) \sim h \{ 2 \xi c'_{(x=l')} - \xi_B - \xi_F \} (s)$$

Substituting  $\xi_F$ ,  $\xi_B$ , and  $\xi c'$  from equations 7.35, 7.36, and 7.37 respectively in the above equation yields:

$$\begin{aligned}
\{ 2 \xi c'_{(x=l')} - \xi_B - \xi_F \} (s) &= 2 D1(s) \left\{ \frac{e^{-st'} + R_B e^{st'} e^{-2sT}}{1 - R_F R_B e^{-2sT}} \right\} - \\
&D1(s) \left\{ \frac{(1 + R_B) e^{-sT}}{1 - R_F R_B e^{-2sT}} \right\} - D1(s) \left\{ \frac{1 + R_B e^{-2sT}}{1 - R_F R_B e^{-2sT}} \right\}
\end{aligned}$$

$$= D1(s) \left\{ \frac{-e^{-sT} + 2e^{-st} - 1 - R_B e^{-sT} + 2R_B e^{-2sT} e^{st} - R_B e^{-2sT}}{1 - R_F R_B e^{-2sT}} \right\}$$

$$\Rightarrow \{ 2 \xi c'_{(x=l)} - \xi_B - \xi_F \} (s) = D1(s) K_{FI}(s)$$

This equation explains the existence of  $K_{FI}(s)$  in the forward path in the block diagrams.  $K_{FI}(s)$  is called the reverberation factor of the particle displacement within the transducer in the presence of the inversion layer.

When no inversion layer exists this term will be equal to the different in displacement between the front and the back face of the transducer as explained by Hayward [35].

The term  $h$  is the piezoelectric constant relating the particle displacement to voltage or electrical charge to force.

When a force is incident on the transducer front face, a fraction is transmitted into the device, determined by  $T_F$ . This force then reverberates in the transducer cavity according to  $K_{FI}$ , producing a net strain, which creates a voltage due to  $h$ , which is then modified by the external load, producing a voltage across the electrodes. This voltage then produces three sets of secondary forces as shown in Fig 7.22. Two of these are generated at the piezoelectric boundaries between the device and the external load media. These two are non symmetric (the term  $X$  in the front face feedback loop), due to the inversion layer. The third component is generated at the piezoelectric boundary between the two piezoelectric layers and is described by the term  $e^{st} - e^{-st}$ . The in advance term  $e^{st}$  arises from the terms  $e^{-s(2T-t)}$ ,  $e^{-s(4T-t)}$  ... during the derivation of equation 7.37 which are normal delay terms, so in reality all the terms are delay terms and the system is stable.

### 7.5.2 The Transmitter Transfer Function Feedback System:

Equation 7.28 giving the transfer function of the transmitter incorporating a front face inversion layer, can be represented as the feedback system shown in the block diagram in Fig 7.24.

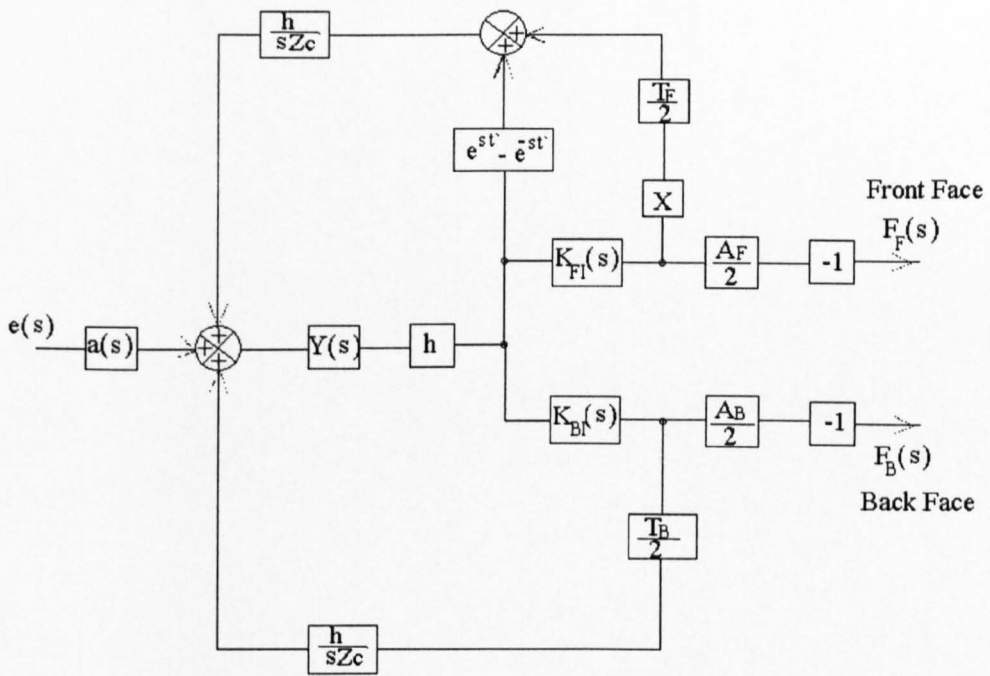


Fig (7.24): The block diagram of the feedback system for the transducer as a transmitter.

In the forward path  $Y(s)$  can be placed before the sum in both the front face and back face feedback loops and in the input path resulting in the block diagram shown in Fig 7.25.



$$I(s) = \frac{Z_E}{\frac{Z_0 + Z_E}{sC_0} + Z_0 Z_E} \cdot e(s)$$

This is similar to equation 7.38 except that it does not contain  $\frac{1}{s}$ . But  $I(s)$  flowing through a capacitor is related to the charge developed on the capacitor electrodes as follows:

$$I(s) = s Q_C(s)$$

Hence, equation 7.38 representing the input path of the block diagram is a transfer function relating the charge on the bulk capacitance  $C_0$  to the driving voltage  $e$ .

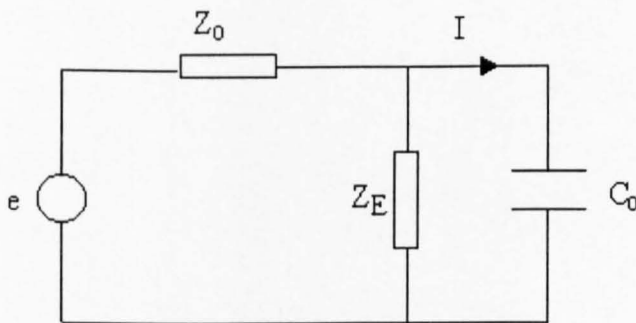


Fig (7.26): The equivalent electrical circuit at the transducer input.

While in each feedback path:

$$Y(s) = \frac{1}{s} \frac{sC_0}{1 + b(s)C_0s} = \frac{1}{s} \left\{ \frac{sC_0}{1 + \frac{Z_E Z_0 s C_0}{Z_E + Z_0}} \right\} \quad \text{--- 7.39}$$

The term inside the brackets is identical to the admittance of the electrical circuit shown in Fig 7.27. Here,  $V_F$  denotes the feedback voltage and  $I_F$  the feedback current.

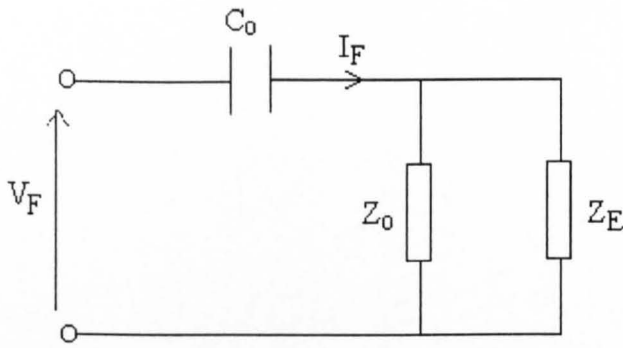


Fig (7.27): The equivalent electrical circuit for each feedback path.

The applied voltage on the transducer due to the inverse piezoelectric effect will produce a force  $h Q(s)$  on both the front and the back faces of the transducer. Part of this force will propagate into the transducer and the other part will go to the front and back face media. Another two forces will also be produced at the inversion-original layer boundary. These forces are illustrated in Fig 7.28, where the notation is that of Redwood [49], i.e. the forces generated into the transducer are positive, while the forces generated into the surrounding media are negative. But here, because the inversion layer has opposite polarity to the original one, i.e.  $h$  has opposite sign, the sign will change at the border of the inversion layer.

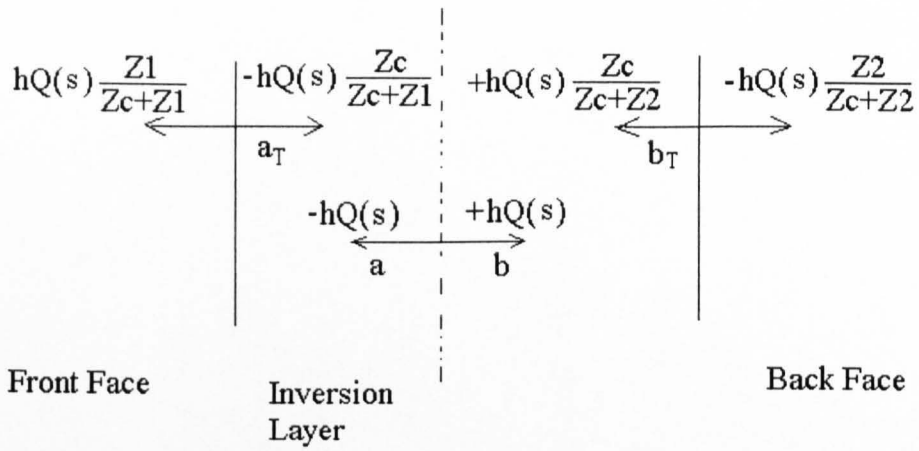


Fig (7.28): Initial stress waves generated at the transducer faces and the inversion-original layer boundaries.

The initial forces shown in the above Figure will undergo a reverberation between the front and the back face of the transducer as shown in Fig 7.29.

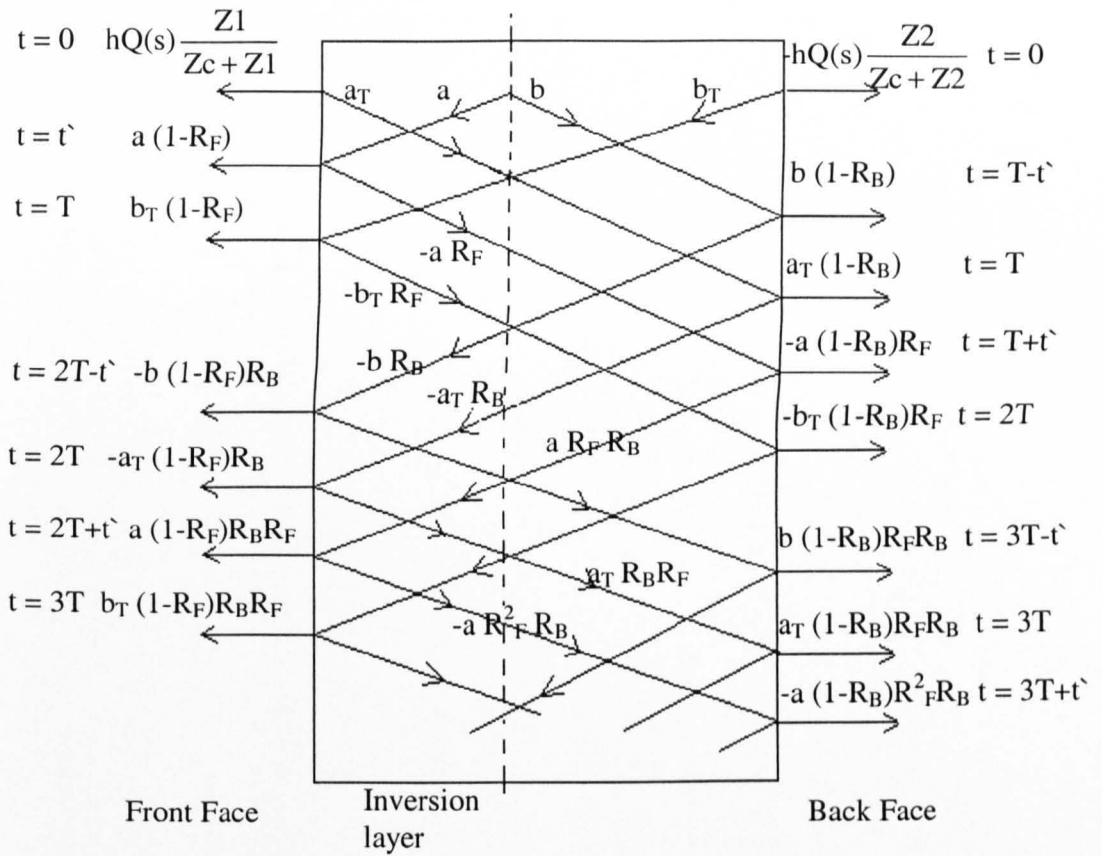


Fig (7.29): Lattice diagram of the forces generated in the transmission mode. Where  $a_T$ ,  $b_T$ ,  $a$  and  $b$  are given in Fig 7.28.

From the above figure, and taking in account that:

$$\frac{Z_c}{Z_c + Z_1} = \frac{1 + R_F}{2}, \quad \frac{Z_c}{Z_c + Z_2} = \frac{1 + R_B}{2}, \quad \frac{Z_1}{Z_c + Z_1} = \frac{1 - R_F}{2}, \quad \frac{Z_2}{Z_c + Z_2} = \frac{1 - R_B}{2}$$

It is possible to obtain the following series in the  $s$ - domain for the stress waves leaving the front face of the transducer:

$$F_1(s) = h Q(s) \left\{ \left( \frac{1 - R_F}{2} \right) - (1 - R_F) e^{-st'} + (1 - R_F) \left( \frac{1 + R_B}{2} \right) e^{-sT} \right. \\ \left. - (1 - R_F) R_B e^{-s(2T-t')} + R_B (1 - R_F) \left( \frac{1 + R_F}{2} \right) e^{-2sT} - (1 - R_F) R_B R_F e^{-s(2T+t')} \right\}$$

$$\begin{aligned}
& + (1-R_F) \left( \frac{1+R_B}{2} \right) R_F R_B e^{-3sT} - (1-R_F) R_B^2 R_F e^{-s(4T+t')} \\
& + (1-R_F) \left( \frac{1+R_F}{2} \right) R_B^2 R_F e^{-4sT} - (1-R_F) R_B^2 R_F^2 e^{-s(4T+t')} + \dots \} \\
F1(s) = & -h Q(s) \left( \frac{1-R_F}{2} \right) \{ -1 - (1+R_B) e^{-sT} - (1+R_F) R_B e^{-2sT} \\
& - (1+R_B) R_B R_F e^{-3sT} - (1+R_F) R_B^2 R_F e^{-4sT} - \dots \} \\
& -h Q(s) (1-R_F) \{ e^{-st'} + R_B e^{-2sT} e^{st'} + R_B R_F e^{-2sT} e^{-st'} \\
& + R_B^2 R_F e^{-4sT} e^{st'} + R_B^2 R_F^2 e^{-4sT} e^{-st'} + \dots \} \\
= & -h Q(s) \left( \frac{1-R_F}{2} \right) \{ -1 - (1+R_F) R_B e^{-2sT} \sum_{n=0}^{\infty} (R_F R_B)^n e^{-2nsT} \\
& - (1+R_B) e^{-sT} \sum_{n=0}^{\infty} (R_F R_B)^n e^{-2nsT} \} \\
& -h Q(s) (1-R_F) \{ e^{-st'} \sum_{n=0}^{\infty} (R_F R_B)^n e^{-2nsT} \\
& + R_B e^{-2sT} e^{st'} \sum_{n=0}^{\infty} (R_F R_B)^n e^{-2nsT} \}
\end{aligned}$$

Taking the sum to infinity for a geometric progression gives the following formula for the wave of force leaving the transducer's front face:

$$\begin{aligned}
F1(s) = & -h Q(s) \left( \frac{1-R_F}{2} \right) \left\{ -1 - \frac{(1+R_F) R_B e^{-2sT}}{1-R_F R_B e^{-2sT}} - \frac{(1+R_B) e^{-sT}}{1-R_F R_B e^{-2sT}} \right\} \\
& -h Q(s) (1-R_F) \left\{ \frac{e^{-st'}}{1-R_F R_B e^{-2sT}} + \frac{R_B e^{-2sT} e^{st'}}{1-R_F R_B e^{-2sT}} \right\}
\end{aligned}$$

Hence:

$$F1(s) = -h Q(s) \left( \frac{1 - R_F}{2} \right) \left\{ \frac{-e^{-sT} + 2e^{-st} - 1 - R_B e^{-sT} + 2R_B e^{-2sT} e^{st} - R_B e^{-2sT}}{1 - R_F R_B e^{-2sT}} \right\}$$

The term between the brackets { } is  $K_{FI}(s)$ , called the reverberation factor of the forces within the transducer when a function of charge is deposited on the device electrodes in the presence of the inversion layer, therefore:

$$F1(s) = -h Q(s) \left( \frac{1 - R_F}{2} \right) K_{FI}(s)$$

In the same manner, the series of forces or stress waves leaving the transducer back face can be found to be:

$$F2(s) = -h Q(s) \left( \frac{1 - R_B}{2} \right) K_{BI}(s)$$

These two equations are identical in form to equations 7.23 and 7.24. Hence, the inverse Laplace transform of equations 7.23 and 7.24 represents a time series of stress waves leaving the transducer's front and back face respectively. The series is produced as a result of the multiple reflections of the forces inside the transducer.

It is very important at this stage to point out that although  $K_{FI}$  and  $K_{BI}$  for both the transmitter and the receiver have the same mathematical form, they differ physically. In the case of the receiver they are related to the displacement reverberation but in the transmitter they demonstrate force reverberation, according to the nomenclature adopted.

### 7.5.3 The Transducer Admittance Transfer Function Feedback System:

The transducer impedance described in equation 7.31 can not be represented in the form of a feedback system, but the admittance can be represented as shown in Fig 7.30.

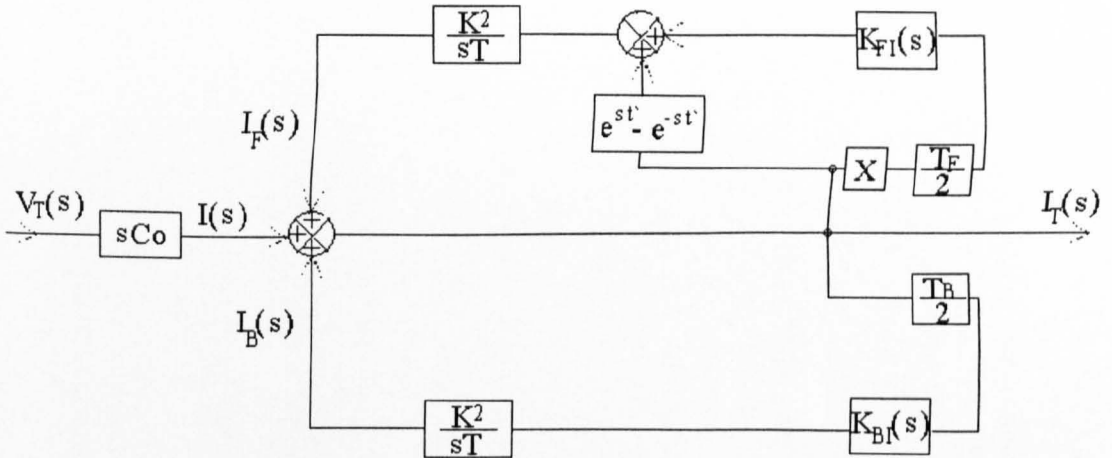


Fig (7.30): The block diagram feedback system for the admittance of the transducer.

In order to be able to describe the physical implications of the transducer admittance transfer function, it is more convenient to substitute for  $\frac{k^2}{T}$  in the previous block diagram. Doing this and rearranging the blocks gives the block diagram shown in Fig 7.31.

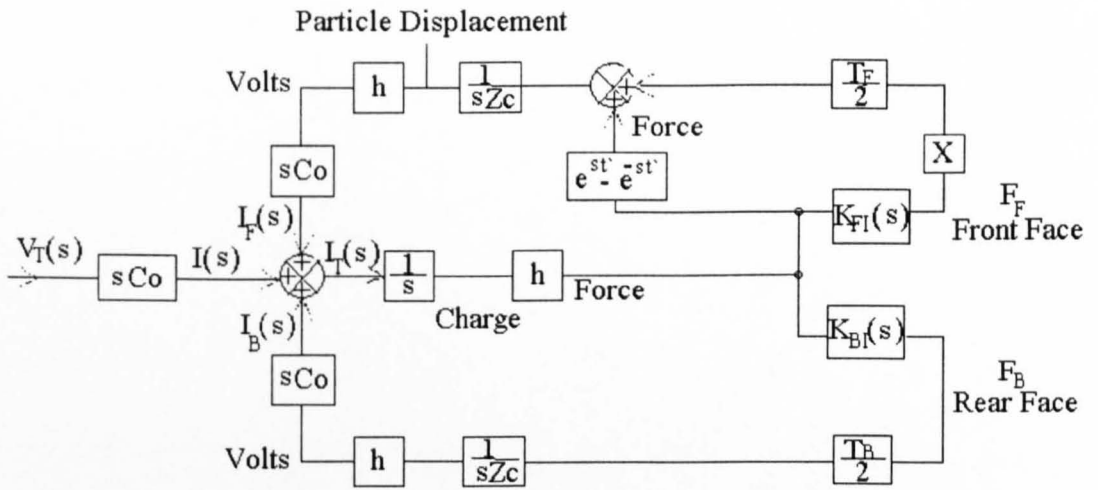


Fig (7.31): The expanded block diagram feedback system for the admittance of the transducer.

When a voltage  $V_T$  is applied to the transducer electrodes a current will flow through the bulk capacitance  $C_o$  of the transducer. The forces described before are produced on the front and the back faces of the transducer and on the inversion-original layer boundary. A fraction of each force developed on the front and the back face is transmitted into the surrounding media and the rest into the transducer. Due to the secondary piezoelectric action, these forces within the transducer produce feedback currents  $I_F$  and  $I_B$  at the input summing point. Also the forces generated at the inversion layer boundary will contribute to these currents as represented by both  $K_{FI}(s)$  and  $K_{BI}(s)$  and the term  $e^{st} - e^{-st}$  (Fig 7.31). All these processes are outlined in Fig 7.31 and the various relationships between force, particle displacement and current are illustrated.

## **7.6 Concluding Remarks:**

This chapter provided a physical insight into the behaviour of the ILT devices and enabled more understanding of the transmitter and receiver mode compared to the typical thickness mode device.

The results confirmed that such devices will have a wider bandwidth than the typical devices, but the pulse width, and hence the axial resolution, required for skin thickness measurements does not seem to be improved. The pulse width is required to be as short as possible. These devices can be operated at higher frequencies for the same thickness, but more reverberations or cycles appeared in the output signal giving at the end a pulse width equal to that obtained from a typical thickness mode transducer.

One advantage of the ILT over the typical devices is that the sensitivity is better. This improvement in the sensitivity gives the ILT devices preference for skin thickness measurement over the typical devices.

The transducer specifications outlined at the end of Chapter 5 are still not fulfilled, specifically the high resolution. ILT's suffer similar problems to conventional devices that are listed in Chapter 5, such as the requirement for a very short pulse width and a new transducer technology is needed for ultra high resolution application on a realistic skin structure.

## **CHAPTER 8**

### **Concluding Remarks & Future Work**

## **8.1 Concluding Summary:**

This thesis has explained the use of ultrasound for skin thickness measurement, the requirements for an ideal ultrasonic system were outlined and the problems and limitations associated with the current ultrasonic systems identified. The problem of interpreting backscattered signals arising from a layered structure like the skin were investigated using the Finite Element Modelling (FEM) package, PZFlex.

The technique was initially used on an idealised skin structure having planar interfaces. The effect of irregular interfaces was modelled and it was found that the backscattered signal had a lower amplitude with more reflections due to the structure of the interface. The modelled transducer and the interaction of the ultrasonic signal with the non planar structure was used to clarify the axial and lateral resolution requirement for high accuracy thickness measurements.

The model was also used to investigate the influence of the shape of a different rubber shoe mounted at the top of the transducer on the backscattered signal to be used in future as a dry coupling medium.

The effect of the real interfaces in the skin on the output backscattered signal was investigated using an FE mesh superimposed on a real skin micrograph, which lead to further refinement of the requirements of the ultrasonic system suitable for resolving such a structure. In order to obtain the axial resolution to resolve the low thickness of the SC a transducer operating at least at 111 MHz is required. In order to resolve the lateral interdigitation high lateral resolution is required. The high lateral resolution can be

obtained by strong focusing the acoustic field, but at the same time this will reduce the depth that can be explored.

Lithium niobate is one of the most commonly used piezoelectric materials for high frequency applications, but a very thin transducer is required to obtain high frequencies, even for the 36° Y-cut specimens. It is difficult to manufacture transducer of the required thickness; repeated fracture of the material occurred during the lapping process to make a transducer of 40 MHz [2] and the 30  $\mu\text{m}$  thickness required for a 111 MHz transducer will be extremely difficult or impossible to obtain.

An inversion layer lithium niobate device may produce higher frequency transducers without the requirement to lap the transducer to a low thickness. Such transducers are expected to have a wider frequency bandwidth giving a preference and better performance for high frequency applications, such as skin thickness measurement, than the normal thickness mode transducers.

An inversion layer device can be obtained by bonding two specimens of opposite polarity using a bonding line, but for high frequency applications, where the thickness of the piezoelectric material is very low, the bonding line can affect the behaviour of the device. Heat treatment of lithium niobate may be a route to obtaining such a multi-layer structure without a bonding line.

This new inversion layer transducer can be obtained from the normal thickness mode transducer using heat treatment of the lithium niobate specimen at a specific temperature for a specific time. Heat treatment of the specimen will cause the formation of an inversion layer having a reversed electrical polarity. This will induce the higher

frequency harmonics to appear in the impedance profile. The number and the thickness of the inversion layers determine the most efficient harmonic frequency.

The behaviour of ILT's was modelled using FEA and a new mathematical model. The results showed that these ILT's had a better efficiency than the typical thickness mode devices, but the pulse width, and hence the axial resolution was not improved in the ILT compared to the typical devices. Although higher frequency was obtained for the same thickness, the output signal from the transducer contained more reverberations giving the same pulse width and hence the same axial resolution compared to the lower frequency normal device.

A 1-D linear mathematical model was developed for one front face inversion layer transducer using Laplace methods. The results of the mathematical model closely matched with FEM results. In this mathematical model closed form solutions were obtained for the operational impedance, in addition to the transmission and reception transfer functions when the device was interfaced to an arbitrary electrical load. By representing device behavior in a block diagram, systems feedback format, cause and effect relationships were readily identified and the underlying differences between the ILT and conventional thickness mode transducer demonstrated clearly.

ILT devices may have potential in some areas of ultrasound, such as harmonic imaging, multi-frequency sonar and non-linear ultrasound. For example, the same transducer that can operate at the first and the second harmonic is required for second harmonic imaging.

Skin structure measurements are still problematic adding to this the reality that because the biology of the skin is so variable an extremely precise distance measurement is very

difficult to be attained. This thesis concludes that ultrasound is able to give an impression of the skin structure rather than a detailed image.

## **8.2 Future Work:**

### **8.2.1 FEM Modelling:**

In this thesis only the effect of the real skin interfaces were modelled, more investigations of the real skin structure are required. All the skin layers were treated as homogeneous linear elastic materials, but PZFlex should be used to model a more detailed inhomogeneous skin structure. More modelling is required for the coupling medium between the transducer and the skin.

The effect of focusing needs to be investigated, but this will be difficult and requires a combination of PZFlex and PSFlex, as mentioned before. Such an analysis will give a clearer insight into the requirements of high lateral resolution.

### **8.2.2 Manufacturing:**

The reproducibility of the heat treatment effect for lithium niobate was not very good. A systematic study of the effects of heat treatment and the production of inversion layers should be made. The heat treatment carried out during the process of this work used only heat treated specimens in air, and more investigations of heat treatment using Ti diffusion are required.

### **8.2.3 Skin Measurement System:**

In this thesis it was shown that the axial resolution of ILT's was not improved at the higher frequency, although they had a better efficiency than the normal thickness mode devices. To obtain the high frequencies required for axial resolution of skin measurement, a new alternative single crystal piezoelectric material, which is more amenable to lapping, is required.

The inhomogeneous and localised variation of the structure of the skin is still a major problem in ultrasonic imaging. Strong focusing is required to obtain high lateral resolution, this will lead to two problems. Firstly, it will reduce the depth that can be explored because the axial length of the focal area becomes very short. Secondly, only a narrow field is being explored. Hence, highly focused transducer with spatial averaging of the data is needed to obtain a detailed image of the skin structure. This will include a suitable scanning technique such as B/D scanning described in the literature to explore the area of interest.

Another area of research needs to be explored that is the effect of water bath or gel, used widely as the coupling medium, on the skin properties and hence the measurement. The use of the silicone rubber coupling medium requires further refinement.

## **References:**

1. K. A. Snook, J. J. Zhao, K. K. Shung et al, "Design, Fabrication and Evaluation of High frequency Single-element Transducers Incorporating Different Materials", IEEE Transaction, UFFC, Vol. 49, No. 2, Feb. 2002.
2. P. Kerr, "Ultrasonic Measurement of Skin Thickness", M. Phil, July 2002, Strathclyde University.
3. G. Wojcik, B. Fornberg, R. Waag, L. Carcione, J. Mould, L. Nikodym and T. Driscoll, "PseudoSpectral Methods for long-scale Bio-Acoustic Models", Ultrasonic Symposium Proceedings 1997.
4. F. Martini, "Fundamentals of ANATOMY and PHYSIOLOGY", Forth Edition, Prentice-Hall, Inc. 1998.
5. R. Warwick and P.L Williams, "Gray's Anatomy, 35<sup>th</sup> Edition", Longman group Ltd. 1973.
6. Diane M. Thiboutot, "Dermatological Applications of High-Frequency Ultrasound", Copyright 1999 Society of Photo-Optical Instrumentation Engineers (SPIE Conference Proceedings).
7. J. Serup and G. B. E. Jemec, "Handbook of NON-INVASIVE METHODS and the SKIN", CRC Press, Inc. 1995.

8. I. A. Brown, G. L. Wilkes and R. H. Wildnauer, "THE BIOMECHANICAL PROPERTIES OF THE SKIN", CRC Critical Reviews in Bioengineering pp. 453-495 August 1973.
9. W. W. Abas and J. C. Barbenel, "The response of human skin to small tensile loads in vitro", Engineering In Medicine, MEP Ltd. pp (43-46), 1982.
10. P. Elsner, E. Berardesac, and H. I. Maibach, "Bioengineering of the Skin: Water and the Stratum Corneum", CRC Press, Inc. 1994.
11. P. Elsner, A. O. Barel, E. Berardesca, B. Gabard and J. Serup, "Skin Bioengineering, Techniques and Applications in Dermatology and Cosmetology", S. Karger AG, P.O. Box, CH-4009 Basel (Switzerland) 1998.
12. E. Berardesca, P. Elsner, Klaus-P. Wilhelm and H. I. Maibach, "Bioengineering of the Skin: Methods and Instrumentation", CRC Press, Inc. 1995.
13. M. Hussey, "Basic Physics and Technology of Medical Diagnostic Ultrasound", Matthew Hussey 1985.
14. P. N. T Wells, "Current Status and Future Technical Advances of Ultrasonic Imaging", IEEE ENGINEERING IN MEDICINE AND BIOLOGY September/October 2000.
15. C. Y. Tan, B. Statham, R. Marks and P. A. Payne, "Skin thickness measurement by pulsed ultrasound: its reproducibility, validation and variability", British Journal of Dermatology 106, pp. 657-667 1982.
16. F. J. Fry, "Methods and Phenomena 3, Ultrasound: Its Application in Medicine and Biology Part II", Elsevier Scientific Publishing Company, Amsterdam 1978.

17. J. L. Rose and B. B. Goldberg, "Basic Physics in Diagnostic Ultrasound", John Wiley & sons, Inc. 1979.
18. C. Passmann and H. Ermert, "A 100-MHz Ultrasound Imaging System for Dermatologic and Ophthalmologic Diagnostics", IEEE transactions on Ultrasonics, Ferroelectrics, and Frequency control, 43(4) July 1996.
19. T. D. Mast, "Empirical Relationships Between Acoustic parameters in Human soft Tissues", Acoustic Research letters online published 16 November 2000, Acoustic Society of America.
20. J. H. Cantrell, R. E. Goans, and R. L. Roswell, "Acoustic impedance variations at burn-nonburn interfaces in porcine skin", J. Acoust. Soc. Am. 64(3), pp. 731-735 Sept. 1978.
21. H. Alexander and D. L. Miller, "Determining Skin Thickness with Pulsed Ultrasound", The Journal of Investigative Dermatology, 72:17-19, 1979.
22. C. Y. Tan, R. Marks, and P. Payne, "Comparison of Xeroradiographic and Ultrasound Detection of Corticosteroid Induced Dermal Thinning", The Journal of Investigative Dermatology, 76:126-128, 1981.
23. J. de Rigal, C. Escoffier, B. Querleux, B. Faivre, P. Agache, and J. Leveque, "Assessment of Ageing of the Human Skin by In Vivo Ultrasonic Imaging", The Journal of Investigative Dermatology, 93(5): 621-625, November 1989.

24. H. Ermert, M. Pollakowski, C. Passmann, and L. von Bernus, "Acoustical imaging using an optimal combination of signal pre-filtering and pulse compression", *Acoustical Imaging*, vol. 21, J. P. Jones, Ed. New York: Plenum, 1994.
25. S. El Gammal, C. El Gammal, K. Kaspar, C. Pieck, P. Altmeyer, M. Vogt, and H. Ermert, "Sonography of the Skin at 100 MHz Enables In Vivo Visualisation of Stratum Corneum and Viable Epidermis in Palmar Skin and Psoriatic Plaques", *The Journal of Investigative Dermatology*, 113(5): 821-829, November 1999.
26. P. D. Lopath, R. J. Meyer, S. Ayappan, K. Snook, T. Ritter and K. K. Shung, "High Frequency Transducers for Ultrasonic Backscatter Microscopy", Copyright 1999 Society of Photo-Optical Instrumentation Engineers (SPIE Conference Proceedings).
27. M. Lebertre, F. Ossant, L. Vaillant, S. Diridollou and F. Patat, "Human Dermis Ultrasound Characterisation: Backscattering Parameters Between 22-45MHz", *IEEE INTERNATIONAL ULTRASONIC SIMPOSIUM* October 22-25, 2000.
28. S. Iraniha, M. E. Cinat, V. M. Vanderkam, A. Boyko, D. Lee, J. Jones, and B. M. Achauer, "Determination of burn Depth with Noncontact Ultrasonography", *Journal of Burn Care & Rehabilitation*, 21(4): 333-338, July/August 2000.
29. T. A. Ritter, K. K. Shung, J. Cannata, and T. R. ShROUT, "High Frequency Ultrasound Array for Medical Imaging", *IEEE Ultrasonics Symposium* 2000.
30. NAFEMS. NAFEMS A Finite Element Primer, COPYRIGHT 1992, NAFEMS BIRNIEHILL EAST KELBRIDE GLASGOW, G75 0QU, UK.

31. D. A. Knapik, B. Starkoski, C. J. Pavlin, and F. S. Foster, "A 100-200 MHz Ultrasound Biomicroscope", IEEE Transactions on Ultrasonics, Ferroelectrics and Frequency Control, 47(6), November 2000.
32. F. A. Duck, "PHYSICAL PROPERTIES OF TISSUE", ACADEMIC PRESS LIMITED 1990.
33. J. C. Mould, G. L. Wojcik, L. M. Carcione, M. Tabei, T. D. Mast, and R. C. Waag, "Validation of FFT-Based Algorithms for large-scale Modelling of Wave Propagation in Tissue", IEEE Ultrasonics Symposium 1999.
34. J. T. Bennett, "Development of a finite element modelling system for piezocomposite transducers", PhD thesis 1995, Department of Electrical and Electronic Engineering, University of Strathclyde, Glasgow-Scotland.
35. G. Hayward, "Time and Frequency Domains Modelling of The Piezoelectric Transducer", PhD Thesis, 1982, Strathclyde University.
36. [www.bostonpiezooptics.com](http://www.bostonpiezooptics.com), **Boston Piezo-Optics Inc.** USA
37. [www.tasitechnical.com](http://www.tasitechnical.com), *TASI Technical Software Inc. Canada (the PRAP Code)*
38. R O'Leary, G. Hayward, A. Parr, G. Smillie and C. Desilets, "Experimental Characterisation of Low Velocity Passive Materials Employed in Piezoelectric Transducer Design", Presented at ONR Transducer workshop, Baltimore May 2002.

39. B. W. Drinkwater, "The Use of Dry Coupling in Ultrasonic Non-destructive Testing", Ph.D. thesis 1995, University of London, Department of Mechanical Engineer.
40. S. Hagusawa, T. Shimada, H. Arao and Y. Asada, "Morphological architecture and distribution of blood capillaries and elastic fibres in the human skin", *Journal of Tissue Viability* 2001 Vol. 11 No 2 pp(59-63).
41. [www.mathworks.com](http://www.mathworks.com), The MathWorks, Inc. USA.
42. K. Nakamura, K. Fukazawa, K. Yamada and S. Saito, "Broadband Ultrasonic Transducers Using LiNbO<sub>3</sub> Plate with Ferroelectric Inversion Layer", *IEEE Trans. Ultrason. Ferroelect. Freq. Contr*, Munich- Germany 2002, pp (1199-1203).
43. K. Nakamura, H. Ando, and H. Shimizu, "Ferroelectric domain inversion caused in LiNbO<sub>3</sub> plates by heat treatment", *Appl. Phys. Lett.* 50 (20), 18 May 1987, pp (1413-1414).
44. L. Huang and N. Jaeger, "Discussion of domain inversion in LiNbO<sub>3</sub>", *Appl. Phys. Lett.* 65 (14), 3 October 1994, pp (1763-1765).
45. S. Miyazawa, "Ferroelectric domain inversion in Ti-diffused LiNbO<sub>3</sub> optical waveguide", *J. Appl. Phys.* 50(7), July 1979, pp (4599-4603).
46. M. Redwood, "Transient performance of piezoelectric transducer", *Journal of the Acoustic Society of America*, Vol. 33, No. 4, April 1961, pp 527-536.

47. W. P. Mason, "Electromechanical transducers and wave filters (2nd Edit)", Van Nostrand Co Inc., NewYork, 1948.
48. J. Blitz, "Fundamentals of ultrasonics", Butterworths 1963.
49. M. Redwood, "A study of waveforms in the generation and detection of short ultrasonic pulses", Applied materials research, April 1963, pp 76-84.

## **APPENDIXES**

## **Appendix A**

The mechanical properties for the materials used in PZFlex.

### **1- The mechanical properties of the PZT5H material:**

The dielectric constants matrix:

$$E_{xx} / E_{\text{vacuum}} = 1700$$

$$E_{zz} / E_{\text{vacuum}} = 1470$$

The stiffness constants matrix:  $[N/m^2]$

$$C_{11} = 12.72e10$$

$$C_{12} = 8.02e10$$

$$C_{13} = 8.47e10$$

$$C_{33} = 11.74e10$$

$$C_{44} = 2.30e10$$

$$C_{66} = 0.5 * (C_{11} - C_{12})$$

The piezoelectric constants matrix:  $[C/m^2]$

$$E_{31} = -6.5$$

$$E_{33} = 23.3$$

$$E_{15} = 17.0$$

### **2- The mechanical properties of the Lithium Niobate Given by the company (Boston -Optics):**

The dielectric constants matrix:

(These parameters are given at constant Strain)

$$E_{xx} / E_{\text{vacuum}} = 44.3$$

$$E_{zz} / E_{\text{vacuum}} = 27.9$$

The stiffness constants matrix (Elastic constants):  $[N/m^2]$

$$C_{11} = 2.03e11$$

$$C_{12} = 0.573e11$$

$$C_{13} = 0.752e11$$

$$C_{14} = 0.085e11$$

$$C_{33} = 2.424e11$$

$$C_{44} = 0.595e11$$

$$C_{66} = 0.728e11$$

The piezoelectric constants matrix:  $[C/m^2]$

E31 = 0.23  
E33 = 1.8  
E15 = 3.83  
E22 = 2.37

### **3- The mechanical properties of the Lithium Niobate measured by the PRAP CODE:**

The dielectric constants matrix:  
(These parameters are measured at constant Strain).

$E_{xx} / E_{vacuum} = 44.3$   
 $E_{zz} / E_{vacuum} = 37.2819$

The stiffness constants matrix (Elastic constants): [N/m<sup>2</sup>]

C11 = 2.03e11  
C12 = 0.573e11  
C13 = 0.752e11  
C14 = 0.085e11  
C33 = 1.80811e11  
C44 = 0.595e11  
C66 = 0.728e11

The piezoelectric constants matrix: [C/m<sup>2</sup>]

E31 = 0.23  
E33 = 4.43658  
E15 = 3.83  
E22 = 2.37

Note: The main differences are in the 33 (or zz) direction parameters.

For the 36° Y-cut the wave speed is 7340 [m/s] and the coupling factor is 0.485.

### **4- The mechanical properties of the Rubber material:**

This material is RTV 664 silicone Rubber (2.649mm).

All this properties are measured at 2.25MHz.

The longitudinal Velocity	1014.8 [m/s]
The Shear Velocity	139.8 [m/s]
Density	1293.68 [kg/m <sup>3</sup> ]
Longitudinal Attenuation	851 [dB/m]
Shear Attenuation	5212 [dB/m]

## 5- The Mechanical properties of other materials:

### 5.1 Water:

Density = 1000	[kg/m <sup>3</sup> ]
Longitudinal wave velocity = 1500	[m/s]
Shear wave velocity = 0.0	[m/s]

### 5.2 Air:

Density = 1.294	[kg/m <sup>3</sup> ]
Longitudinal wave velocity = 330.0	[m/s]
Shear wave velocity = 0.0	[m/s]

### 5.3 Aluminium:

Density = 2700	[kg/m <sup>3</sup> ]
Young's Modulus = 808.1e9	[m. s <sup>-2</sup> .kg]
Poisson Ratio = 0.355	

### 5.4 Tungsten Epoxy:

Density = 16800	[kg/m <sup>3</sup> ]
Bulk Modulus = 3.49e10	[m. s <sup>-2</sup> .kg]
Shear Modulus = 2.58e10	[m. s <sup>-2</sup> .kg]

## Appendix B

The MATLAB programme used to create the table containing the x, y of each pixel in the skin image and the material in that pixel. This table was then used in PZFlex to build the FE mesh of the real skin structure.

```
%***** START *****
clear all; close all;

% "Mat=['watr'; 'derm'; 'epid'; 'scrn']; The names of the diverse skin layers"
%   watr is water
%   derm is dermis
%   epid is epidermis
%   scrn is Stratum Corneum
%
Mat_Value=[255 150 100 50]; % "The greyscale intensity of each layer respectively"

Img_Magnification=210; % "The ratio in which the skin image was magnified"

x_Dim=774.7/Img_Magnification; % "Width of the image, Dimension in mm"
y_Dim=27.8/Img_Magnification; % "Length of the image, Dimension in mm"
[Im,map]=imread('skinb-stitched-big.tif','tif'); % "Read the image"

[ys,xs]=size(Im);
Ds=xs*ys;
x=0:xs; % "Form the x, y of each pixel"
y=0:ys;
x=((x_Dim./xs)*x);
y=((y_Dim./ys)*y);

fid=fopen('table.skin1','wt'); % "Open a text file to write the table"

fprintf(fid,' hedr      0); % "Some headers required by PZFlex"
fprintf(fid,'\n info      1');
fprintf(fid,'\n xcrd      ');
fprintf(fid,'%d\n',xs+1);

num_of_samples_per_row=8; % "No. of columns in the table file"

d=floor((xs+1)/num_of_samples_per_row);
r=rem(xs+1,num_of_samples_per_row);
t=1;
for i=1:d;
    for j=1:num_of_samples_per_row;
        if x(t)<0
            fprintf(fid,'%E ',x(t));
        else
            fprintf(fid,' %E ',x(t));
        end
    end
end
```

```

    end
    t=t+1;
    end
    fprintf(fid,'\n');
end

if r>0;
    for j=1:r;
        fprintf(fid,' %E ',x(t));
        t=t+1;
    end
end

fprintf(fid,'\n ycrd      ');
fprintf(fid,'%d\n',ys+1);

d=floor((ys+1)/8);
r=rem(ys+1,num_of_samples_per_row);
t=1;
for i=1:d;
    for j=1:num_of_samples_per_row;
        if y(t)<0
            fprintf(fid,' %E ',y(t));
        else
            fprintf(fid,' %E ',y(t));
        end
        t=t+1;
    end
    fprintf(fid,'\n');
end

if r>0;
    for j=1:r;
        fprintf(fid,' %E ',y(t));
        t=t+1;
    end
end

fprintf(fid,'\nmatr      %d',Ds);
fprintf(fid,'\n');

c=1;
for y=1:ys;          % "Write the material name of each pixel"
    for x=1:xs;
        if Im(y,x)==Mat_Value(1)
            fprintf(fid,'watr ');
        elseif Im(y,x)==Mat_Value(2)
            fprintf(fid,'derm ');
        end
    end
end

```

```
elseif Im(y,x)==Mat_Value(3)
    fprintf(fid,'epid ');
elseif Im(y,x)==Mat_Value(4)
    fprintf(fid,'scrn ');
else
    fprintf(fid,'watr ');
end
c=c+1;
if c>24
    c=1;
    fprintf(fid,'\n');
end
end
end

fclose(fid);

%***** STOP *****
```